A Hybrid Seismic Design Method for Steel Irregular Space Moment Resisting Frames

Tzimas, Angelos S.; Skalomenos, Konstantinos A.; Beskos, Dimitri E.

DOI:
10.1080/13632469.2020.1733140

Document Version
Peer reviewed version

Citation for published version (Harvard):
Tzimas, AS, Skalomenos, KA & Beskos, DE 2020, 'A Hybrid Seismic Design Method for Steel Irregular Space Moment Resisting Frames', *Journal of Earthquake Engineering*. https://doi.org/10.1080/13632469.2020.1733140

A Hybrid Seismic Design Method for Steel Irregular Space Moment Resisting Frames

Journal:	*Journal of Earthquake Engineering*
Manuscript ID	UEQE-2019-3771.R2
Manuscript Type:	Full Length Papers
Date Submitted by the Author:	n/a
Complete List of Authors:	Tzimas, Angelos; Atkins Skalomenos, Konstantinos; University of Birmingham Edgbaston Campus, Civil Engineering Beskos, Dimitri; University of Patras School of Engineering
Keywords:	Steel space frames, Hybrid force/displacement design, Space moment resisting frames, Plan view irregular frames, Frames with setbacks, Mass irregular heightwise frames, Behavior factors, Deformation control

A Hybrid Seismic Design Method for Steel Irregular Space Moment Resisting Frames

Angelos S. Tzimas[1]; Konstantinos A. Skalomenos[2,*]; Dimitri E. Beskos[3,4]

[1] Atkins, Woodcote Grove, Ashley Road, Epsom KT18 5BW, United Kingdom

[2] Department of Civil Engineering, University of Birmingham, Edgbaston, Birmingham B15 2TT, United Kingdom

[3] Department of Disaster Mitigation for Structures, College of Civil Engineering, Tongji University 200092 Shanghai, China

[4] Department of Civil Engineering, University of Patras 26500 Patras, Greece

ABSTRACT

A hybrid force/displacement seismic design method for space steel moment resisting frames irregular in plan view and in elevation is developed. Irregularity in elevation is either due to non-uniform distribution of mass or due to the presence of setbacks along the height of the frame. More specifically, 30 different frames irregular in plan view for the first case (plan-irregularities), 40 frames with setbacks (vertical stiffness irregularities) for the second case, and 18 frames with mass discontinuities (vertical mass irregularities) at the first, intermediate and top storey for the third case are considered. All these frames are designed according to Eurocodes 3 and 8 and subjected to 42 pairs of ordinary ground motions. Through nonlinear seismic analyses, seismic response databanks for these three types of irregular frames are generated corresponding to four performance levels. These databanks are then utilized for the development of simple expressions that determine the behavior (or strength reduction) factors of the frames. These are functions of frames geometrical/dynamic characteristics including measures of their irregularities as well as the target maximum interstorey drift ratio and member local ductility. The proposed design method, even though it is mainly a force-based design method, controls deformation and therefore damage through the proposed deformation-controlled behavior factors. Design examples are presented to validate the effectiveness of the method to account for the irregularity effects on the preliminary design stage while time-history analysis results demonstrate its advantages to control better the inelastic response of the frames over the conventional force-based seismic design method of Eurocode 8.

Keywords: Steel space frames, Hybrid force/displacement design, Space moment resisting frames, Plan view irregular frames, Frames with setbacks, Mass irregular heightwise frames, Behavior factors, Deformation control

1. INTRODUCTION

Irregular building structures may suffer significantly more damages compared to regular structures [1], indicating that their inelastic seismic response cannot be always estimated with safety by utilizing the methods of current seismic design codes [2,3]. The various structural irregularities over the floor plan or along the height of structures lead to a combined non-uniform distribution of stiffness, strength and mass which in turn negatively affects the seismic performance of structures.

Common types of geometrical irregularities in building structures are mainly related to floor plan irregularity, e.g., L, Π, or T-shaped buildings in plan view or to the presence of setbacks along the height of the building, i.e., the presence of abrupt reductions of the floor area. In urban areas, for instance, plan-irregular or setback buildings are often used since they increase ventilation and sunlight and use effectively the often irregular available lot area. It is also a common trend, nowadays, for buildings to accommodate different functions at specific levels of the elevation, such as floors with heavy mechanical or electrical equipment, floors used for commercial purposes (shopping centers, entertainment and leisure facilities) or car parking floors. This could result in a significant mass irregularity along the height that cannot be ignored in the design. As a result, stronger beams tend to be installed at floors that sustain the heavier masses.

Many researchers in the past have examined the seismic response of structures with irregularities. A review of research on the seismic behavior of irregular building structures can be found in [1,4]. A detailed description of the inelastic behavior of plan-irregular structures was made by De la Llera and Chopra [5], where the torsional effects by non-uniform distribution of strength and stiffness were considered. Many studies thereafter investigated the influence of strength deterioration on the seismic response of plan-irregular structures under

*Corresponding author e-mail: k.skalomenos@bham.ac.uk

biaxial seismic excitations adopting more sophisticated modelling approaches [6]. Recent works on multi-degree-of-freedom asymmetric reinforced concrete and steel braced frame structures [7] demonstrate the necessity of considering a more uniform distribution of ductility demands among adjacent members in the seismic design of asymmetric structures.

A larger inelastic deformation demand (i.e., member ductility or story drift) was also observed in buildings with setbacks either in members near setbacks or in the tower (i.e., the part with the smallest number of bays) [8]. Duan and Chandler [9] pointed out that the current design methodologies cannot prevent the members near the setback from a severe damage concentration and as a result a stronger design for the tower should be considered. Chen et al. [10] observed that the tower exhibits a local vibration mode enough to result in higher mode effects indicating the necessity for controlling its response, while Karavasilis et al. [11] concluded that the extensive local damages of the tower members could reduce the ductility classification of the building. Very few studies have also examined the influence of biaxial seismic excitations and torsional effect on setback space buildings [12-14].

The seismic response of planar frames with vertical mass irregularities has also been a subject of research over the last years. Valmundsson and Nau [15] observed that mass discontinuity at the higher floors affects primarily the elastic response of the frames and that at the lower floors affects mostly their inelastic response, while Das and Nau [16] found that mass irregularity at the lower or upper floors lead to the worst behavior with respect to energy absorption. However, Magliulo et al. [17] concluded that elastic and inelastic responses are slightly affected by mass discontinuities which is in accordance with the findings in the study of Tremblay and Poncet [18], for steel buildings with diagonal braces. An estimation methodology of the seismic damage of planar steel moment-resisting frames with vertical mass irregularities is presented in [19].

The above research studies (mostly on two-dimensional (2-D) frames) highlight the importance of treating irregular structures as a special type of structures and the need of developing effective design procedures or upgrading existing ones to account for the new drift and ductility demands. The three-dimensional (3D) frame modelling appears to be a sufficient solution for the study of irregular building structures for which torsional motion may not be treated adequately by traditional, simplified plane models [7,14].

A new seismic design method, namely the hybrid force/displacement (HFD) design method, has been proposed by the present authors and co-workers and its effectiveness has been confirmed in several types of regular and irregular planar steel frames [20-22], regular space steel frames [23] and regular planar composite steel/concrete frames [24]. The HFD seismic design method combines the advantages of both the force-based design (FBD) method [2,3] and the direct displacement-based design (DBD) method [25] in a hybrid force/displacement design scheme and works within the framework of the performance-based seismic design (PBSD) [26]. The main advantages of HFD is the fact that directly controls both structural and non-structural damage and requires fewer design iterations than the conventional FBD method as well as it does not use substitute SDOF structures and highly damped displacement response spectra as the DBD method. A deformation-controlled behavior factor q (or strength reduction factor R) is determined to limit the global ductility and seismic design forces are calculated by utilizing the familiar to engineers response spectrum analysis.

In this study, the HFD is developed for irregular in elevation and floor plan space steel moment resisting frames (MRF) as well as for frames with vertical mass irregularities. A large seismic response databank is generated on the basis of 88 space irregular MRFs databank according to Eurocodes 3 and 8 [27,3], four different performance levels with respect the IDR and $\mu_{\theta,}$ and non-linear dynamic analysis under 42 pairs of ordinary ground motions. This response databank is utilized to develop the necessary empirical equations employed by the HFD. Realistic performance-based design examples of three irregular MRFs are presented and evaluated with nonlinear time-history analyses for three performance levels. Comparisons with the design results of the FBD method of EC8 [3] demonstrate the advantage of the proposed design method to account in a direct manner for the irregularity effects and control the inelastic response of these irregular frames.

2. SEISMIC DESING OF STEEL IRREGULAR SPACE FRAMES

2.1. Space frames irregular in plan view

In this section, 30 steel space MRFs regular along their height and irregular in plan view (L-shaped plan) are designed. The frames have a storey height equal to 3.00 m and a bay span 5.00 m. Figure 1a shows in plan view the 6 types of the frames considered. Each type has 3, 6, 9, 12 and 15 storeys, hence there are 6×5=30 such MRFs. Figure 1b depicts in perspective form a 6-storey space frame of type 5 in Figure 1a. The present space frames constitute frame Group A. A torsional response is expected in the frames of Group A due to their

stiffness and mass irregularity caused by their L-shaped plan view, and therefore, accidental eccentricity is not considered as a part of the design and assessment of their structural response. This design approach may be considered to be against the clause 4.3.2 of EC8 [3], but it is used to investigate if the torsional response of the frames of Group A is higher compared to the torsional response of the corresponding regular frames with 5% accidental eccentricity (see Section 4.1). It should be noted that one of the EC8 [3] criteria to characterize a building as irregular in plan, is when the slenderness ratio $\lambda = L_{max}/L_{min}$ of the building in plan is higher than 4, where L_{max} and L_{min} are respectively its larger and smaller dimension. In the current design cases of the buildings of Group A, the range of λ ratio is between 1.33 and 4 and thus the level of the building irregularities can be considered low to moderate.

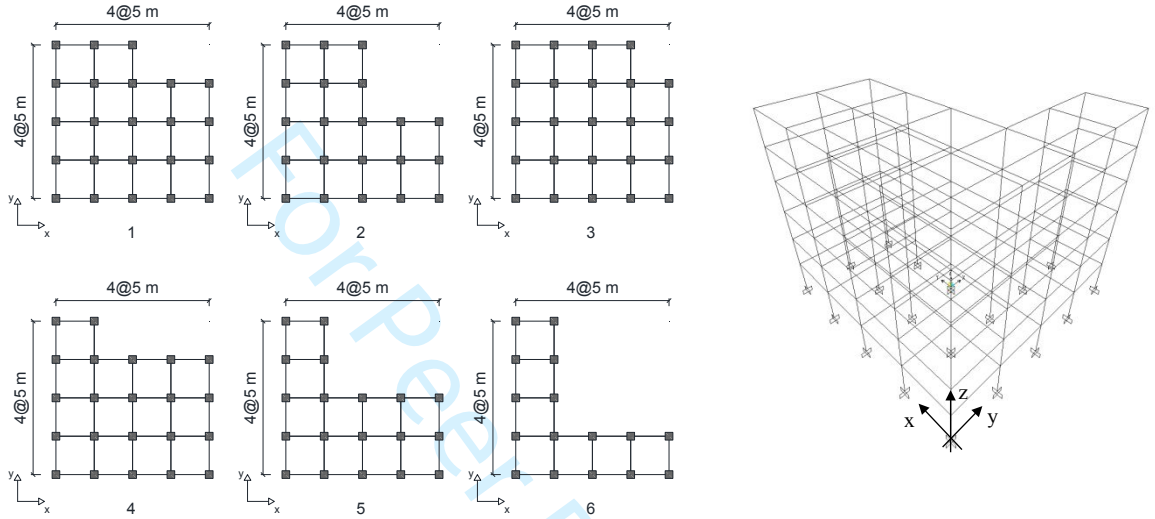

(a) (b)

Figure 1. Group A of space steel frames: (a) frames plan view (Type 1-6); (b) perspective view of the six-storeys four-bays space MRF (Type 5 in plan view)

The gravity loads combination was 1.35G + 1.5Q. The dead and live design loads were G = 6.5 kN/m^2 and Q = 2.0 kN/m^2, respectively, while structural self-weight was considered in the structural analysis process. The earthquake load was determined by the Type 1 elastic design spectrum of EC8 [3] for soil class B. The peak ground acceleration (PGA) was taken equal to 0.24g (g = 9.81m/s^2), while a behavior factor q = 6.5 was used to size the frames for both the x and y directions of the building. It should be noted that in accordance with EC8 [3], for buildings which are not regular, the q factor should be reduced by 20%. This reduction of q has been considered in the design of all frames of this work. The seismic design combinations were $G + 0.3Q \pm E_x \pm 0.3E_y$, $G + 0.3Q \pm E_y \pm 0.3E_x$, where E_x and E_y are the seismic loads in x and y direction, respectively.

Every frame was designed according to Eurocodes 3 and 8 [27,3] by using the commercial software SAP 2000 [28] and conducting spectrum analysis. For the beams, compact IPE structural sections of grade S235 were selected while for the columns compact square-hollow-sections (SHS) of grade S355 as a practical way to satisfy efficiently the capacity design of joints. In dissipative elements, all the sections are classified as Class 1. SHS columns are part of the lateral resisting system in both x and y directions, and thus are subjected to bidirectional bending and axial load due to the gravity and seismic design situation. The use of SHS in the frames of this work is preferable since the strength and stiffness is the same in both local axes compared to other H commercial sections. Same design approach applies also for the buildings of Group B and C. The beam-to-column joints were designed to be rigid. Second order effects (P−Δ) were considered through the interstorey drift sensitivity coefficient θ [3]. As additional design quantities to quantify the mechanical characteristics of the designed frames, the column-to-beam flexural strength ratio α and the mid-height beam-to-column stiffness ratio ρ were adopted in the present study as defined in [21,29].

For all frame cases, the coefficient θ [3] governs the seismic design resulting in a cross-section enlargement to satisfy the drift requirements. This is a known issue of EC8 [3] for steel MRFs, in particular when high q factors are used in low to moderate seismicity designs. However, the initial choice of a high q factor plays a direct role in the design solution [30] and lighter solutions can very likely be adopted if a lower q factor was initially adopted instead, especially in the case of tall buildings. The cross-sections of the 6-stories and 12 stories frames are given in Table 1. Cross-sections for the 3-storeys, 9-storieys and 15-storeys frames can be found in [22]. In Table 1, B denotes beam and C denotes column. The subscripts x and y stand for the respective

directions while *e* and *i* mean "exterior" and "interior", respectively. Section dimensions are given in mm. Minimum and maximum values of ρ and α are also provided for which ρ decreases as α increases and vice versa. In addition, the three first natural periods are provided in Table 2.

Table 1. Sections of space steel frames of Group A.

*Six storey space MRF			
Floor	Group A		
	IPE		SHS
	B_{xe}, B_{ye}	B_{xi}, B_{yi}	C_i, C_e
1	330	360	350x16
2	330	360	300x16
3	330	360	300x16
4	300	330	300x12
5	300	330	300x12
6	300	330	300x12

*$0.24 < \rho < 0.43$ and $1.60 < \alpha < 2.27$

*Twelve storey space MRF			
Floor	Group A		
	IPE		SHS
	B_{xe}, B_{ye}	B_{xi}, B_{yi}	C_i, C_e
1	360	450	400x20
2	400	450	400x20
3	400	450	400x20
4	360	450	400x20
5	360	400	400x20
6	360	400	400x16
7	330	400	400x16
8	330	360	350x16
9	300	360	300x16
10	300	360	300x16
11	270	330	300x12
12	270	330	300x12

*$0.19 < \rho < 0.30$ and $2.60 < \alpha < 3.63$

Table 2. Three first vibration periods of the 6-storeys and 12-storeys space steel frames of Group A.

Frames of Group A				
Number of storeys	Frame type	Period (sec)		
		T_1	T_2	T_3
6	1	1.21	1.21	1.09
6	2	1.19	1.19	1.09
6	3	1.22	1.22	1.09
6	4	1.20	1.20	1.08
6	5	1.17	1.17	1.07
6	6	1.12	1.12	1.05
12	1	1.92	1.92	1.76
12	2	1.91	1.90	1.76
12	3	1.93	1.92	1.77
12	4	1.92	1.91	1.76
12	5	1.89	1.89	1.75
12	6	1.87	1.87	1.73

2.2 Space frames with setbacks along the height

In this section, 40 steel space MRFs regular in the plan view and irregular along the height (with setbacks) are designed following the same assumptions and design methodologies adopted for the frames of Group A. The number of the bays in x direction reduces with the number of storeys along the height, as shown in Figure 2a, thereby creating a geometrical discontinuity along that height. Figure 2b shows in 3D a representative 6-storeys space frame with 3 bays in both directions for the first, second and third storey, and one bay in x direction for the rest three storeys. Figure 2c illustrates all the frames under consideration. The current space frames constitute frame Group B and have 3, 6 and 9 storeys. Similarly, with the frames of Group A, a torsional response is expected in the frames of Group B due to their stiffness and mass irregularity along their height caused by the setbacks, and therefore, accidental eccentricity is not considered. The cross-sections of the frames of Group B had dimensions similar to those of Group A. Sections of the 6-storey and 9-storey frames are shown in Table 3 as the most representative, while the rest can be found in Tzimas [22]. The three first natural periods of Group B frames are provided in Table 4.

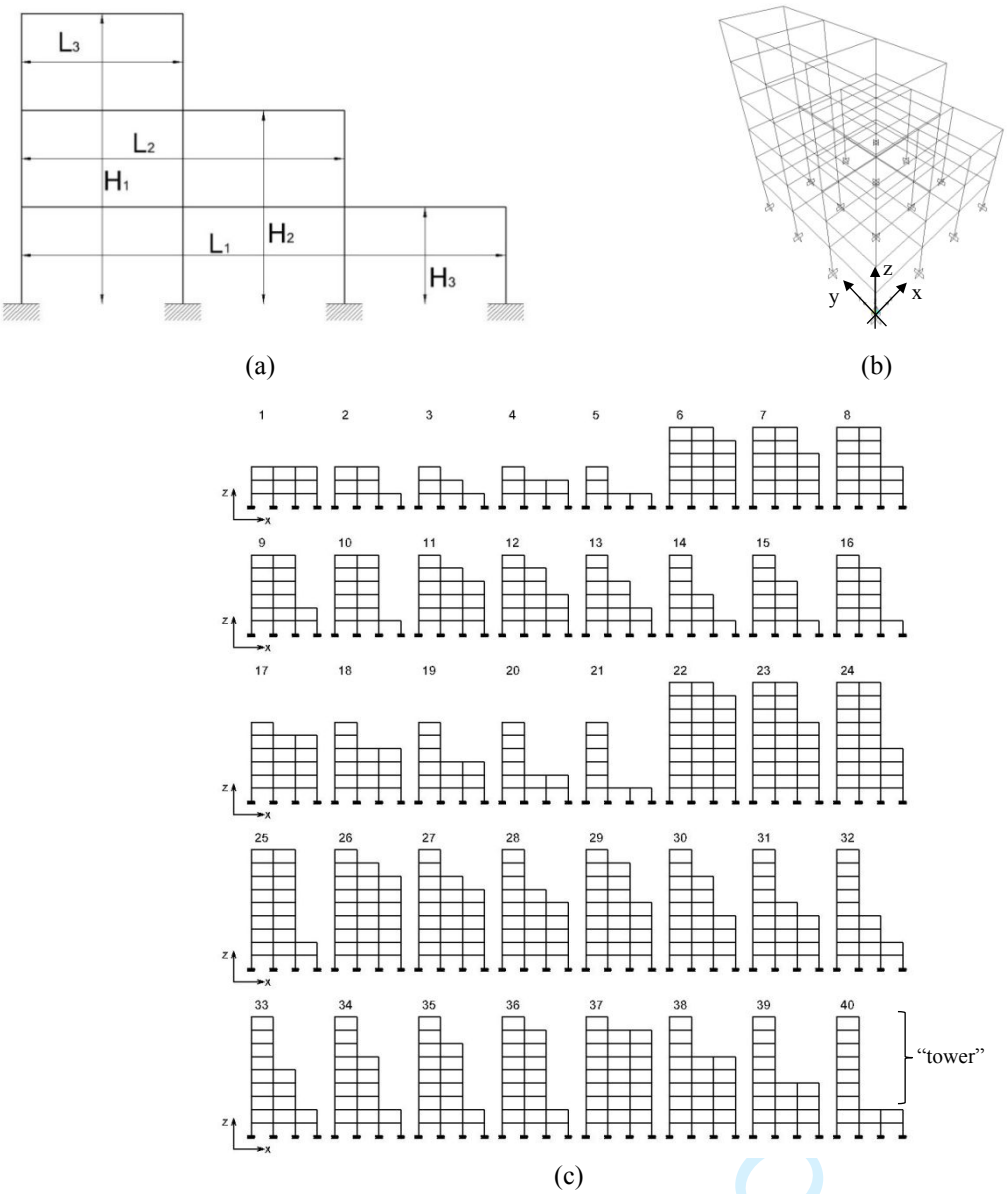

Figure 2. (a) Geometry of frames with setbacks; (b) perspective view of a six-storey with setbacks along the height; (c) all the frames with setbacks considered (Frame type 1 – Frame type 40)

Table 3 Section of the six-storey and nine-storey space steel frames of Group B.

*Six storey space MRF			
	Group B		
Floor	IPE		SHS
	F_{xe}, F_{ye}	F_{xi}, F_{yi}	C_i, C_e
1	330	360	350x16
2	330	360	300x16
3	330	360	300x16
4	300	330	300x12
5	300	330	300x12
6	300	330	300x12

*$0.24 < \rho < 0.43$ and $1.60 < \alpha < 2.27$

*Nine storey space MRF			
	Group B		
Floor	IPE		SHS
	F_{xe}, F_{ye}	F_{xi}, F_{yi}	C_i, C_e
1	300	360	400x16
2	330	400	400x16
3	330	400	400x16
4	330	400	400x16
5	330	400	400x16
6	300	360	350x16
7	270	330	350x16
8	270	300	300x12
9	270	300	350x12

*$0.18 < \rho < 0.32$ and $2.19 < \alpha < 2.93$

In the adopted frame design with setbacks, the storey area is reduced approximately by 33% and 66% in x direction because of the setbacks. The criterion of the EC8 [3] to characterize a building with setbacks as irregular in elevation, is when the individual setbacks are greater than 10 % of the previous plan dimension, thus the level of the building irregularities can be considered high. The geometrical irregularity introduced by setbacks is quantified through the Φ_s and Φ_b indices which according to Figure 2a can be taken from [11,31]

$$\Phi_s = \frac{1}{n_s - 1} \cdot \sum_{i=1}^{i=n_s-1} \frac{L_i}{L_{i+1}} \qquad \Phi_b = \frac{1}{n_b - 1} \cdot \sum_{i=1}^{i=n_b-1} \frac{H_i}{H_{i+1}} \tag{1}$$

where n_s is the number of storeys and n_b the bays number of the first storey. Figure 2a defines H_i and L_i.

Table 4. Three first vibration periods of the 6-storeys space steel frames of Group B.

Frames of Group B					
Frame case (See Figure 2c)	Φ_s	Φ_d	Period (sec)		
			T_1	T_1	T_1
6	1.10	1.10	1.14	1.12	0.96
7	1.10	1.25	1.11	1.07	0.87
8	1.10	1.50	1.10	1.06	0.85
9	1.10	2.00	1.11	1.09	0.90
10	1.10	3.50	1.18	1.17	1.03
11	1.30	1.23	1.04	0.99	0.81
12	1.30	1.43	1.03	0.97	0.75
13	1.30	1.75	0.98	0.92	0.69
14	1.30	2.50	0.97	0.94	0.74
15	1.30	2.75	0.99	0.95	0.75
16	1.30	3.10	1.05	1.03	0.85
17	1.40	1.10	1.07	1.05	0.91
18	1.40	1.25	0.99	0.93	0.76
19	1.40	1.50	0.96	0.90	0.69
20	1.40	2.00	0.97	0.96	0.78
21	1.40	3.50	1.06	1.01	0.90
22	1.06	1.06	1.53	1.52	1.36
23	1.06	1.25	1.48	1.42	1.19
24	1.06	1.40	1.48	1.42	1.16
25	1.06	2.75	1.51	1.49	1.27
26	1.19	1.13	1.44	1.39	1.22
27	1.19	1.23	1.37	1.28	1.08
28	1.19	1.35	1.32	1.21	0.96
29	1.19	1.36	1.41	1.32	1.07
30	1.19	1.52	1.36	1.25	0.97
31	1.19	1.53	1.30	1.19	0.91
32	1.19	2.13	1.32	1.26	0.99
33	1.19	2.15	1.32	1.24	0.95
34	1.19	2.25	1.34	1.25	0.98
35	1.19	2.39	1.38	1.30	1.05
36	1.19	2.56	1.43	1.39	1.16
37	1.25	1.06	1.47	1.45	1.32
38	1.25	1.25	1.33	1.24	1.04
39	1.25	1.625	1.31	1.22	0.94
40	1.25	2.75	1.38	1.38	1.14

2.3. Space frames with mass discontinuity along their height

In this section, 18 steel space MRFs regular in plan view and with a non-uniform distribution of mass along the height are designed. These space frames constitute frame Group C. The mass discontinuity is located either at the bottom storey (Frame B) or at the middle storey (Frame M) or at the top storey (Frame T), as shown in Figure 3. The mass discontinuity is quantified by the mass ratio, m_r. The quantity m_r is defined as the ratio of the mass of the storey that sustains the large weight (critical storey) to the smaller mass of the masses of the adjacent storeys. This means that the critical storey of each frame carries higher gravity loads compared to the adjacent storeys and this has been considered in frames design. Based on the recommendation of ASCE 7-10 [32], a building structure is considered irregular in terms of vertical mass discontinuity, when the quantity m_r takes a value higher than 1.5. EC8 [3] does not provide any corresponding mr limit as a vertical irregularity criterion. In the examined space frames, m_r equals 2 and 3. The frames have 3, 6 and 9 storeys with 4 bays. An accidental eccentricity of 5% in directions x and y, separately, is taken into account in the design. Table 5 shows the final cross-sections of the 6-storeys and 9-storeys frames, while the three natural periods of these frames are provided in Table 6. Based on Table 6, it is observed that the period of frames increases when the mass discontinuity is located at the upper storeys. Cross-sections for the 3-storeys frames can be found in [22].

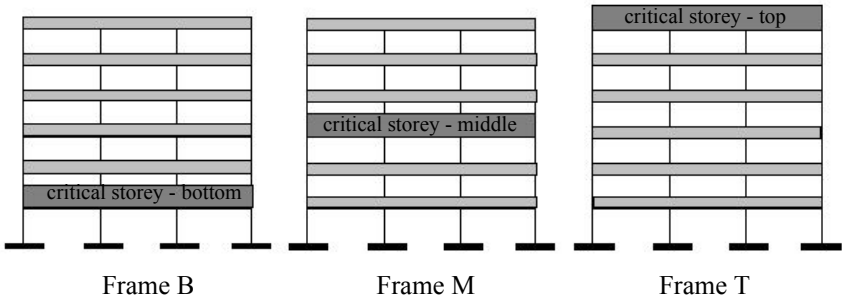

Figure 3. The location of mass discontinuity considered in this study

Table 5. Sections of the 6-storeys and 9-storeys space steel frames of Group C.

***Six storey space MRF**							
	$m_r = 2$				$m_r = 3$		
	Frame B				Frame B		
Floor	IPE		SHS	Floor	IPE		SHS
	B_{xe}, B_{ye}	B_{xi}, B_{yi}	C_i, C_e		B_{xe}, B_{ye}	B_{xi}, B_{yi}	C_i, C_e
1	330	360	350x16	1	330	500	350x16
2	330	360	300x16	2	330	360	350x16
3	330	360	300x16	3	330	360	350x16
4	300	330	300x12	4	300	330	300x16
5	300	330	300x12	5	300	330	300x16
6	300	330	300x12	6	300	330	300x16
	Frame M				Frame M		
1	330	360	350x16	1	330	360	350x16
2	330	360	300x16	2	330	360	350x16
3	330	360	300x16	3	330	500	350x16
4	300	330	300x12	4	300	330	300x16
5	300	330	300x12	5	300	330	300x16
6	300	330	300x12	6	300	330	300x16
	Frame T				Frame T		
1	330	360	350x16	1	330	360	400x16
2	330	360	300x16	2	330	360	400x16
3	330	360	300x16	3	330	360	400x16
4	300	330	300x12	4	300	330	350x12
5	300	330	300x12	5	300	330	350x12
6	300	330	300x12	6	300	450	350x12

*$0.19 < \rho < 0.30$ and $4.26 < \alpha < 5.79$

***Nine storey space MRF**							
	$m_r = 2$				$m_r = 3$		
	Frame B				Frame B		
Floor	IPE		SHS	Floor	IPE		SHS
	B_{xe}, B_{ye}	B_{xi}, B_{yi}	C_i, C_e		B_{xe}, B_{ye}	B_{xi}, B_{yi}	C_i, C_e
1	300	360	400x16	1	300	500	400x16
2	330	400	400x16	2	330	400	400x16
3	330	400	400x16	3	330	400	400x16
4	330	400	400x16	4	330	400	400x16
5	330	400	400x16	5	330	400	400x16
6	300	360	350x16	6	300	360	350x16
7	270	330	300x12	7	270	330	350x16
8	270	300	300x12	8	270	300	300x12
9	270	300	300x12	9	270	300	300x12
	Frame M				Frame M		
1	300	360	400x16	1	300	400	400x20
2	330	400	400x16	2	330	450	400x20
3	330	400	400x16	3	330	450	400x20
4	330	400	400x16	4	330	450	400x20
5	330	400	400x16	5	330	500	400x16
6	300	360	350x16	6	300	360	400x16
7	270	330	350x16	7	270	330	350x16
8	270	300	300x12	8	270	300	300x16
9	270	300	300x12	9	270	300	300x16

Frame T				Frame T			
1	300	360	400x16	1	330	400	400x20
2	330	400	400x16	2	360	450	400x20
3	330	400	400x16	3	360	450	400x20
4	330	400	400x16	4	360	450	400x20
5	330	400	400x16	5	330	400	400x16
6	300	360	350x16	6	330	360	400x16
7	270	330	350x16	7	300	330	350x16
8	270	330	300x12	8	300	330	300x16
9	270	330	300x12	9	300	450	300x16

*$0.15 < \rho < 0.27$ and $5.04 < \alpha < 6.28$

Table 6. Three first vibration periods of the 6-storeys and 9-storeys space steel frames of Group C.

Frames of Group C					
Frame case (See Figure 3)	Number of storeys	m_r	Period (sec) T_1	T_1	T_1
B	6	2	1.23	1.23	1.10
B	6	3	1.14	1.14	1.05
B	9	2	1.63	1.63	1.53
B	9	3	1.58	1.58	1.52
M	6	2	1.28	1.28	1.15
M	6	3	1.23	1.23	1.14
M	9	2	1.69	1.69	1.60
M	9	3	1.58	1.58	1.56
T	6	2	1.43	1.43	1.28
T	6	3	1.47	1.47	1.33
T	9	2	1.81	1.81	1.71
T	9	3	1.80	1.80	1.68

3. FRAME MODELING AND GROUND MOTIONS FOR INELASTIC ANALYSIS

3.1 Frame modelling

Nonlinear dynamic analyses were performed with the aid of Ruaumoko 3D software (Carr [33]) by taking into account the effect of large displacements. The frame modeling considers simple center-line representation for frame members with a rigid diaphragmatic action at every floor along the frame height. Rayleigh type damping corresponding to 3% of critical damping in the first and n^{th} mode (n is the number of the frame storeys), in conjunction with the tangent stiffness matrix was assumed. The abovementioned damping modeling assumptions are based on the recommendations of [33] to avoid potential unrealistic damping forces that result in underestimation of peak displacement demands and overestimation of peak strength demands. It is noted that for all models, the first and second periods were translational, while the third one was torsional. The use of the first and n^{th} mode in Rayleigh damping definition considers that the effective mass for the first n modes of vibration is at least 90% of the total mass of the structure.

Bilinear elastoplastic hinges were considered at beam and column ends with a strain hardening equal to 3% [33]. This modeling is considered adequate for time-history analysis under design level ground motions [3, 34]. Based on Skalomenos et al. [35], at high seismic intensities, the use of more refined models that capture stiffness and strength deterioration phenomena in beams, columns and panel zone connections is recommended in determining the ductility demands of plane composite frames and smaller behavior factors can be observed than those determined by simplified model assumptions [36]. The influence of the modelling sophistication to the frames under consideration is a subject of continuing study. The M-N interaction effect in three dimensions was taken into account. Considering plastic hinge formation in columns, the effect of the axial force on the plastic moment strength is taken into account through the interaction formulae [27]

$$\frac{N}{N_{pl,Rd}}+\frac{M_y}{M_{pl,y,Rd}}+\frac{M_z}{M_{pl,z,Rd}}=1.0 \qquad (2)$$

where N, M_y and M_z are the axial force and the bending moments in the cross-section of the column, $N_{pl,Rd}$ is the axial plastic resistance, and $M_{pl,y,Rd}$ and $M_{pl,z,Rd}$ are the plastic moments of resistance. It should be noted that local buckling limits the ability of SHS to form stable plastic hinges and the behavior is highly dependent on the width-thickness (b/t) and the depth-thickness ratio (h/t). Based on the testing results of [37], SHS members subjected to bending due to cyclic loading start deteriorating behavior at 0.04 rad rotation level. This rotational

level is expected to occur at seismic levels beyond the design earthquake. A sufficient rotational capacity and strength of the columns may be achieved through connection detailing, e.g. by using stiffeners, which can lead to stable hysteretic behavior of the columns for the *IDR* values considered in this work, i.e. up to 4%.

3.2 Ground motions

The space steel frames were subjected to 42 pairs of far-fault seismic excitations [38], where a full list of all these ground motions with their characteristics can be found in [22]. Figure 4 depicts the elastic spectra of the ground motion components. The selection of ground motions was based on the comparison between the spectral ordinates of each ground motion against the spectral ordinates of the design basis earthquake at the fundamental period of each frame. In that way the scaling factor of each ground motion can be controlled in order not to take excessive values at higher performance levels. It should be noted that in the literature there are also different procedures for selecting and scaling acceleration histories such as the one described in FEMA P58 [39].

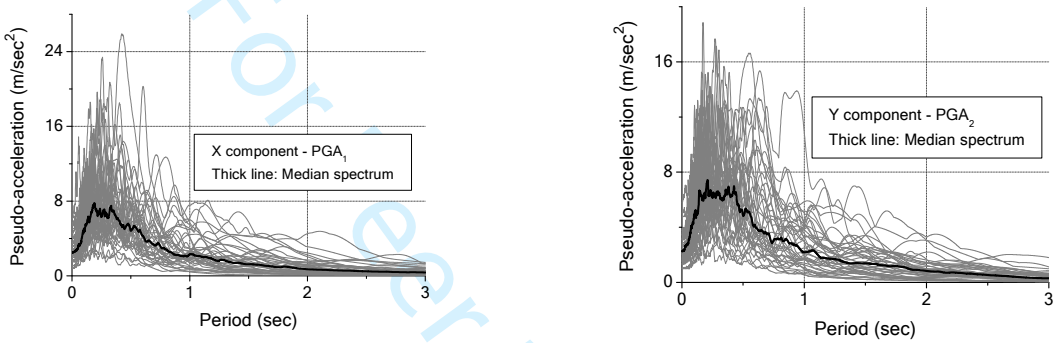

Figure 4. Response spectra for the x and y components of the ground motions.

3.3 Seismic response databank

The seismic response databank of the 88 space irregular MRFs was created by approximately 30000 dynamic nonlinear time histories in the framework of incremental dynamic analysis (IDA). Each IDA analysis subjects the structure to a single ground motion with repeatedly scaling its amplitude. The IDA curve that correlates the peak structural response quantity with the seismic intensity was made. The scaling factors (*SF*) of the ground motion that drives the structure to the four performance levels proposed by SEAOC [40] were identified and recorded for every structure and ground motion pair. Those four performance levels were: (a) formation of first plastic hinge in the frame; (b) peak value for the target interstory drift ratio along the frame height (IDR_{max}) equal to 1.8%; (c) IDR_{max} equal to 3.2 and (d) IDR_{max} equal to 4%. The two components of the 42 ground motions were alternated along the x and y axis of the buildings as those axes were defined in the schematic views of Section 2. The bisection method [21,22,24] was programmed in MATLAB [41] which operated the time history analyses and determined accurately the appropriate scale factor for each performance level (SF_{PL}).

Once the SF_{PL} was known, the response quantities of interest were obtained for each performance level. These were: (1) the roof displacement at the onset of first plastic hinge, $u_{r,y}$, (2) the peak roof displacement, $u_{r,max}$, (3) the IDR_{max}, (4) the maximum local rotational ductility of beams and columns, μ_θ, (5) the maximum roof displacement ductility, μ_r, (6) the behavior factor q, (7) irregularity metrics quantified through indices, e.g. Φ_s and Φ_b; and (8) the fundamental periods of vibration. The μ_θ is defined as $1+\theta_p/\theta_y$, where θ_y and θ_p are the yield chord rotation and the plastic rotation the member's ends, respectively. The μ_r is defined as $u_{r,max} / u_{r,y}$ for each performance level. The corresponding behavior factor q is calculated as the ratio of the SF_{PL} over the SF_y (scale factor that drives the structure to the first yielding) [35,39]. The proposed q factor, unlike the traditional constant q factor used in EC8 [3], is determined for each performance level and depends on the deformation demands in terms of *IDR* and μ_θ. It should be noted that peak floor acceleration (PFA) can be used as an additional performance metric for the non-structural elements, e.g. acceleration sensitive equipment. The inclusion of acceleration measures in HFD method can be considered as an important future development

4. TIME HISTORY ANALYSIS RESULTS

On the basis of the developments and assumptions presented in this work, the current section introduces the seismic behavior of the steel space irregular MRFs under consideration. A discussion on seismic responses for each type of structural irregularity is presented for representative frames. The results highlight the importance of considering the irregularity design parameters and are assessed accordingly to develop the proposed design method. A future goal is to further extend the current design method to other types of building structures with, e.g., strength and stiffness degradation, semi-rigid joints, I sections for columns, or combination of irregularities.

4.1. Space frames irregular in plan view

Figure 5 shows the normalized median of the *IDR* along the height of the 6 and 12 storey frames of Group A. Accordingly, Figure 6 shows the normalized median of the peak values of lateral storey displacements along the frame elevation. Results are shown only for the performance levels of IDR_{max}=1.8% and IDR_{max}=4.0%. For the performance levels at the first plastic hinge and IDR_{max}=3.2% one can look at [22]. It was found that the seismic response is similar along the x or y direction, and therefore, only the results of the x direction are presented. For comparison reasons, the responses of the corresponding regular-in-plan-view frames (with square plan view) are also plotted in these figures (labeled as Reg. Frame). It is noted that an accidental eccentricity of 5% was considered in the design of these regular-in-plan-view frames. An observation of Figures 5 and 6 and the remaining ones in [22], reveals that the response of the frames is similar with a dispersion that increases slightly with the number of storeys. In particular, the response of Frames type 1 – 5 is very similar with the response of the Reg. Frame, indicating that the plan irregularity considered in this study may not play an important role in the seismic response of the frames. However, the response of Frame 6 appears to be the one with the higher difference compared to the rest of frames and requires further investigation. In addition, it is observed from the *IDR* profiles that peak values in tall buildings are recorded in higher storeys. To make the *IDR* distribution more uniform along the frame elevation, a solution could be to increase the beam and/or the column dimensions at the upper floors. However, this may increase the weight of the building disproportionately. Finally, Figure 7 illustrates the normalized median inter-storey twist by the storey height at x and y direction of the 6 storey frames for the performance level with *IDR* = 4.0%. The torsional response is smaller in all Frames 1 – 6 of Figure 1a compared to the torsional response of the Regular Frame, as shown in Figure 7. This result can also demonstrate that the EC8 [3] slenderness λ criterion for regularity in plan is valid, considering that all the other regularity in plan criteria of clause 4.2.3.2 of EC8 [3] are met.

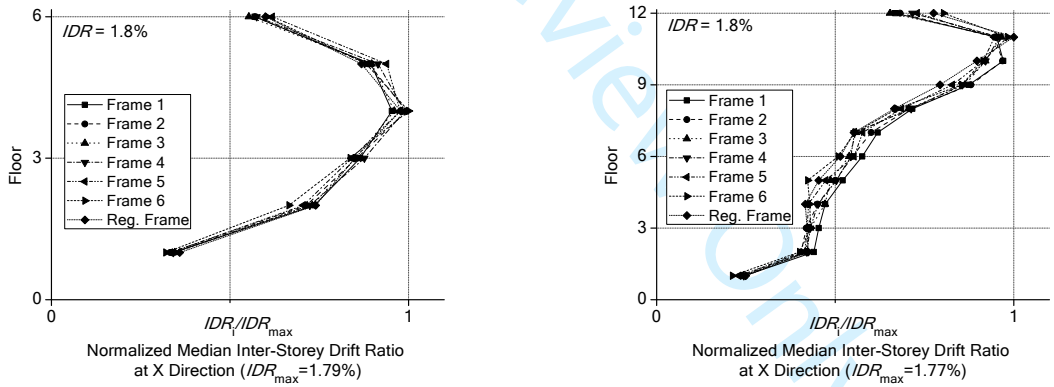

(a)

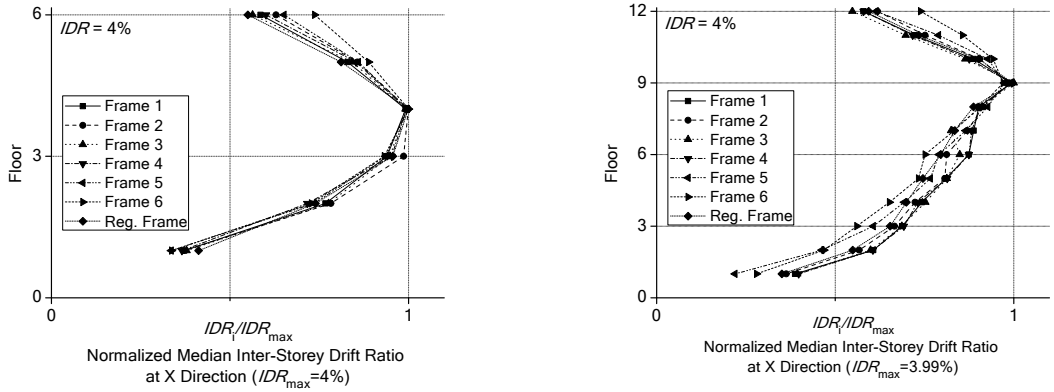

(b)

Figure 5. *IDR* profile of the 6 and 12 storey frames of Group A: (a) first plastic hinge; (b) *IDR* = 1.8%; (c) *IDR* = 3.2%; (d) *IDR* = 4%.

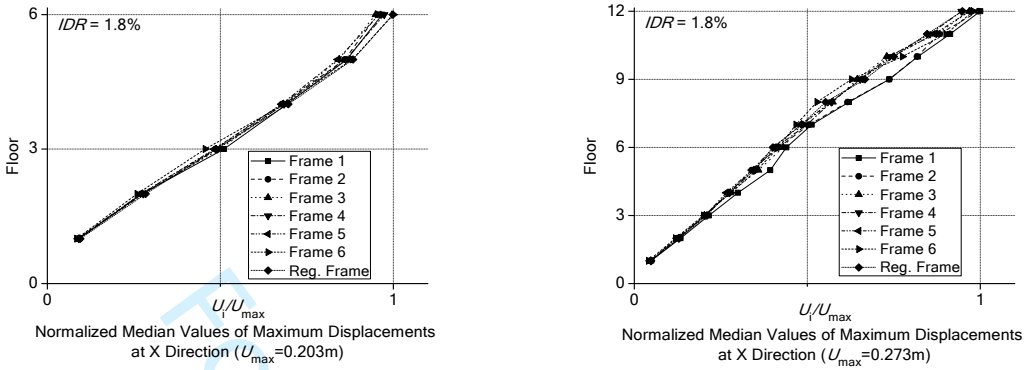

(a)

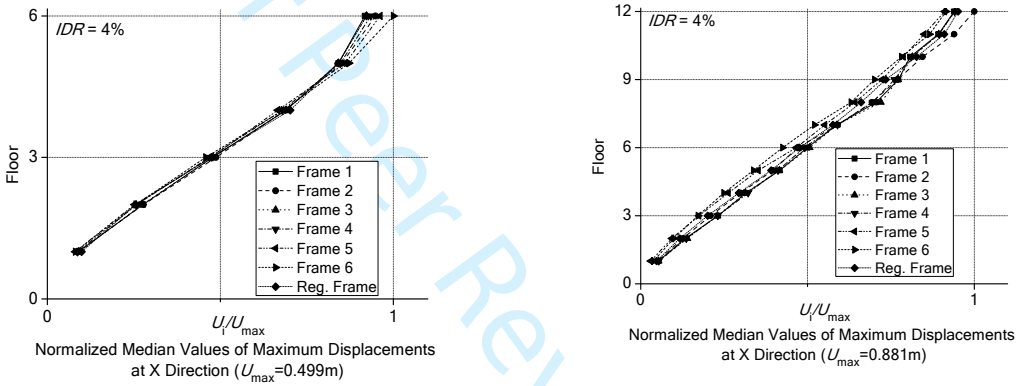

(b)

Figure 6. Floor displacements profile of the 6 and 12 storey frames of Group A: (a) *IDR* = 1.8%; and (b) *IDR* = 4%.

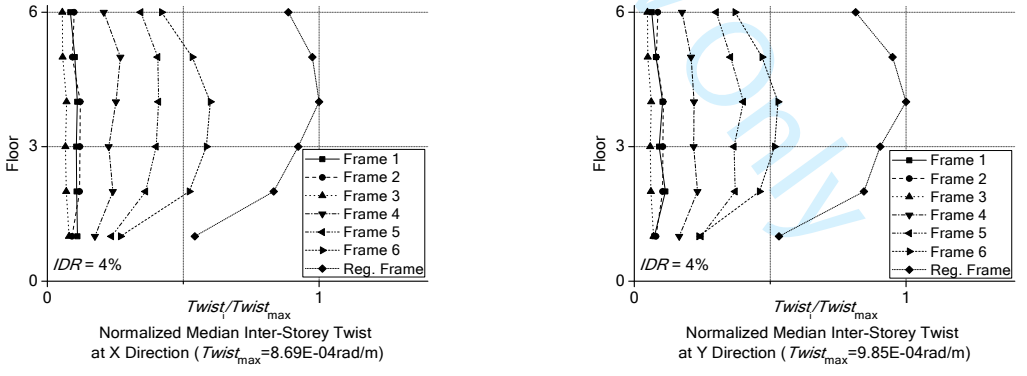

(a) (b)

Figure 7. Normalized median inter-storey twist of the 6-storey frames of Group A: *IDR* = 4.0% at: (a) x direction and (b) y direction.

5.2 Space frames with setbacks along the height

Figure 8 depicts with the same manner as Figures 5 and 6 the lateral storey displacements and *IDR* profiles of the Group B frames, for the first three performance levels. The 6-storey frames (See Figure 2, Frames 6 to 21) are shown in those figures. The figures illustrate the frame responses along the x direction. The displacement and *IDR* profiles were created by using the maximum values obtained from the frame nodes at the perimeter of

each storey. In Figure 8 the responses of Frame 10, 19 and 21 are highlighted with dark marked lines as more representative ones among the 16 six-storey frames, while the remaining frame responses are depicted by light gray lines. For comparison reasons, the responses of the corresponding regular frames (no setbacks and an accidental eccentricity of 5%) are also plotted in those figures (labeled as Reg. Frame).

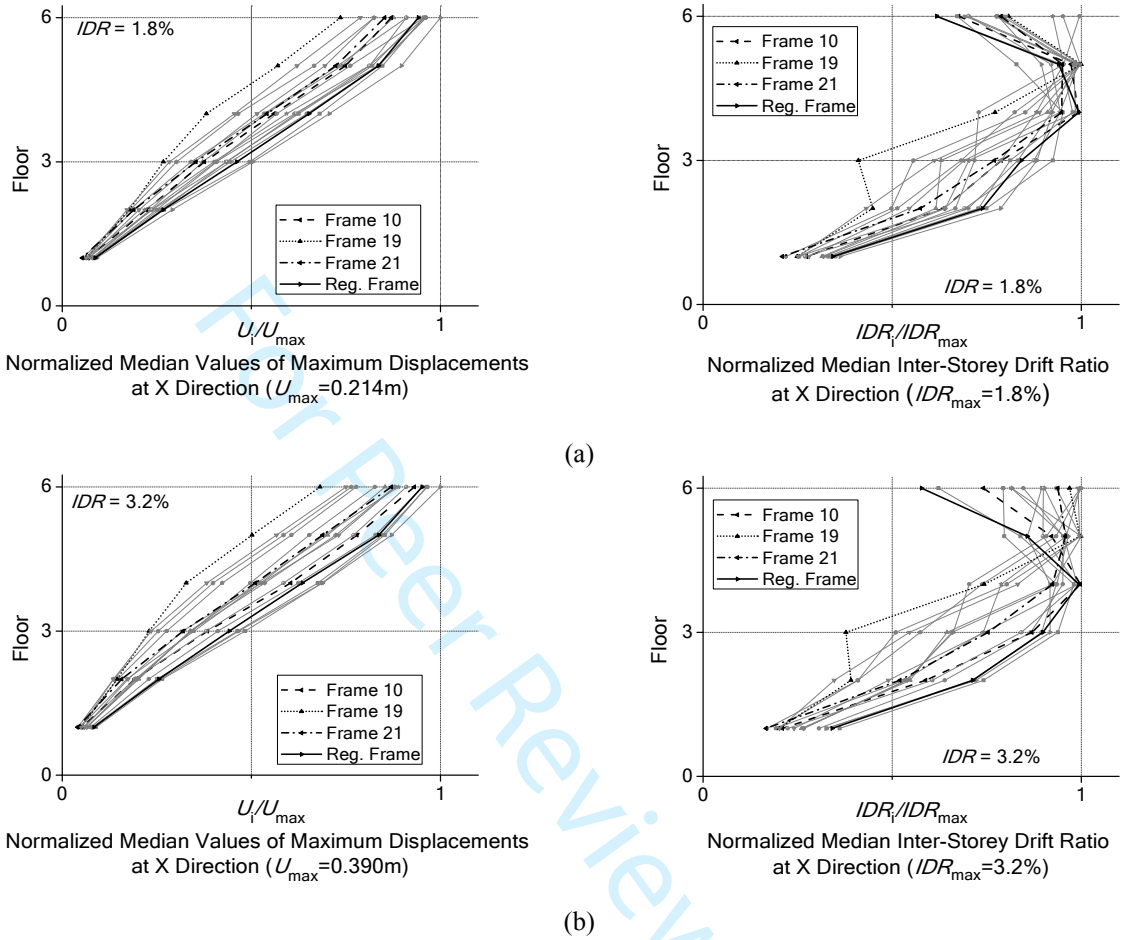

Figure 8. Peak floor displacements and *IDR* profiles of the 6-storey frames of Group B: (a) *IDR* = 1.8%; and (b) *IDR* = 3.2%.

Table 7. Frames exhibiting the minimum and maximum floor displacement along the x and y direction among all the frames of Group B (See Figure 2), including the corresponding regular frame.

3-storey				6-storey				9-storey			
x direction		y direction		x direction		y direction		x direction		y direction	
min	max	min	max	min	max	min	max	min	max	min	max
Frame 5	Regular Frame	Frame 5	Regular Frame	Frame 19	Frame 11	Frame 14	Frame 18	Frame 40	Regular Frame	Frame 39	Frame 26

The indices Φ_s and Φ_b considered here, appear to be adequate to quantify the influence of the setbacks on the dynamic behavior of frames. For all the performance levels, those frames with values of Φ_s and Φ_b close to unity exhibit larger floor displacements than those frames which form a "tower" along their height. This is also observed in Table 7, where the frames that exhibit the minimum and maximum displacement along the x and y direction among all the frames of Group B (including the corresponding regular frame) are summarized. It should be noted that the frame responses along the x direction show a larger dispersion compared with the ones along the y direction because of the flexibility of the "tower" along the x direction.

Figure 8 shows that *IDR* profiles among all the frames have the same shape for the low performance level. In high-damage performance levels, the shape of *IDR* profiles is becoming less uniform due to the inelastic deformations. The dispersion with respect to the amplitudes increases between the lower and higher floors. The

torsional behavior was also found to be larger in all frames of Group B compared to the torsional behavior of the Reg. Frame. Figure 9 illustrates the normalized median inter-storey twist by the storey height for the 6-storey and 9-storey frames associated with *IDR* = 3.2% along the x direction.

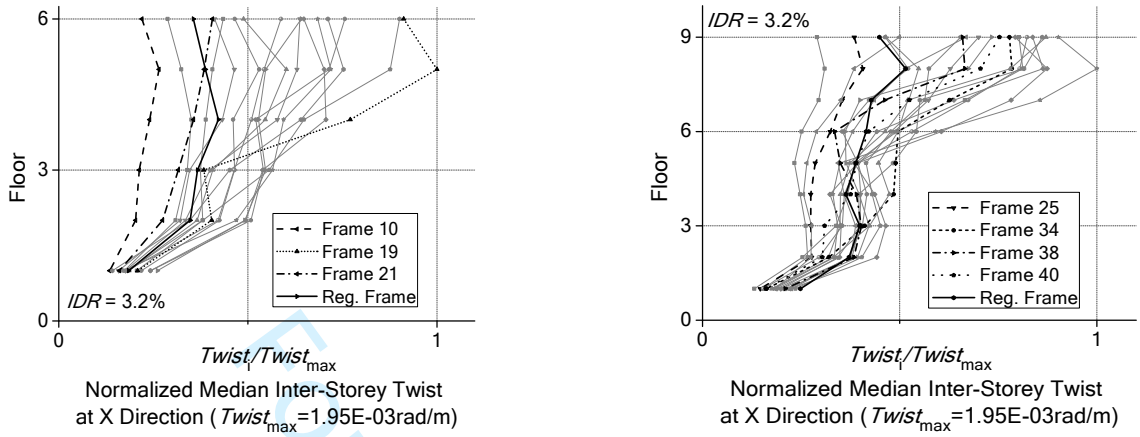

Figure 9. (a) Normalized median inter-storey twist of the 6-storey; and (b) 9-storey frames of Group B associated with *IDR* = 3.2% along the x direction.

Frame structures with setbacks along their height are expected to exhibit a larger level of damage compared to the corresponding regular structures. To further justify this discussion on the frame considered, the inelastic behavior of the frames of Group B was evaluated for a common level of seismic intensity by conducting time-history nonlinear analyses with five pairs of semi-artificial accelerograms. The accelerograms were generated to be compatible to the elastic design spectrum of EC8 [3] (PGA = 0.36g and soil class B) in order to evaluate the response of the frames under a seismic intently beyond the design-based level. The two components of the artificial motions shown in Figure 10 were alternated in x and y direction, respectively. The analyses were performed for 10 of the 40 frames shown in Figure 2c (Frame 3, 4, 5, 10, 19, 21, 25, 34, 40) and their corresponding regular frames (labeled as R). Figure 11 shows bar charts of the results in terms of IDR_{max} and μ_θ for the 6-storeys and 9-storeys frames along the x and y direction.

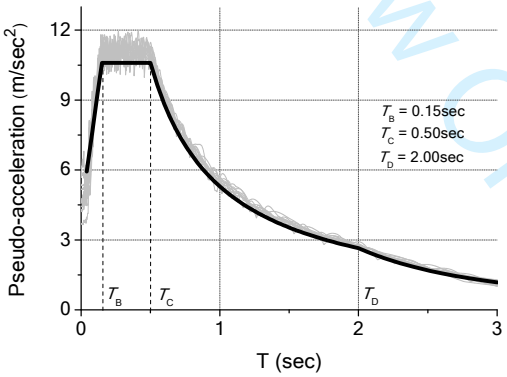

Figure 10. Response spectra of the semi-artificial ground motions.

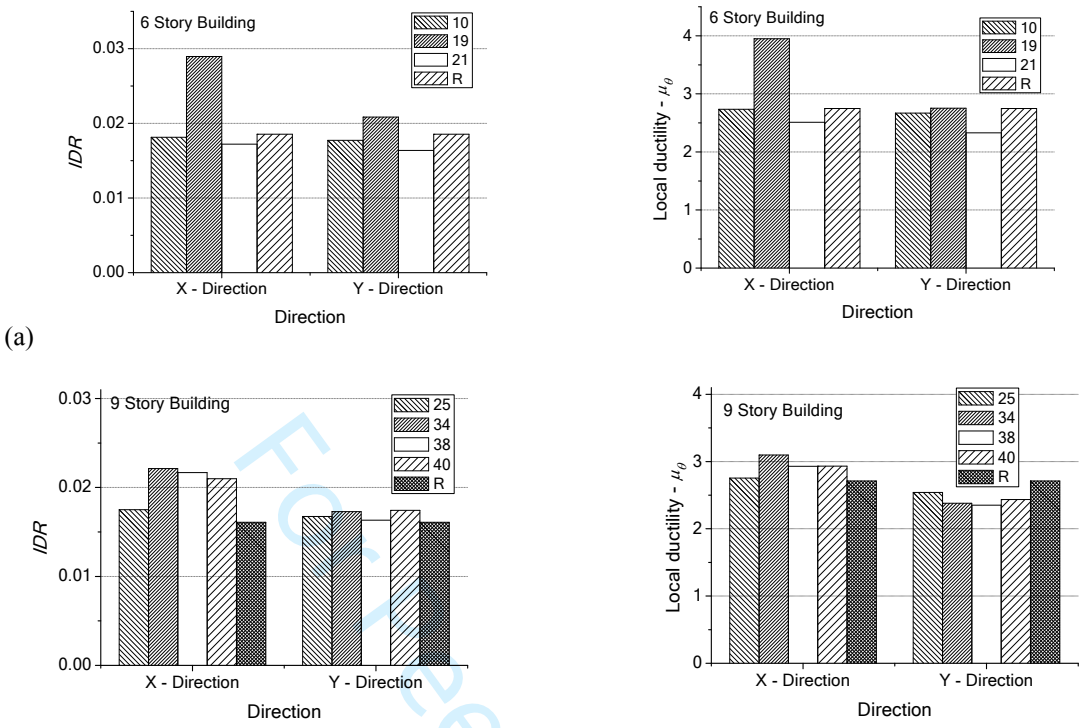

Figure 11. IDR_{max} and μ_θ along the x and y direction for the: (a) 6-storey [Frames 10, 19, 21]; and (c) 9-storey frames [Frames 25, 34, 38, 40] of Group B.

It is observed from Figure 11 that frames with setbacks experienced a larger damage along the x direction, while along the y direction regular frames often exhibited a larger level of damage than the irregular frames. In addition, regarding the x direction, increasing the height of the frames leads to an increase of drift and ductility demands for all irregular frames as compared with the regular ones.

5.3. Space frames with mass irregularity along their height

Figure 12 shows peak lateral storey displacements and *IDR* profiles in elevation of the 6-storey frames of Group C, for the two performance levels. The remaining performance levels can be found in [22]. For comparison reasons, the responses of the corresponding regular frames (no mass discontinuity and an accidental eccentricity of 5%) are also plotted in these figures (labeled as R). It is observed that the regular frames exhibited a larger displacement and *IDR* profile at the onset of the first plastic hinge compared with the irregular ones. Only the case of Frame T2 (mass discontinuity is at the top storey and mass ratio m_r = 2.0) provides with slightly higher values at the top storeys. The same trend with the results of the 6-storey frames is observed for the 3-storey and 9-storey frames.

The 6-storey and 9-storey frames behaved in a similar way at higher performance levels. In general, smaller displacements exhibited in frames with the mass discontinuity at the top storey (T) of the frame, followed by the frames with the mass discontinuity at the bottom storey (B) of the frame, and then by those with the mass discontinuity at the middle storey (M) of the frame. On the contrary, in case of 3-storey frames, the trend appears to be different. Frames with the mass discontinuity at the top storey (T) exhibited larger displacements.

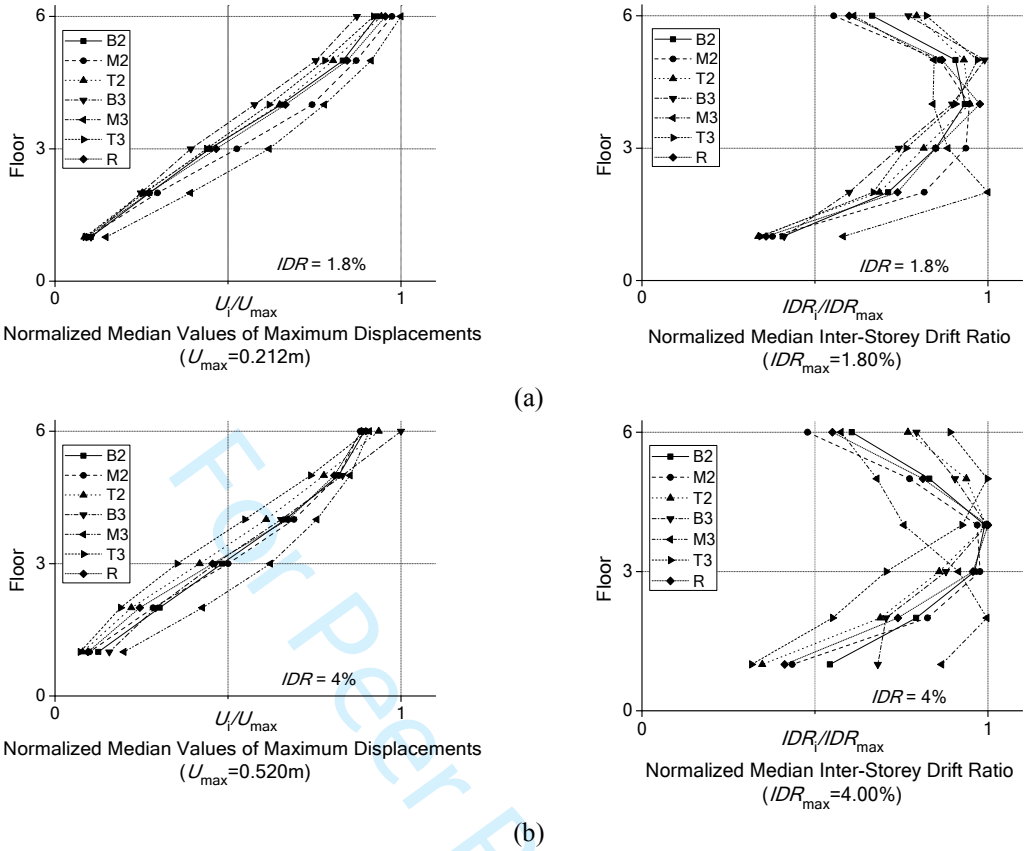

Figure 12. Peak floor displacements and *IDR* profiles of the 6-storey frames of Group C: (a) *IDR* = 1.8%; (b) *IDR* = 4.0%

5. HFD DESIGN METHOD

The HFD method [21-24] determines the roof displacement $u_{r,max(d)}$ at design as the minimum of the peak roof displacements $u_{r,max(IDR)}$ and $u_{r,max(\mu)}$ which correspond to non-structural and structural deformation respectively,

$$u_{r,max(d)} = \min\left(u_{r,max(IDR)},\ u_{r,max(\mu)}\right) \tag{3}$$

The roof ductility $\mu_{r,d}$ as the design quantity is then determined as

$$\mu_{r,d} = \frac{u_{r,max(d)}}{u_{r,y}} \tag{4}$$

The designer can obtain $u_{r,y}$ by conducting an elastic strength-based design (q=1) for frequent earthquake. The behavior factor q is given as a function of $\mu_{r,d}$.

In this section, empirical formulae for $u_{r,max(IDR)}$, $u_{r,max(\mu)}$ and q as functions of basic geometrical/dynamical characteristics of the frames are developed by a nonlinear regression analysis in MATLAB [41]. By analyzing the created response databank of frames with irregular plan view (Group A), $u_{r,max(IDR)}$ is expressed as

$$u_{r,max(IDR)} = b_1 \cdot H \cdot IDR^{b_2} \tag{5}$$

where *IDR* is the targeted interstory drift ration and *H* is the height of the frame (in m). The parameters b_1 and b_2 are provided in Table 8. By analyzing the response databank of frames with setbacks along the height (Group B), the ratio $\beta = u_{r,max(IDR)} / (H \cdot IDR)$ was found to be the most representative parameter to quantify the design demand. The ratio β is calculated by

$$\beta = 1 - b_1 \cdot (n_s - 1)^{b_2} \cdot \Phi_s^{b_3} \cdot \Phi_b^{b_4} \tag{6}$$

where constants b_1, b_2, b_3, and b_4 are given in Table 9 for motions along the x and y directions. Equation (6) is simple and satisfies the natural condition $\beta = 1$ for $n_s = 1$. By analyzing the response databank of frames with

mass discontinuities along the height (Group C), the $u_{r,max(IDR)}$ can be expressed as in Eq. (5). The parameters b_1 and b_2 are given in Table 10 with respect to the storeys number and the location of mass discontinuity (bottom, middle, or top).

With *IDR* to be known, the ratio $u_{r,max,app}/u_{r,max,exact}$ is taken for all irregular frames. The "appx" subscript stands for the word "approximate" and refers to the value obtained by the empirical Eqs (5) and (6), while the "exact" subscript refers to the seismic response databanks. The mean, median and standard deviation (Stdev) values are also provided. For the frames of Group A, Eq. (5) provides a mean value equal to 1.04, median value equal to 0.99 and dispersion value equal to 0.30 for the ratio $u_{r,max,app}/u_{r,max,exact}$. The same equation for the frames of Group C provides a mean value equal to 1.01, median value equal to 0.98 and dispersion value equal to 0.26 for the ratio $u_{r,max,app}/u_{r,max,exact}$. Similar results can be obtained from the use of Eq. (6) for the frames of Group B.

Table 8. Values of parameters b_1 and b_2 of Eq. (5) for steel space frames with irregular plan view

Number of storeys	$IDR_y - IDR_{1.8\%}$		$IDR_{1.8\%} - IDR_{3.2\%}$		$IDR > IDR_{3.2\%}$	
	b_1	b_2	b_1	b_2	b_1	b_2
3	0.84	1.01	1.03	1.06	0.99	1.05
6	0.37	0.88	0.93	1.11	1.51	1.25
9	0.29	0.88	2.07	1.37	2.38	1.41
12	0.28	0.91	1.46	1.32	5.58	1.71
15	0.22	0.89	5.04	1.67	6.88	1.76

Table 9. Values of parameters $b_1 - b_4$ of Eq. (6) for steel space frames with setbacks

Direction	b_1	b_2	b_3	b_4
x	0.18	0.36	0.85	0.24
y	0.18	0.36	0.17	0.10

Table 10. Values of parameters b_1 and b_2 of Eq. (5) for steel space frames with mass discontinuities

Number of storeys	Location of mass discontinuity	b_1	b_2
3	B	0.83	1.01
	M	0.83	1.01
	T	1.26	1.11
6	B	1.16	1.17
	M	0.72	1.03
	T	0.82	1.07
9	B	1.95	1.34
	M	1.47	1.24
	T	1.38	1.27

The $u_{r,max(\mu)}$ can be estimated from

$$u_{r,max(\mu)} = \mu_{r,\theta} \cdot u_{r,y} \tag{7}$$

where $\mu_{r,\theta}$ is the maximum ductility of the top storey with respect the μ_θ and can be calculated for the frames with irregular plan view (Group A) as

$$\begin{aligned} \mu_{r,\theta} &= 1 + 0.81 \cdot (\mu_\theta - 1) \qquad \text{for } \mu_\theta \le 4.68 \\ \mu_{r,\theta} &= 2.58 + 0.38 \cdot (\mu_\theta - 1) \qquad \text{for } \mu_\theta > 4.68 \end{aligned} \tag{8}$$

and for the frames with setbacks (Group B) and vertical mass discontinuities (Group C) as

$$\mu_{r,\theta} = 1 + b_1 \cdot (\mu_\theta - 1)^{b_2} \tag{9}$$

Table 11a and b provides the constants b_1 and b_2 respectively. Eq. (8) provides a mean value equal to 0.94, median value equal to 0.94 and dispersion value equal to 0.24 for the ratio $\mu_{r,\theta,app}/\mu_{r,\theta,exact}$. For the Group B frames, Eq. (9) provides a mean value equal to 1.02, median value equal to 0.97 and dispersion value equal to 0.28 for the ratio $\mu_{r,\theta,app}/\mu_{r,\theta,exact}$, while for the Group C frames and the same ratio, Eq. (9) provides a mean value equal to 1.04, median value equal to 1.02 and dispersion value equal to 0.24.

Table 11. Values of constants b_1 and b_2 of Eq. (9) for:

(a) Steel space frames with setbacks		
Direction	b_1	b_2
x and y	0.79	1.00
(b) Steel space frames with mass discontinuities		
Location of mass discontinuity	b_1	b_2
B	1.22	0.60
M	1.17	0.59
T	1.26	0.61

As it was mentioned in the Section 3.3, the behavior factor q was defined as $q = SF_{IDR} / SF_y$. Figure 13a illustrates schematically the relation of behavior factor q versus the targeted *IDR* for the 6-storey space frames of Group A, while Figure 13b plots the median values of all frames for each type of irregular plan-view introduced in Figure 1a. Number of storeys had no influence on q. The *q-IDR* relation did not significantly differ from the corresponding one for regular frames for the case studies examined in the present work. Moreover, the period of vibration and frequency of the ground motion was found to not have a significant effect on the *q-IDR* relation. A similar finding is also valid for the Groups B and C frames.

For the Group B frames there is an influence of the torsional response on the *q-IDR* relation as it is shown in Figure 14. Figures 14a and 14b show the *q-IDR* relation along the x and y direction, respectively, for some representative Group B fames and the corresponding regular frames. Figure 14 shows the median values for the four performance levels considered here. Having as reference the trend of the regular frame, a large dispersion of the *q-IDR* relation for the frames with setbacks is observed. Figure 15 illustrates the relation of behavior factor q with the *IDR* for mass ratio $m_r = 2$. Figure 15a shows the *q-IDR* relation of the 6-storey frames of Group C for the three cases of mass discontinuity considered against the corresponding regular frame, while Figure 15b the *q-IDR* relation of the 3-storey, 6-storey and 9-storey frames where the mass discontinuity is located at the middle storey (M) of the frames. The trend of the *q-IDR* relation was found to be similar for mass ratio $m_r = 3$. For frames with a mass discontinuity along their height, a larger behavior factor q than the corresponding one for regular frames can be used to satisfy the targeted *IDR*, as shown in Figure 15a. Accordingly, the q factor increases also with the number of storeys for a given level of performance, as shown in Figure 15b. Table 12 summarizes the median values of scale factors (SF) used in time-history analyses to drive the frames of Group C to reach the target performance level. Only results for the *IDR* = 1.8% and *IDR* = 4.0% performance levels are provided. Results for the remaining performance levels can be found in [22]. It is concluded that frames with a mass discontinuity along their height satisfy the various performance levels for a lower seismic intensity than the corresponding regular frames, since the SF is smaller for the former case study. It should be noted here that the design of the frames affects the analysis results and could lead into a different conclusion. More frame cases should be examined in the future with additional mass discontinuities to generalize the abovementioned findings.

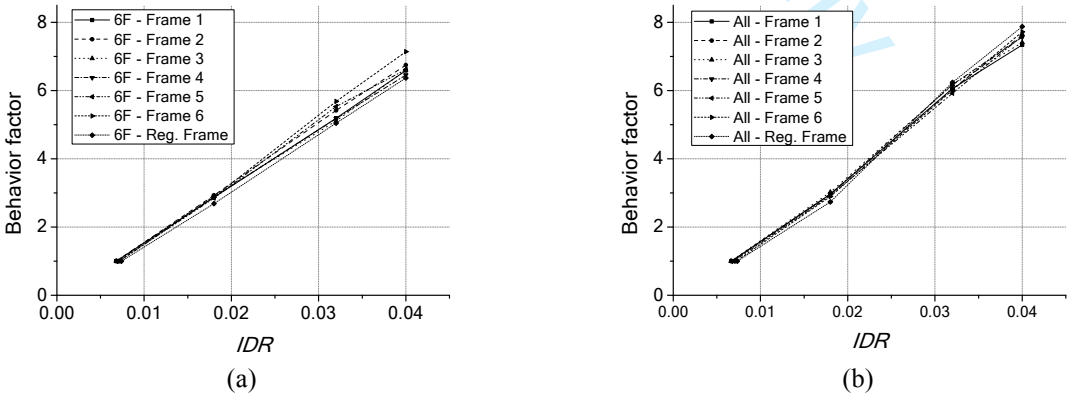

(a) (b)

Figure 13. Behavior factor q versus *IDR* for the frames of Group A: (a) 6-storey frames; and (b) all frames (median values)

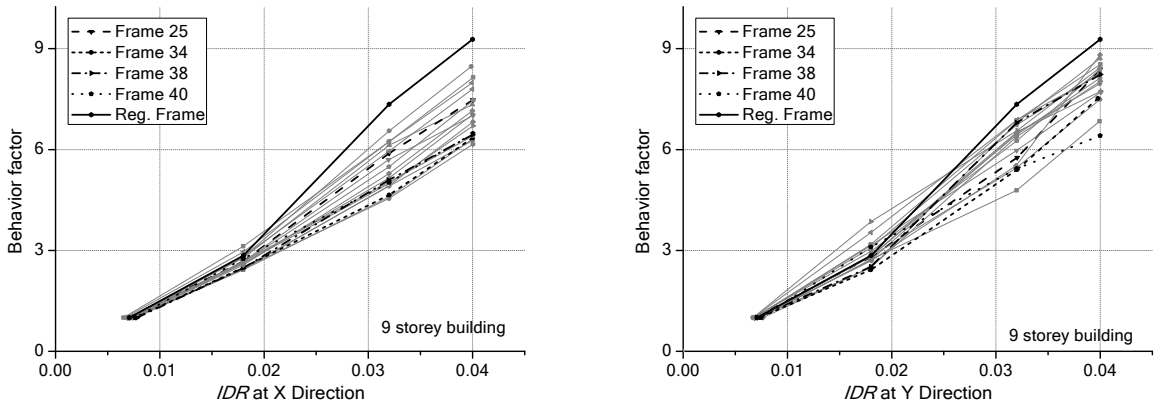

(a) (b)

Figure 14. Behavior factor q versus IDR for the 9-storey frames of Group B at: (a) along x direction; and (b) along y direction

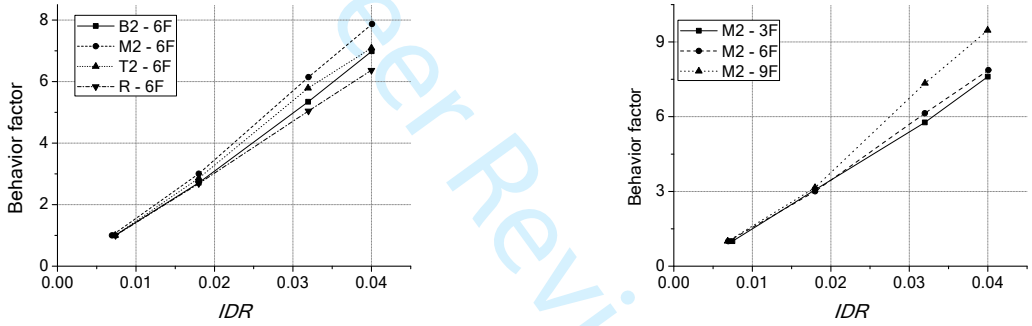

(a) (b)

Figure 15. Behavior factor q versus IDR for mass ratio $m_r = 2$: (a) 6-storey frames of Group C for the three cases of mass discontinuity considered against the corresponding regular frame; (b) 3-storey, 6-storey and 9-storey frames where the mass discontinuity is located at the middle storey (M) of the frames.

Table 12. Median values of scale factors (SF) that correspond to performance levels IDR = 1.8% and IDR = 4.0% for the Group C frames.

Performance level	Design case	Scale Factor (SF) 3 storey	6 storey	9 storey
	B2	1.74	1.97	1.85
	M2	2.02	2.02	2.19
	T2	1.97	2.04	2.10
IDR=1.8%	B3	1.91	1.91	1.70
	M3	2.03	2.27	1.87
	T3	2.14	2.04	1.70
	R	**1.76**	**1.87**	**2.00**
	B2	3.49	3.71	4.03
	M2	3.14	3.81	3.89
	T2	3.07	3.61	3.53
IDR=4%	B3	2.87	3.56	3.49
	M3	3.47	3.80	4.32
	T3	3.24	3.75	3.29
	R	**3.34**	**4.01**	**4.32**

Table 13. Values of parameters b_1 and b_2 for: Eqs (11) and (12).

(a) Steel space frames with setbacks – Eq. (11)			
Direction	b_1	b_2	b_3
x	1.39	1.05	-0.06
y	1.39	1.05	-0.34
(b) Steel space frames with mass discontinuities – Eq. (12)			
Location of mass discontinuity		b_1	b_2
B		1.38	1.00
M		1.50	1.00
T		1.43	1.00

The expression providing q was found to be of the form

$$q = 1 + 1.35 \cdot (\mu_r - 1) \quad \text{for the frames of Group A} \tag{10}$$

$$q = 1 + b_1 \cdot (\mu_r - 1)^{b_2} \cdot \Phi_s^{b_3} \quad \text{for the frames of Group B} \tag{11}$$

$$q = 1 + b_1 \cdot (\mu_r - 1)^{b_2} \quad \text{for the frames of Group C} \tag{12}$$

where the parameters b_1 and b_2 of Eqs (11) and (12) are obtained from Table 13 and μ_r is the $\mu_{r,d}$ of Eq. (4). Equations (10), (11) and (12) fulfill the condition q=1 for μ_r=1. These equations show that the equal-displacement rule of EC8 [3] overestimates the peak floor displacements.

The proposed equations can be applied to frames with stiffness parameter ρ and strength parameter α within their minimum and maximum values in Section 2. The created database can be further increased by considering buildings which will be designed using different values of behavior factor q. This will also contribute to the inclusion of the ρ and α parameters in the proposed equations and further development of the regression coefficients considered in this work. It should be also noticed that based on the analysis results no effect of the period of vibration and frequency content of the ground motion on the relationship between q and μ_r, $u_{r,max}$ and IDR_{max}, μ_r and μ_θ was identified and for this reason their effect has not been included in all proposed equations. In addition, the inclusion of peak floor acceleration as an additional performance metric of the HFD method can further control non-structural damage as well as residual drifts in the design equations and provide useful information for estimating potential losses and repair costs at different performance levels.

Figure 16 shows graphically Eqs (10) and (11) for the Group A and B frames together with the corresponding databank results and the equal displacement rule, while in Figure 18b the q-μ_r relation introduced in [11] for planar frames with setbacks is also plotted here for comparison reasons assuming Φ_s = 2. Accordingly, Figure 17 plots Eq. (12) for the Group C frames together with the corresponding databank results, the equal displacement rule and the relations introduced in [19] for planar frames with vertical mass discontinuities. Figures 16 and 17 show higher dispersion in the q value at higher roof ductility levels which can be related to the variability induced from each seismic record. The present results appear to be more accurate than those of EC8 [3], which overestimates ductility demands in all cases.

Furthermore, for a realistic range of q (less than 8), the comparison in Figures 16 and 17 of the proposed q-μ_r relations for space irregular frames to the corresponding relations for planar irregular frames, reveal a difference in their seismic response. For a targeted level of seismic performance, space frames require higher ductility demands and lower behavior factors than the corresponding planar ones. This finding is in accordance with the current design codes [3], where a proper reduction on the behavior factor is recommended for space irregular structures for which torsional response plays an important role. A larger lateral resistance seems to be required in order to control the seismic response of these type of structures.

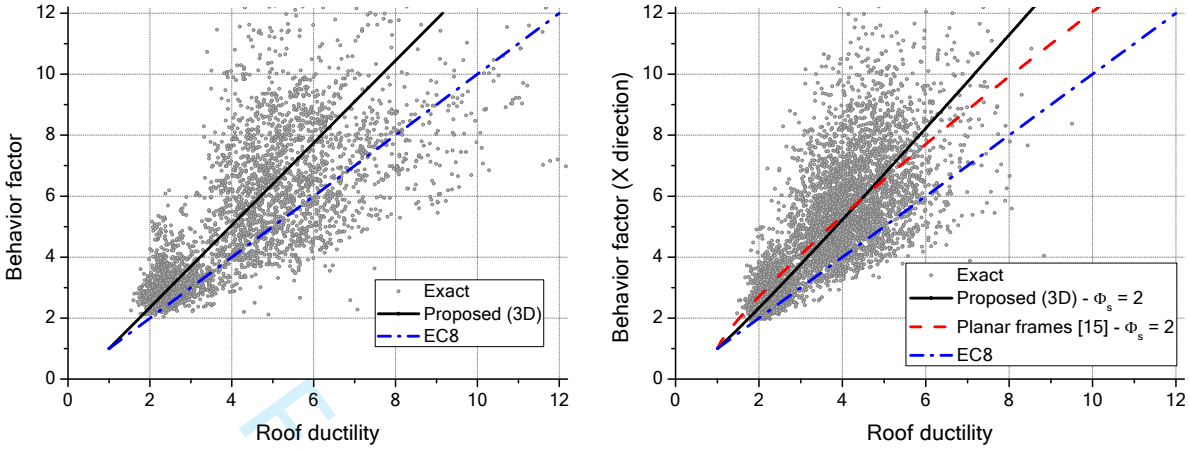

(a) (b)

Figure 16. Graphical depiction of the response databank results and approximation by the proposed relation for space MRFs. Comparison with the proposed in [11] relation for planar MRFs and the equal-displacement rule (EC8 [3]), for the case of frames with: (a) irregular plan view (Group A); (b) setbacks (Group B) with $\Phi_s = 2$.

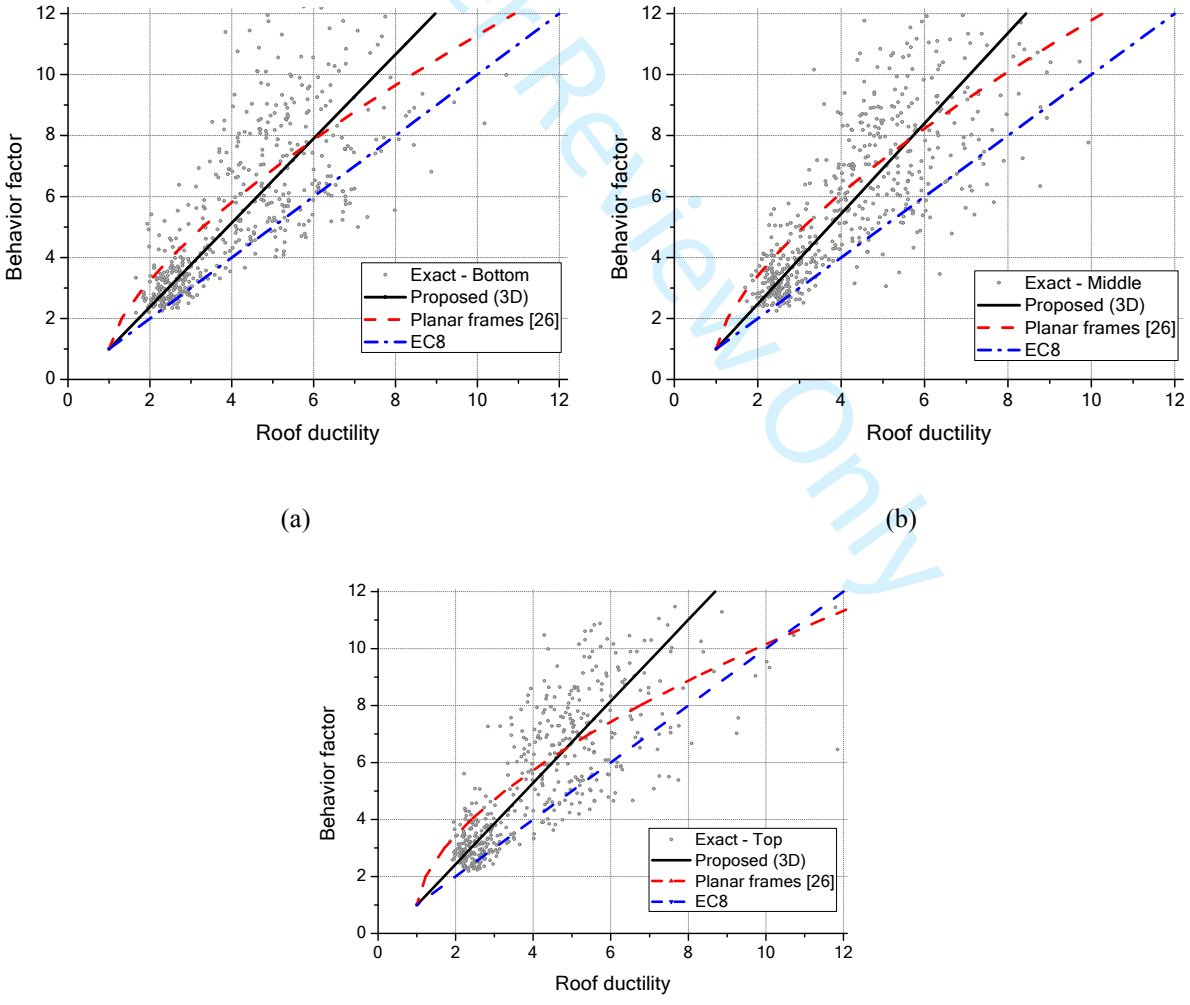

(a) (b)

(c)

Figure 17. Graphical depiction of the response databank results and approximation by the proposed relation for space MRFs. Comparison with the proposed in [19] relation for planar MRFs and the equal-displacement rule (EC8 [3]) for the frames with vertical mass discontinuities (Group C) on: (a) bottom floor; (b) middle floor; and (c) top floor.

6. SEISMIC DESIGN EXAMPLES

This section utilizes the developed relationships within the framework of the HFD seismic design method [21-24] for designing the three space steel irregular frames shown in Figure 18. The frames were first designed according to EC8 [3] and EC3 [27] provisions assuming the same grade of steel and load combinations as those introduced in Section 2. All buildings have 3m storey height and 6m bay width in both directions (Figure 18). The performance levels for seismic design are: (a) IO (Immediate Occupancy) under the FOE (Frequently Occurring Earthquake), (b) LS (Life Safety) under the DBE (Design Basis Earthquake), (c) CP (Collapse Prevention) under the MCE (Maximum Considered Earthquake). Figure 19 shows the Type 1 (soil class B) elastic design spectra of EC8 [3] for the FOE, DBE and MCE levels. For the DBE level, the peak ground acceleration (PGA_{DBE}) was taken equal to 0.36g. The PGAs under the FOE and the MCE were taken equal to 0.25 x PGA_{DBE} and 1.5 x PGA_{DBE}, respectively. Based on ASCE 41-13 [42], the *IDR* and μ_θ should be lower than 0.7% and 1.0 under the FOE, lower than 2.5% and 9.0 under the DBE and lower than 5.0% and 11.0 under the MCE, respectively. Table 14 summarizes all the relevant information of the design.

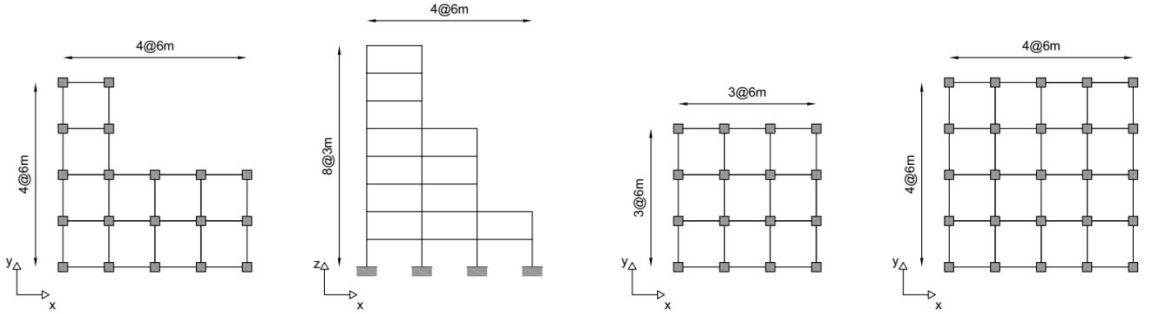

(a) (b) (c)

Figure 18. Building structures considered here for the design examples: (a) 6-storey space frame with L-shaped plan view; (b) 8-storey setback space frame; and (c) 9-story space frame with a vertical mass irregularity at 5th floor.

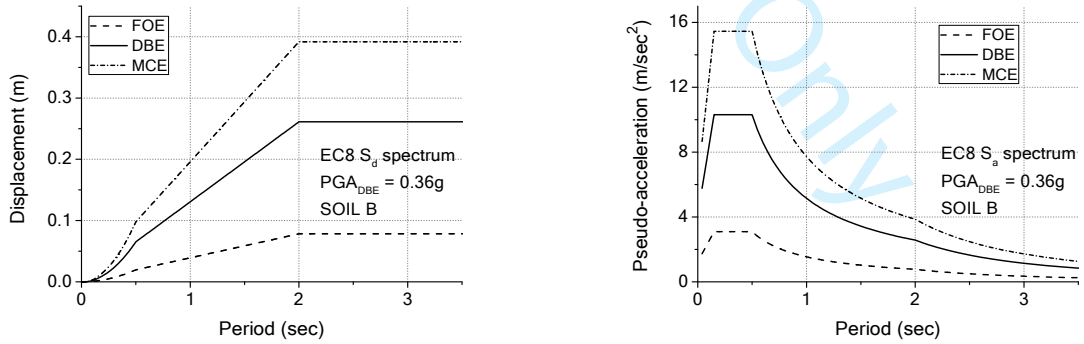

(a) (b)

Figure 19. Design spectra of EC8 [3] for soil class B and PGA_{DBE} = 0.36g: (a) displacement design spectra; (b) pseudo-acceleration design spectra.

Table 14. Types and steel grade for designed frames (3* means that the 5th floor has a mass three times larger the one of the adjacent floors)

Design Example	Storeys Number	Lateral-resistant system	PGA_{DBE}	Metrics of Irregularity			Grade of steel
				Φ_s	Φ_b	Mass	Beam - Column
1	6	MRF with L shaped plan	0.36g	-	-	-	S235 – S355

2	8	MRF Setback	0.36g	1.21	2.05	-	S235 – S355
3	9	MRF Mass Irregular	0.36g	-	-	3*	S235 – S355

6.1. Six storey space MRF with L shaped floor plan.

Figure 18a illustrates a six storey space MRF with L shaped floor plan. The story height is 3.0 m. Table 15 provides the sections under a first elastic design for the FOE and the natural periods. The fundamental period is translational and equal to 1.24 sec. Considering that the initial FOE design is to determine the yielding roof displacement, $u_{r,y}$ equals to 0.076 m and IDR_y = 0.58%. This value of *IDR* fulfils the limit states of IO performance level as defined in ASCE 41-13 [42]. The designed structure is further assessed for the LS and the CP performance levels. For estimating the frame response under the DBE, the behavior factor q in DBE level can be taken from PGA_{DBE}/PGA_{FOE} = 4.00. By using Eq. (10) and Eq. (4), $\mu_{r,d} = (4\text{-}1)/1.35+1 = 3.22$ and $u_{r,max} = 0.076\times3.22 = 0.245$ m, respectively. By employing Eq. (8) and Eq. (5), $\mu_\theta = (3.22\text{-}1)/0.81+1 = 3.74$ and $IDR_{max} = (0.245/(3\times6\times0.93))^{1/1.11} = 2.22\%$, respectively. For estimating the frame response under the MCE, the factor q in MCE level can be taken from $(PGA_{MCE}/PGA_{DBE})\times q_{DBE} = 6$. Accordingly, by using Eq. (10) and Eq. (4), $\mu_{r,d} = (6\text{-}1)/1.35+1 = 4.7$ and $u_{r,max} = 0.076\times4.7 = 0.357$ m, respectively. By employing Eq. (8) and Eq. (5), $\mu_\theta = (4.7\text{-}2.58)/0.38+1 = 6.58$ and $IDR_{max} = (0.357/(3\times6\times0.93))^{1/1.11} = 3.12\%$, respectively. In the view of the above results and considering the limit values of ASCE 41-13 [42], one can observe that the frame design which fulfils the IO performance level fulfils the LS and CP requirements as well.

A second design is made for the LS performance level. The target values of the IDR_{max} and μ_θ are equal to 2.5% and 9, respectively (ASCE 41-13 [42]). Eq. (5) estimates the target roof displacement $u_{r,max(IDR)}$ as $3\times6\times0.93\times0.025^{1.11} = 0.279$ m. Then, the target roof displacement ductility $\mu_{r,IDR}$ is estimated by employing Eq. (4) as 0.279/0.076 = 3.67. By using Eq. (8), the target local rotational ductility $\mu_{r,\theta}$ is calculated as $2.58+0.38\times(9\text{-}1) = 5.62$. The design roof ductility $\mu_{r,d}$ is determined by taking the minimum values of $\mu_{r,IDR}$ and $\mu_{r,\theta}$ and is equal to the min (3.67, 5.62) = 3.67. It is found that drift controls the LS performance level. For a SDOF system with the same period as the designed frame (T_1 = 1.24 sec), the peak displacement can be determined from the DBE displacement design spectrum shown in Figure 19a and is equal to 0.165 m. Then, this displacement is increased to account for the frame response. The calculations give $0.165\times1.4 = 0.231$ m, where the multiplier 1.4 is proposed by ASCE 41-13 [42] for six storey buildings. The estimated roof displacement appears to be smaller than the $u_{r,max(IDR)}$ = 0.279 m, and the target values of the IDR_{max} and μ_θ for DBE performance level require revision according to [25,27]. By revising the target displacement to 0.231 m, the target values of IDR_{max} and μ_θ for this design example should be around 2.11% and 3.52, respectively, based on the Eqs. (4), (5) and (8). Based on Eq. (10) and implementing the new values of IDR_{max} and μ_θ, the required behavior factor q is calculated equal to 3.75. The designer performs a response spectrum analysis using the DBE design spectrum (Figure 19b) reduced by the obtained q factor. The resulted cross-sections are the same as the ones determined in IO level (Table 15).

A third design is prepared for the CP performance level. The target values of the IDR_{max} and μ_θ are equal to 5% and 11, respectively (ASCE 41-13 [42]). Eq. (5) estimates $u_{r,max(IDR)} = 3\times6\times1.51\times0.025^{1.25} = 0.643$ m. Then, by using Eq. (4), $\mu_{r,IDR} = 0.643/0.076 = 8.46$. Based on Eq. (8), $\mu_{r,\theta} = 2.58+0.38\times(11\text{-}1) = 6.38$. Thus, the $\mu_{r,d}$ is equal to 6.38. It is found here that local ductility controls the CP performance level and $u_{r,max(d)} = u_{r,max(\mu)} = 6.38\times0.076 = 0.485$ m. Based on the MCE displacement design spectrum shown in Figure 19a and the assumption of the SDOF system introduced before, the maximum displacement is found to be $0.248\times1.4 = 0.347$ m. The estimated roof displacement appears to be smaller than the $u_{r,max(IDR)}$ = 0.485 m, and the target values of the IDR_{max} and μ_θ for the MCE performance level require revision. By revising the target displacement to 0.347 m, the target values of IDR_{max} and μ_θ for this design example should be around 3.04% and 6.24, respectively, based on the Eqs. (4), (5) and (8). The required behavior factor q = 5.82 based on Eq. (10). The designer performs a response spectrum analysis using the MCE design spectrum (Figure 19b) reduced by the obtained q factor. The resulted cross-sections are the same as the ones determined in IO level (Table 15). In the view of the above results, one can observe that IO performance level determines the frame dimensions in the current example.

The conventional FBD method [3, 27] using a behavior factor $q = 6.5 \times 0.8 = 5.2$ is also applied to design the current space irregular MRF. The obtained cross-section and first three natural periods are given in Table 15. It is observed that the LS performance level determines the frame dimension in the FBD (EC8 [3]). The frame behaves elastically under FOE and it is expected to experience $u_{r,y}$ = 0.073 m and IDR_{max} = 0.55%. Accordingly, under the DBE the $u_{r,max}$ can be computed as $0.073\times PGA_{DBE}/PGA_{FOE} = 0.292$ m and the IDR_{max} as $0.55\%\times PGA_{DBE}/PGA_{FOE} = 2.20\%$. Under the MCE the $u_{r,max}$ can be computed as $0.292\times PGA_{MCE}/PGA_{DBE} = 0.438$ m and the IDR_{max} as $2.20\%\times PGA_{MCE}/PGA_{DBE} = 3.30\%$.

6.2. *Eight storey setback steel space MRF*

Figure 18b illustrates a steel space MRF with setbacks consisting of eight storeys of height 3.0m each. According to Eq. (1), the values of the indexes Φ_s and Φ_b of the MRF are equal to 1.21 and 2.05, respectively. Eq. (6) determines a value equal to 0.49 for the parameter β. As was mentioned in Section 4.2, based on the analyses results of this work, in most cases the direction with setback determines the performance level and thus only the equations of that direction are considered in this example. Table 16 provides the sections under FOE and the natural periods. The fundamental period is translational. The $u_{r,y}$ equals 0.079 m, while IDR_y equals 0.58% satisfying the IO level [42]. The q factor of the frame in DBE is 4.00. By using Eq. (11) and Eq. (4), $\mu_{r,d} = ((4\text{-}1)/(1.39\times1.21^{-0.06}))^{1/1.05} + 1 = 3.10$ and $u_{r,max} = 3.10\times0.079 = 0.245$ m, respectively. By employing Eq. (9) and Eq. (6), $\mu_\theta = (3.10\text{-}1)/0.79+1 = 3.66$ and $IDR_{max} = u_{r,max} / (H\times\beta) = 2.07\%$, respectively. For estimating the frame response under the MCE, the q factor for the space MRF is 6. Accordingly, by using Eq. (11) and Eq. (4), $\mu_{r,d} = ((6\text{-}1)/(1.39\times1.21^{-0.06}))^{1/1.05} + 1 = 4.42$ and $u_{r,max} = 4.42\times0.079 = 0.350$ m, respectively. By employing Eq. (9) and Eq. (6), $\mu_\theta = (4.42\text{-}1)/0.79+1 = 5.33$ and $IDR_{max} = u_{r,max} / (H\times\beta) = 2.96\%$, respectively. Based on the limit values of ASCE 41-13 [42], designing the frame under IO, both the LS and CP performance levels are satisfied.

If the design starts from the LS performance level, the $u_{r,max(IDR)} = H\times\beta\times IDR_{max} = 0.294$ m and therefore, the $\mu_{r,IDR}$ is equal to 0.294/0.079 = 3.72. By using Eq. (9), the $\mu_{r,\theta} = 1+0.79\times(9\text{-}1) = 7.32$ and therefore, the $\mu_{r,d} = \min(3.72, 7.32) = 3.72$. It is found that drift controls the LS design. For a SDOF system with T = 1.47 sec, the maximum displacement is found 0.197×1.4 = 0.276 m under DBE (Figure 19a). The multiplier 1.4 is for eight storey buildings [42]. The displacement is smaller than the $u_{r,max(IDR)} = 0.294$ m and the revised values of IDR_{max} and μ_θ based on Eqs. (4) and (9) are 2.23% and 4.16, respectively. These values fulfil the limit states of ASCE 41-13 [42]. Based on Eq. (11) the required behavior factor q = 4.90. The resulted cross-sections are the same as the ones of IO level (Table 16).

If the design starts from the CP performance level, the $u_{r,max(IDR)} = H\times\beta\times IDR_{max} = 0.588$ m and therefore, the $\mu_{r,IDR}$ equals 0.588/0.079 = 7.44. By using Eq. (9), the $\mu_{r,\theta} = 1+0.79\times(11\text{-}1) = 8.90$ and thus $\mu_{r,d} = 7.44$. It is found that drift controls the CP design in current example as well. The maximum displacement expected under MCE would not be larger than 0.300×1.4 = 0.420 m (Figure 19a) which is smaller than the $u_{r,max(IDR)} = 0.588$ m. The revised values of IDR_{max} and μ_θ are 3.57% and 6.46, respectively. These values fulfil the limit states of ASCE 41-13 [42]. The use of $IDR_{max} = 3.57\%$ lead to similar structure with the IO level.

The FBD method [3, 27] is also applied here using factor $q = 6.5 \times 0.8 = 5.2$. The LS performance level determines the frame dimension. The obtained cross-section and first three natural periods are given in Table 16. The frame behaves elastically under FOE and it is expected to experience $u_{r,y} = 0.079$ m and $IDR_{max} = 0.58\%$. Accordingly, under the DBE the $u_{r,max} = 0.316$ m and the $IDR_{max} = 2.32\%$. Under the MCE the $u_{r,max} = 0.474$ m and the $IDR_{max} = 3.48\%$.

6.3 *Nine storey steel space MRF with mass discontinuity along the height*

Figure 18c illustrate the floor plan of the nine storey steel space MRF with mass discontinuity along the height. The frame has an accidental eccentricity of 5% while the 5th floor has three times the mass of the adjacent floors. Table 17 provides the sections under FOE and the natural periods. The $u_{r,y} = 0.117$ m and $IDR_y = 0.62\%$ which fulfils the IO limit state values [42]. The q factor for DBE is 4.00. By using Eq. (12), $\mu_{r,d} = 1+(4.00\text{-}1)/1.48 = 3.03$, and Eq. (4), $u_{r,max} = 3.03\times0.117 = 0.354$ m. Eq. (9) determines $\mu_\theta = 1+((3.03\text{-}1)/1.17)^{1/0.59} = 3.54$ and Eq. (5) $IDR_{max} = (0.354/(1.47\times3\times9))^{1/1.24} = 2.22\%$. For estimating the frame response under the MCE, the q factor for the space MRF is 6. Accordingly, by using Eq. (12) and Eq. (4), $\mu_{r,d} = 1+(6\text{-}1)/1.48 = 4.38$ and $u_{r,max} = 4.38\times0.117 = 0.512$ m, respectively. By employing Eq. (9) and Eq. (5), $\mu_\theta = 1+((4.38\text{-}1)/1.17)^{1/0.59} = 7.03$ and $IDR_{max} = (0.512/(1.47\times3\times9))^{1/1.24} = 3.00\%$, respectively. Based on the limit values of ASCE 41-13 [42], designing the frame under IO, both the LS and CP performance levels are satisfied.

Under LS performance level design, Eq. (5) estimates $u_{r,max(IDR)}$ as $9\times3\times1.47\times0.025^{1.24} = 0.409$ and therefore, the $\mu_{r,IDR}$ is 0.409/0.117 = 3.50. By using Eq. (9), the $\mu_{r,\theta} = 1+1.17\times(9\text{-}1)^{0.59} = 4.99$ and thus $\mu_{r,d} = 3.50$. For a SDOF system with T = 1.95 sec, the maximum displacement is found to be 0.26×1.48 = 0.384 m under the DBE displacement design spectrum (Figure 19a). The multiplier 1.48 is for nine storey buildings [42]. The is smaller than 0.409 m and the revised values of the IDR_{max} and μ_θ are 2.24% and 4.10, respectively. These values satisfy the limit values of ASCE 41-13 [42]. Based on Eq. (12) the required behavior factor q = 4.38. The resulted cross-sections are the same as the ones of IO level (Table 17).

Under CP performance level design, $u_{r,max(IDR)} = 9\times3\times1.47\times0.05^{1.24} = 0.967$ m and therefore, $\mu_{r,IDR} = 0.967/0.117 = 8.26$. The $\mu_{r,\theta}$ is calculated as $1+1.17\times(11-1)^{0.59} = 5.55$ and thus $\mu_{r,d} = 5.55$. As a result, local ductility controls the CP design in the current example and placing the attention, the $u_{r,max(d)} = u_{r,max(\mu)} = 5.55\times0.117 = 0.65$ m. Under the MCE displacement design spectrum, the maximum roof displacement of the frame is expected to be $0.39\times1.48 = 0.577$ m (Figure 19a). The value is smaller than 0.65 m and revised values of IDR_{max} and μ_θ are 3.30% and 7.80, respectively. These values satisfy the limit value of ASCE 41-13 [42]. The use of IDR_{max} = 3.30% lead to similar structure with the IO level.

The FBD method [3,27] is also applied here using factor $q = 6.5 \times 0.8 = 5.2$. The LS performance level determines the frame dimension. The obtained cross-section and first three natural periods are given in Table 17. The frame behaves elastically under FOE and it is expected to experience $u_{r,y} = 0.087$ m and $IDR_{max} = 0.51\%$. Accordingly, under the DBE the $u_{r,max} = 0.348$ m and the $IDR_{max} = 2.04\%$. Under the MCE the $u_{r,max} = 0.522$ m and the $IDR_{max} = 3.06\%$.

Table 15. Columns and beams sections and first three natural periods of the 6-storey steel space MRF with irregular floor plan (L-shaped)

Design Example 1: 6-storey steel space MRF with L shaped floor plan						
Floor	Hybrid method			EC8 method		
	IPE		SHS	IPE		SHS
	B_{xe} - B_{ye}	B_{xi} - B_{yi}	C_i - C_e	B_{xe} - B_{ye}	B_{xi} - B_{yi}	C_i - C_e
1	330	450	340x20	400	450	350x16
2	330	500	340x20	400	500	350x16
3	330	450	320x20	400	500	350x16
4	300	400	320x20	360	450	300x16
5	300	360	300x20	330	360	300x16
6	300	360	300x20	330	360	300x16
	T_1=1.24sec - T_2=1.23sec - T_3=1.19sec			T_1=1.11sec - T_2=1.10sec - T_3=1.04sec		

Table 16. Columns and beams sections and first three natural periods of the 8-storey steel space MRF with setbacks

Design Example 2: Eight storey steel space MRF with setbacks						
Floor	Hybrid and EC8 method					
	IPE		SHS	IPE		SHS
	F_{xe}	F_{ye}	C_e	F_{xi}	F_{yi}	C_i
1	330	300	400x16	360	330	400x16
2	330	300	400x16	400	330	400x16
3	330	300	400x16	400	330	400x16
4	330	300	350x16	400	330	350x16
5	330	300	350x16	360	330	350x16
6	330	300	350x16	360	-	-
7	300	300	300x16	330	-	-
8	300	300	300x16	330	-	-
	T_1=1.47sec - T_2=1.37sec - T_3=1.13sec					

Table 17. Columns and beams sections and first three natural periods of the 9-storey steel space MRF with vertical mass discontinuities

Design Example 3: Nine storey steel space MRF with vertical mass discontinuity						
Floor	Hybrid method			EC8 method		
	IPE		SHS	IPE		SHS
	B_{xe} - B_{ye}	B_{xi} - B_{yi}	C_i - C_e	B_{xe} - B_{ye}	B_{xi} - B_{yi}	C_i - C_e
1	300	400	400x20	450	550	400x20
2	330	450	400x20	450	550	400x20
3	330	450	400x16	450	550	400x20
4	330	450	400x16	400	550	400x16
5	400	500	400x16	400	500	400x16
6	330	400	350x16	360	450	350x16
7	300	330	350x16	360	400	350x16

8	300	330	300x16	330	360	300x16
9	300	330	300x16	330	360	300x16
	T_1=1.95sec - T_2=1.95sec - T_3=1.91sec			T_1=1.56 sec - T_2=1.56 sec - T_3=1.49 sec		

6.4 Comparison and seismic assessment using semi-artificial accelerograms

The three design frames introduced in previous sections were subjected to the five pairs of semi-artificial accelerograms shown in Figure 10. The time history analysis results were then used to evaluate the frames performance as well as to both design methods.

The dynamic nonlinear analysis results are summarized in Table 18. Compared to the FBD method, one can observe that the hybrid design method provides a better control for the structural damage in terms of drift and ductility. This is because the hybrid design method utilizes a deformation and damage control q factor which can obtain several values based on the targeted performance level, while the FBD method employs a q factor that takes a general and constant value uncoupled from specific damage objectives. Moreover, IDR_{max} and $u_{r,max}$ obtained from the dynamic nonlinear analysis are constantly overestimated by FBD method, while those values are well predicted by the proposed method. However, a better prediction is observed for the six storey MRF by the hybrid method whereas an underestimation is observed for the nine storey MRF. Both design methods provided structures with similar weights. HFD and FBD designs of Example 1 have weight equal to 1211 kN and 1198 kN, respectively, while in Example 2 both methods determined a weight equal to 916. For the design Example 3, the hybrid design method provided a 15% lighter structure. The total weight of the steel (transformed in kN) was measured equal to 2536 kN. The FBD method provided a heavier structure with weight equal to 2946 kN. Table 19 provides the total mass of the structures and the performance level that controls the design in each case.

It should be noted that in all MRFs designed by the FBD, the interstorey drift sensitivity coefficient θ of EC8 [3] governs the design under the DBE thus determining a smaller actual behavior factor q than the one chosen initially. However, the initial choice of the q factor plays a direct role in the design solution by FBD and lighter solutions can very likely be adopted if a lower q factor was adopted instead. HFD appears to be more rational in estimating a behavior factor which satisfies both the targeted performance levels and drift requirements without implying later any indirect revision. As a result, a lighter structure is very likely to be adopted.

Table 18. Dynamic analyses results and comparison with both design methods for the 3 examples considered here

Six storey steel space MRF with L shaped floor plan - PGA_{DBE} = 0.36g												
Example 1	Hybrid method						Force based desing (EC8)					
	FOE		DBE		MCE		FOE		DBE		MCE	
	TH[a]	EST[a]	TH[a]	EST[a]	TH[a]	EST[a]	TH[a]	EST[b]	TH[a]	EST[b]	TH[a]	EST[b]
IDR (%)	0.58	0.58	2.06	2.22	2.78	3.12	0.55	0.55	1.75	2.20	2.40	3.30
$u_{r,max}$ (m)	0.078	0.076	0.245	0.245	0.346	0.357	0.074	0.073	0.225	0.292	0.332	0.438
μ_θ	1.00	1.00	3.17	3.74	4.22	6.58	1.00	1.00	2.93	-	4.80	-
Eight storey steel space MRF with setbacks - PGA_{DBE} = 0.36g												
Example 2	Hybrid method						Force based desing (EC8)					
	FOE		DBE		MCE		FOE		DBE		MCE	
	TH[a]	EST[a]	TH[a]	EST[a]	TH[a]	EST[a]	TH[a]	EST[b]	TH[a]	EST[b]	TH[a]	EST[b]
IDR (%)	0.60	0.58	2.01	2.07	3.02	2.96	0.60	0.58	2.01	2.32	3.02	3.48
$u_{r,max}$ (m)	0.086	0.079	0.278	0.246	0.418	0.350	0.086	0.079	0.278	0.316	0.418	0.474
μ_θ	1.00	1.00	3.08	3.66	4.39	5.33	1.00	1.00	3.08	-	4.39	-
Nine storey steel space MRF with vertical mass irregularity - PGA_{DBE} = 0.36g												
Example 3	Hybrid method						Force based desing (EC8)					
	FOE		DBE		MCE		FOE		DBE		MCE	
	TH[a]	EST[a]	TH[a]	EST[a]	TH[a]	EST[a]	TH[a]	EST[b]	TH[a]	EST[b]	TH[a]	EST[b]
IDR (%)	0.63	0.62	1.93	2.22	2.57	3.00	0.51	0.51	1.74	2.04	2.39	3.06
$u_{r,max}$ (m)	0.125	0.117	0.333	0.354	0.450	0.512	0.090	0.087	0.283	0.348	0.411	0.522
μ_θ	1.00	1.00	3.37	3.54	4.45	7.03	1.00	1.00	3.42	-	4.64	-

[a]TH: time history analysis; [a]EST: estimations of hybrid design method;
[b]EST (EC8): estimations using the equal displacement rule of EC8

Table 19. Mass and performance level (PL) that controls the design for the frames

Design Example	Hybrid method		Force based desing (EC8)	
	Mass (tons)	Control PL	Mass (tons)	Control PL
1	123.45	IO	122.12	LS
2	93.37	IO	93.37	LS
3	258.51	IO	300.31	LS

7. CONCLUSIONS

The main findings of the present study can be summarized as follows:

(1) Empirical expressions for a hybrid seismic design method (HFD) are developed for space steel moment resisting frames irregular in plan view and in elevation. Irregularity in elevation is either due to non-uniform distribution of mass or due to the presence of setbacks along the height of the frame. The proposed damage-control expressions apply to frames with low values of the mid-height stiffness parameter ρ and high values of the column-to-beam flexural strength parameter α.

(2) A torsional response component is observed in the irregular in-plan frames of this study. However, the level of this response is considerably smaller compared to the torsional response of the corresponding regular frames with 5% accidental eccentricity. This conclusion is limited to frames with the same bay widths and number of bays in both directions, similar to the frames of this work. The torsional response component of irregular setback frames can be more than two times the one of the corresponding regular frames with 5% accidental eccentricity.

(3) Buildings with setbacks only in one direction have different response and global ductility demands along the x and y in-plan direction. Thus, relationships between peak roof displacement – interstorey drift ratio (u_r - *IDR*) and behavior factor - maximum roof displacement ductility (q - μ_r) are different along the x and y direction. Based on the analyses results, in most cases, the setback direction determines the design controlling performance level.

(4) For a certain value of *IDR*, frames with mass discontinuity along their height have higher ductility demands compared to the corresponding regular frames. In addition, these frames satisfy the various performance levels for a lower seismic intensity than the corresponding regular frames.

(5) For a realistic range of q values (less than 8), the comparison of the proposed q-μ_r relationships versus the corresponding relationships proposed for planar irregular frames reveals a difference in the seismic response of space and planar irregular frames. For a targeted level of seismic performance, space frames require higher ductility demands and lower behavior factors than the corresponding planar ones. The above behavior seems to be related to the presence of the torsional response component in space irregular frames.

(6) Nonlinear time-history analyses revealed that HFD design method provides better estimations of critical response quantities, such as, the *IDR*, member ductility μ_θ, and roof displacement u_r under the three performance levels considered than the conventional FBD method.

(7) In the three design examples designed by the FBD method, the interstorey drift sensitivity coefficient θ of EC8 governs the design under the DBE level. As a result, a smaller behavior factor q than the one initially chosen is very likely to be determined by FBD. Following the HFD method, the immediate occupancy (IO) performance level controls the design in current examples without implying any indirect revision to the initial selection of q factor and a lighter structure could very likely be designed.

(8) In the three design examples, resulting total weights of the designed 6-storey irregular-in-plan-view and 8-storey with setbacks buildings by both design methods were found to be similar. In the design of the 9-storey building with vertical mass discontinuities the HFD method led to a 15% lighter structure.

REFERENCES

1. Zembaty Z, De Stefano M, editors. Seismic Behavior and Design of Irregular and Complex Civil Structures II. Switzerland: Springer; 2016
2. International Building Code, IBC. International code council, Inc. U.S.A.: ICC; 2012
3. Eurocode 8, EC8. Design of structures for earthquake resistance, Part 1: General rules, seismic actions and rules for buildings, European Standard EN 1998-1, Stage 51 Draft. European Committee for Standardization (CEN), Brussels; 2004

4. De Stefano M, Pintucchi B. A review of research on seismic behavior of irregular building structures since 2002. Bulletin of Earthquake Engineering 2008; 6: 285-308.
5. De la Llera JC, Chopra AK. Understanding the inelastic seismic behavior of asymmetric-plan buildings. Earthquake Engineering and Structural Dynamics 1995; 24: 549-572.
6. Dutta SC, Das PK. Inelastic seismic response of code-designed reinforced concrete asymmetric buildings with strength degradation. Engineering Structures 2002; 24: 1295-1314.
7. Anagnostopoulos SA, Kyrkos MT, Stathopoulos KG. Earthquake induced torsion in buildings: Critical review and state of the art. Earthquakes and Structures 2015; 8(2): 305-377.
8. Humar JL, Wright EW. Earthquake response of steel framed multistory buildings with setbacks. Earthquake Engineering and Structural Dynamics 1977; 5(1): 15-39.
9. Duan XN, Chandler AM. Seismic torsional response and design procedures for a class of setback frame buildings. Earthquake Engineering and Structural Dynamics 1995; 24: 761-777.
10. Chen C, Lam NTK, Mendis P. The Bifurcation Behavior of Vertically Irregular Buildings in Low Seismicity Regions. In WCEE: Proceedings of the 12th World Conference on Earthquake Engineering; 2000 Jan. 30 – Feb. 4; Auckland, New Zealand. Paper No. 1625.
11. Karavasilis TL, Bazeos, N, Beskos, DE. Seismic response of plane steel MRF with setbacks: estimation of inelastic deformation demands. Journal of Constructional Steel Research 2008; 64(6): 644-654.
12. Bosco M, Ghersi A, Marino E, Rossi PP. Effects of in elevation irregularity on the elastic seismic response of in-plan asymmetric buildings. In: Proceedings of the third European workshop on the seismic behavior of irregular and complex structures; 2002 Sept. 17-18; Florence, Italy. CD ROM.
13. Xilin Lu, Ningfen Su, Ying Zhou. Nonlinear time history analysis of a super-tall building with setbacks in elevation. The Structural Design of Tall and Special Buildings 2011; 22: 593-614.
14. Vasilopoulos AA, Bazeos N, Beskos DE. Seismic design of irregular space steel frames using advanced methods of analysis. Steel and Composite Structures 2008; 8: 53-83.
15. Valmundsson EV, Nau JM. Seismic response of building frames with vertical structural irregularities. Journal of Structural Engineering (ASCE) 1997; 123(1): 30-41.
16. Das S, Nau JM. Seismic design aspects of vertically irregular reinforced concrete building. Earthquake Spectra 2003; 19(3): 455-477.
17. Magliulo G, Ramasco R, Realfonzo R. Seismic behavior of irregular in elevation plane frames. In: Proceedings of the 12th European conference on earthquake engineering; 2002 Sept. 9-13; London, UK. Paper no. 219.
18. Tremblay R, Poncet L. Seismic performance of concentrically braced steel frames in multistory buildings with mass irregularity. Journal of Structural Engineering (ASCE) 2005; 131; 1363-1375.
19. Karavasilis TL, Bazeos N Beskos DE. Estimation of seismic inelastic deformation demands in plane steel MRF with vertical mass irregularities. Engineering Structures 2009; 30(11); 3265-3275.
20. Karavasilis TL, Bazeos N, Beskos DE. A hybrid force/displacement seismic design method for plane steel frames. In: Mazzolani FM, Wada A, editors. STESSA: Proceedings of the International Conference on the Behavior of Steel Structures in Seismic Area; 2006 August 14-17; Yokohama, Japan: Taylor & Fransis; 2006. p. 39-44.
21. Tzimas AS, Karavasilis TL, Bazeos N, Beskos DE. A hybrid force/displacement seismic design method for steel building frames. Engineering Structures 2013; 56: 1452-1463.
22. Tzimas AS. A New Hybrid Force/Displacement Method for Seismic Design of Space Steel Structures. Ph.D. Thesis, Department of Civil Engineering, University of Patras, Patras, Greece; 2013 (in Greek).
23. Tzimas AS, Karavasilis TL, Bazeos N, Beskos DE. Extension of the hybrid force/displacement (HFD) seismic design method to 3D steel moment-resisting frame buildings. Engineering Structures 2017; 147; 486–504.
24. Skalomenos KA, Hatzigeorgiou GD, Beskos DE. Application of the hybrid force/displacement (HFD) seismic design method to composite steel/concrete plane frames, Journal of Constructional Steel Research 2015; 115: 179-190.
25. Priestley MJN, Calvi GM, Kowalsky MJ. Direct Displacement-Based Design. Pavia, Italy: IUSS Press; 2007.
26. Bozorgnia Y, Bertero, VV. Earthquake Engineering: From Engineering Seismology to Performance-Based Engineering. CRC Press, Boca Raton, FL, USA; 2004.
27. Eurocode 3, EC3. Design of Steel Structures, Part 1. 1: General Rules for Buildings, European Prestandard ENV 1993-1-1. European Committee for Standardization (CEN), Brussels; 2005.
28. SAP2000. Static and Dynamic Finite Element Analysis of Structures. Computers and Structures inc., Berkeley, California; 2018.

29. Chopra AK (2007) Dynamics of structures. Pearson Prentice Hall, Berkeley
30. Macedo L, Silva A, Castro JM. A more rational selection of the behavior factor for seismic design according to Eurocode 8. Engineering Structures 2019; 188: 69-86.
31. Mazzolani FM, Piluso V. Theory and Design of Seismic Resistant Steel Frames. New York: FN & SPON an Imprint of Chapman & Hall, London; 1996
32. ASCE Standard ASCE/SEI 7-10. Minimum Design Loads for Buildings and Other Structures. American Society of Civil Engineers, Reston, Virginia, USA; 2010.
33. Carr AJ. Ruaumoko-3D - A Program for Inelastic Dynamic Analysis. Technical Report, Department of Civil Engineering, University of Canterbury, Christchurch, New Zealand; 2005.
34. Gupta A, Krawinkler H. Seismic Demands for Performance Evaluation of Steel Moment Resisting Frame Structures. Report No 132, John A Blume Earthquake Engineering Center, Department of Civil Engineering, Stanford University, Stanford, CA, USA; 1999.
35. Skalomenos KA, Hatzigeorgiou GD, Beskos DE. Modelling level selection for seismic analysis of concrete-filled steel tube/moment resisting frames by using fragility curves, Earthquake Engineering and Structural Dynamics 2015; 44(2): 199-220
36. Skalomenos KA, Hatzigeorgiou GD, Beskos DE. Seismic behavior of composite steel/concrete MRFs: deformation assessment and behavior factors, Bulletin of Earthquake Engineering 2015; 13(12): 3871-3896.
37. Fadden MF. Cyclic Bending Behavior of Hollow Structural Sections and their Application in Seismic Moment Frame Systems. Ph.D. Thesis, Department of Civil Engineering, University of Michigan, USA; 2013.
38. Pacific Earthquake Engineering Research Centre, PEER. Strong Ground Motion Database; 2009, http://peer.berkeley.edu/.
39. FEMA P58. Seismic performance assessment of buildings. ATC. Applied Technology Council: CA. USA; 2012.
40. Structural Engineers Association of California, SEAOC. Vision 2000 – A framework for performance based earthquake engineering. Sacramento, CA; 1995.
41. MATLAB. The language of technical computing. Natick MA: The Mathworks Inc; 2018.
42. ASCE Standard ASCE/SEI 41-13. Seismic Evaluation of Retrofit of Existing Buildings. American Society of Civil Engineers, Reston, Virginia, USA; 2014.

A Hybrid Seismic Design Method for Steel Irregular Space Moment Resisting Frames

Angelos S. Tzimas[1]; Konstantinos A. Skalomenos[2,*]; Dimitri E. Beskos[3,4]

[1] Atkins, Woodcote Grove, Ashley Road, Epsom KT18 5BW, United Kingdom

[2] Department of Civil Engineering, University of Birmingham, Edgbaston, Birmingham B15 2TT, United Kingdom

[3] Department of Disaster Mitigation for Structures, College of Civil Engineering, Tongji University 200092 Shanghai, China

[4] Department of Civil Engineering, University of Patras 26500 Patras, Greece

ABSTRACT

A hybrid force/displacement seismic design method for space steel moment resisting frames irregular in plan view and in elevation is developed. Irregularity in elevation is either due to non-uniform distribution of mass or due to the presence of setbacks along the height of the frame. More specifically, 30 different frames irregular in plan view for the first case (plan-irregularities), 40 frames with setbacks (vertical stiffness irregularities) for the second case, and 18 frames with mass discontinuities (vertical mass irregularities) at the first, intermediate and top storey for the third case are considered. All these frames are designed according to Eurocodes 3 and 8 and subjected to 42 pairs of ordinary ground motions. Through nonlinear seismic analyses, seismic response databanks for these three types of irregular frames are generated corresponding to four performance levels. These databanks are then utilized for the development of simple expressions that determine the behavior (or strength reduction) factors of the frames. These are functions of frames geometrical/dynamic characteristics including measures of their irregularities as well as the target maximum interstorey drift ratio and member local ductility. The proposed design method, even though it is mainly a force-based design method, controls deformation and therefore damage through the proposed deformation-controlled behavior factors. Design examples are presented to validate the effectiveness of the method to account for the irregularity effects on the preliminary design stage while time-history analysis results demonstrate its advantages to control better the inelastic response of the frames over the conventional force-based seismic design method of Eurocode 8.

Keywords: Steel space frames, Hybrid force/displacement design, Space moment resisting frames, Plan view irregular frames, Frames with setbacks, Mass irregular heightwise frames, Behavior factors, Deformation control

1. INTRODUCTION

Irregular building structures may suffer significantly more damages compared to regular structures [1], indicating that their inelastic seismic response cannot be always estimated with safety by utilizing the methods of current seismic design codes [2,3]. The various structural irregularities over the floor plan or along the height of structures lead to a combined non-uniform distribution of stiffness, strength and mass which in turn negatively affects the seismic performance of structures.

Common types of geometrical irregularities in building structures are mainly related to floor plan irregularity, e.g., L, Π, or T-shaped buildings in plan view or to the presence of setbacks along the height of the building, i.e., the presence of abrupt reductions of the floor area. In urban areas, for instance, plan-irregular or setback buildings are often used since they increase ventilation and sunlight and use effectively the often irregular available lot area. It is also a common trend, nowadays, for buildings to accommodate different functions at specific levels of the elevation, such as floors with heavy mechanical or electrical equipment, floors used for commercial purposes (shopping centers, entertainment and leisure facilities) or car parking floors. This could result in a significant mass irregularity along the height that cannot be ignored in the design. As a result, stronger beams tend to be installed at floors that sustain the heavier masses.

Many researchers in the past have examined the seismic response of structures with irregularities. A review of research on the seismic behavior of irregular building structures can be found in [1,4]. A detailed description of the inelastic behavior of plan-irregular structures was made by De la Llera and Chopra [5], where the torsional effects by non-uniform distribution of strength and stiffness were considered. Many studies thereafter investigated the influence of strength deterioration on the seismic response of plan-irregular structures under

*Corresponding author e-mail: k.skalomenos@bham.ac.uk

biaxial seismic excitations adopting more sophisticated modelling approaches [6]. Recent works on multi-degree-of-freedom asymmetric reinforced concrete and steel braced frame structures [7] demonstrate the necessity of considering a more uniform distribution of ductility demands among adjacent members in the seismic design of asymmetric structures.

A larger inelastic deformation demand (i.e., member ductility or story drift) was also observed in buildings with setbacks either in members near setbacks or in the tower (i.e., the part with the smallest number of bays) [8]. Duan and Chandler [9] pointed out that the current design methodologies cannot prevent the members near the setback from a severe damage concentration and as a result a stronger design for the tower should be considered. Chen et al. [10] observed that the tower exhibits a local vibration mode enough to result in higher mode effects indicating the necessity for controlling its response, while Karavasilis et al. [11] concluded that the extensive local damages of the tower members could reduce the ductility classification of the building. Very few studies have also examined the influence of biaxial seismic excitations and torsional effect on setback space buildings [12-14].

The seismic response of planar frames with vertical mass irregularities has also been a subject of research over the last years. Valmundsson and Nau [15] observed that mass discontinuity at the higher floors affects primarily the elastic response of the frames and that at the lower floors affects mostly their inelastic response, while Das and Nau [16] found that mass irregularity at the lower or upper floors lead to the worst behavior with respect to energy absorption. However, Magliulo et al. [17] concluded that elastic and inelastic responses are slightly affected by mass discontinuities which is in accordance with the findings in the study of Tremblay and Poncet [18], for steel buildings with diagonal braces. An estimation methodology of the seismic damage of planar steel moment-resisting frames with vertical mass irregularities is presented in [19].

The above research studies (mostly on two-dimensional (2-D) frames) highlight the importance of treating irregular structures as a special type of structures and the need of developing effective design procedures or upgrading existing ones to account for the new drift and ductility demands. The three-dimensional (3D) frame modelling appears to be a sufficient solution for the study of irregular building structures for which torsional motion may not be treated adequately by traditional, simplified plane models [7,14].

A new seismic design method, namely the hybrid force/displacement (HFD) design method, has been proposed by the present authors and co-workers and its effectiveness has been confirmed in several types of regular and irregular planar steel frames [20-22], regular space steel frames [23] and regular planar composite steel/concrete frames [24]. The HFD seismic design method combines the advantages of both the force-based design (FBD) method [2,3] and the direct displacement-based design (DBD) method [25] in a hybrid force/displacement design scheme and works within the framework of the performance-based seismic design (PBSD) [26]. The main advantages of HFD is the fact that directly controls both structural and non-structural damage and requires fewer design iterations than the conventional FBD method as well as it does not use substitute SDOF structures and highly damped displacement response spectra as the DBD method. A deformation-controlled behavior factor q (or strength reduction factor R) is determined to limit the global ductility and seismic design forces are calculated by utilizing the familiar to engineers response spectrum analysis.

In this study, the HFD is developed for irregular in elevation and floor plan space steel moment resisting frames (MRF) as well as for frames with vertical mass irregularities. A large seismic response databank is generated on the basis of 88 space irregular MRFs databank according to Eurocodes 3 and 8 [27,3], four different performance levels with respect the IDR and $\mu_{\theta,}$ and non-linear dynamic analysis under 42 pairs of ordinary ground motions. This response databank is utilized to develop the necessary empirical equations employed by the HFD. Realistic performance-based design examples of three irregular MRFs are presented and evaluated with nonlinear time-history analyses for three performance levels. Comparisons with the design results of the FBD method of EC8 [3] demonstrate the advantage of the proposed design method to account in a direct manner for the irregularity effects and control the inelastic response of these irregular frames.

2. SEISMIC DESING OF STEEL IRREGULAR SPACE FRAMES

2.1. Space frames irregular in plan view

In this section, 30 steel space MRFs regular along their height and irregular in plan view (L-shaped plan) are designed. The frames have a storey height equal to 3.00 m and a bay span 5.00 m. Figure 1a shows in plan view the 6 types of the frames considered. Each type has 3, 6, 9, 12 and 15 storeys, hence there are 6×5=30 such MRFs. Figure 1b depicts in perspective form a 6-storey space frame of type 5 in Figure 1a. The present space frames constitute frame Group A. A torsional response is expected in the frames of Group A due to their

stiffness and mass irregularity caused by their L-shaped plan view, and therefore, accidental eccentricity is not considered as a part of the design and assessment of their structural response. This design approach may be considered to be against the clause 4.3.2 of EC8 [3], but it is used to investigate if the torsional response of the frames of Group A is higher compared to the torsional response of the corresponding regular frames with 5% accidental eccentricity (see Section 4.1). It should be noted that one of the EC8 [3] criteria to characterize a building as irregular in plan, is when the slenderness ratio $\lambda = L_{max}/L_{min}$ of the building in plan is higher than 4, where L_{max} and L_{min} are respectively its larger and smaller dimension. In the current design cases of the buildings of Group A, the range of λ ratio is between 1.33 and 4 and thus the level of the building irregularities can be considered low to moderate.

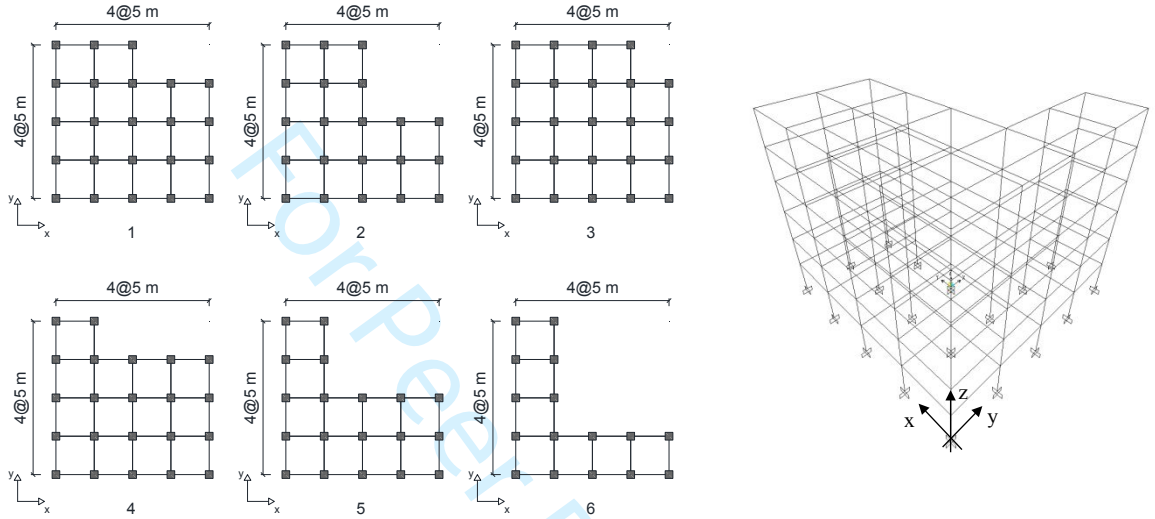

(a) (b)

Figure 1. Group A of space steel frames: (a) frames plan view (Type 1-6); (b) perspective view of the six-storeys four-bays space MRF (Type 5 in plan view)

The gravity loads combination was 1.35G + 1.5Q. The dead and live design loads were G = 6.5 kN/m^2 and Q = 2.0 kN/m^2, respectively, while structural self-weight was considered in the structural analysis process. The earthquake load was determined by the Type 1 elastic design spectrum of EC8 [3] for soil class B. The peak ground acceleration (PGA) was taken equal to 0.24g (g = 9.81m/s^2), while a behavior factor q = 6.5 was used to size the frames for both the x and y directions of the building. It should be noted that in accordance with EC8 [3], for buildings which are not regular, the q factor should be reduced by 20%. This reduction of q has been considered in the design of all frames of this work. The seismic design combinations were G + 0.3Q ± E_x ± 0.3E_y, G + 0.3Q ± E_y ± 0.3E_x, where E_x and E_y are the seismic loads in x and y direction, respectively.

Every frame was designed according to Eurocodes 3 and 8 [27,3] by using the commercial software SAP 2000 [28] and conducting spectrum analysis. For the beams, compact IPE structural sections of grade S235 were selected while for the columns compact square-hollow-sections (SHS) of grade S355 as a practical way to satisfy efficiently the capacity design of joints. In dissipative elements, all the sections are classified as Class 1. SHS columns are part of the lateral resisting system in both x and y directions, and thus are subjected to bidirectional bending and axial load due to the gravity and seismic design situation. The use of SHS in the frames of this work is preferable since the strength and stiffness is the same in both local axes compared to other H commercial sections. Same design approach applies also for the buildings of Group B and C. The beam-to-column joints were designed to be rigid. Second order effects (P−Δ) were considered through the interstorey drift sensitivity coefficient θ [3]. As additional design quantities to quantify the mechanical characteristics of the designed frames, the column-to-beam flexural strength ratio α and the mid-height beam-to-column stiffness ratio ρ were adopted in the present study as defined in [21,29].

For all frame cases, the coefficient θ [3] governs the seismic design resulting in a cross-section enlargement to satisfy the drift requirements. This is a known issue of EC8 [3] for steel MRFs, in particular when high q factors are used in low to moderate seismicity designs. However, the initial choice of a high q factor plays a direct role in the design solution [30] and lighter solutions can very likely be adopted if a lower q factor was initially adopted instead, especially in the case of tall buildings. The cross-sections of the 6-stories and 12 stories frames are given in Table 1. Cross-sections for the 3-storeys, 9-storieys and 15-storeys frames can be found in [22]. In Table 1, B denotes beam and C denotes column. The subscripts x and y stand for the respective

directions while *e* and *i* mean "exterior" and "interior", respectively. Section dimensions are given in mm. Minimum and maximum values of ρ and α are also provided for which ρ decreases as α increases and vice versa. In addition, the three first natural periods are provided in Table 2.

Table 1. Sections of space steel frames of Group A.

*Six storey space MRF			
Floor	Group A		
	IPE		SHS
	B_{xe}, B_{ye}	B_{xi}, B_{yi}	C_i, C_e
1	330	360	350x16
2	330	360	300x16
3	330	360	300x16
4	300	330	300x12
5	300	330	300x12
6	300	330	300x12

*$0.24 < \rho < 0.43$ and $1.60 < \alpha < 2.27$

*Twelve storey space MRF			
Floor	Group A		
	IPE		SHS
	B_{xe}, B_{ye}	B_{xi}, B_{yi}	C_i, C_e
1	360	450	400x20
2	400	450	400x20
3	400	450	400x20
4	360	450	400x20
5	360	400	400x20
6	360	400	400x16
7	330	400	400x16
8	330	360	350x16
9	300	360	300x16
10	300	360	300x16
11	270	330	300x12
12	270	330	300x12

*$0.19 < \rho < 0.30$ and $2.60 < \alpha < 3.63$

Table 2. Three first vibration periods of the 6-storeys and 12-storeys space steel frames of Group A.

Frames of Group A				
Number of storeys	Frame type	Period (sec)		
		T_1	T_2	T_3
6	1	1.21	1.21	1.09
6	2	1.19	1.19	1.09
6	3	1.22	1.22	1.09
6	4	1.20	1.20	1.08
6	5	1.17	1.17	1.07
6	6	1.12	1.12	1.05
12	1	1.92	1.92	1.76
12	2	1.91	1.90	1.76
12	3	1.93	1.92	1.77
12	4	1.92	1.91	1.76
12	5	1.89	1.89	1.75
12	6	1.87	1.87	1.73

2.2 Space frames with setbacks along the height

In this section, 40 steel space MRFs regular in the plan view and irregular along the height (with setbacks) are designed following the same assumptions and design methodologies adopted for the frames of Group A. The number of the bays in x direction reduces with the number of storeys along the height, as shown in Figure 2a, thereby creating a geometrical discontinuity along that height. Figure 2b shows in 3D a representative 6-storeys space frame with 3 bays in both directions for the first, second and third storey, and one bay in x direction for the rest three storeys. Figure 2c illustrates all the frames under consideration. The current space frames constitute frame Group B and have 3, 6 and 9 storeys. Similarly, with the frames of Group A, a torsional response is expected in the frames of Group B due to their stiffness and mass irregularity along their height caused by the setbacks, and therefore, accidental eccentricity is not considered. The cross-sections of the frames of Group B had dimensions similar to those of Group A. Sections of the 6-storey and 9-storey frames are shown in Table 3 as the most representative, while the rest can be found in Tzimas [22]. The three first natural periods of Group B frames are provided in Table 4.

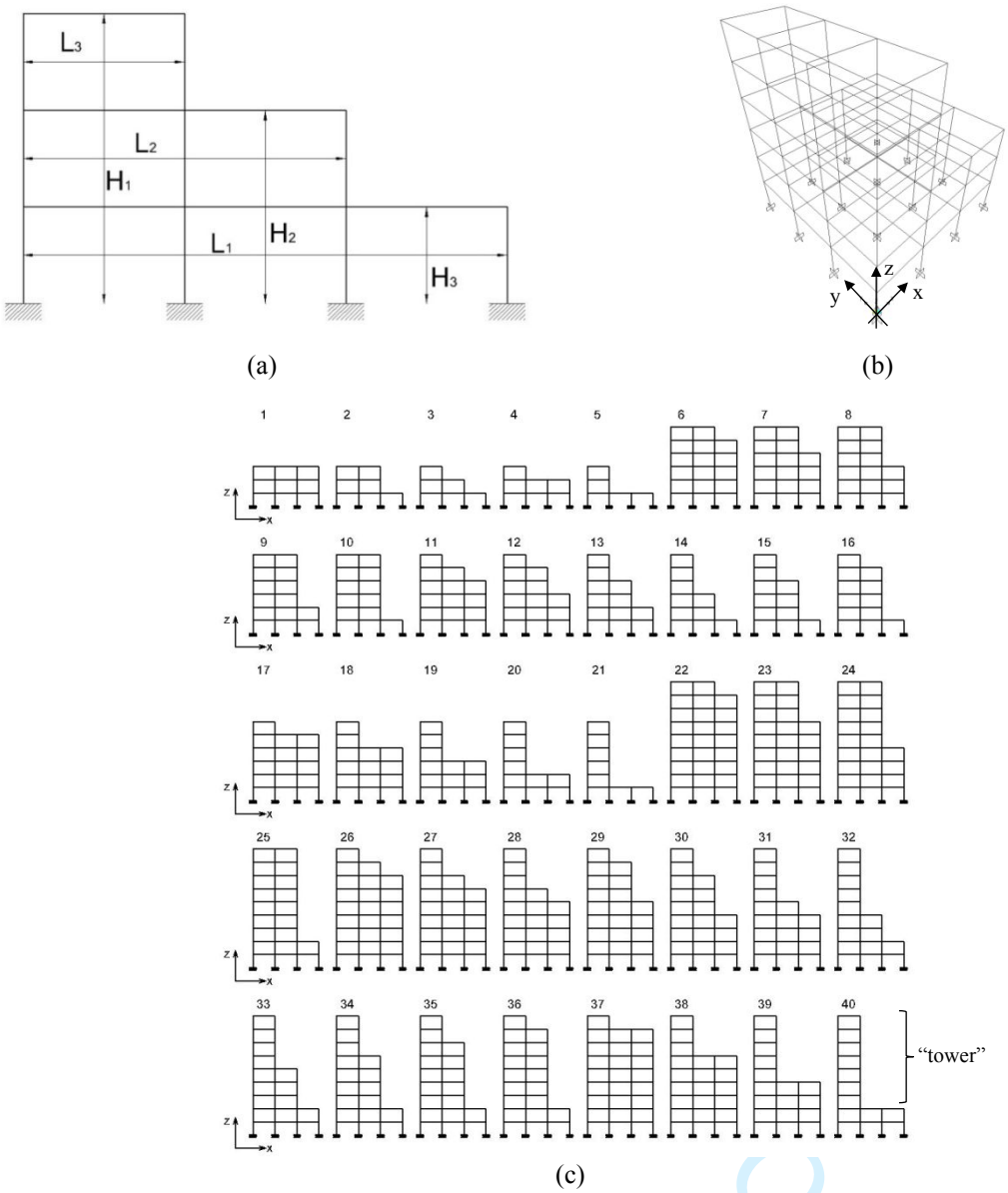

Figure 2. (a) Geometry of frames with setbacks; (b) perspective view of a six-storey with setbacks along the height; (c) all the frames with setbacks considered (Frame type 1 – Frame type 40)

Table 3 Section of the six-storey and nine-storey space steel frames of Group B.

*Six storey space MRF			
	Group B		
Floor	IPE		SHS
	F_{xe}, F_{ye}	F_{xi}, F_{yi}	C_i, C_e
1	330	360	350x16
2	330	360	300x16
3	330	360	300x16
4	300	330	300x12
5	300	330	300x12
6	300	330	300x12

*$0.24 < \rho < 0.43$ and $1.60 < \alpha < 2.27$

*Nine storey space MRF			
	Group B		
Floor	IPE		SHS
	F_{xe}, F_{ye}	F_{xi}, F_{yi}	C_i, C_e
1	300	360	400x16
2	330	400	400x16
3	330	400	400x16
4	330	400	400x16
5	330	400	400x16
6	300	360	350x16
7	270	330	350x16
8	270	300	300x12
9	270	300	350x12

*$0.18 < \rho < 0.32$ and $2.19 < \alpha < 2.93$

In the adopted frame design with setbacks, the storey area is reduced approximately by 33% and 66% in x direction because of the setbacks. The criterion of the EC8 [3] to characterize a building with setbacks as irregular in elevation, is when the individual setbacks are greater than 10 % of the previous plan dimension, thus the level of the building irregularities can be considered high. The geometrical irregularity introduced by setbacks is quantified through the Φ_s and Φ_b indices which according to Figure 2a can be taken from [11,31]

$$\Phi_s = \frac{1}{n_s - 1} \cdot \sum_{i=1}^{i=n_s-1} \frac{L_i}{L_{i+1}} \qquad \Phi_b = \frac{1}{n_b - 1} \cdot \sum_{i=1}^{i=n_b-1} \frac{H_i}{H_{i+1}} \tag{1}$$

where n_s is the number of storeys and n_b the bays number of the first storey. Figure 2a defines H_i and L_i.

Table 4. Three first vibration periods of the 6-storeys space steel frames of Group B.

Frames of Group B					
Frame case (See Figure 2c)	Φ_s	Φ_d	Period (sec)		
			T_1	T_1	T_1
6	1.10	1.10	1.14	1.12	0.96
7	1.10	1.25	1.11	1.07	0.87
8	1.10	1.50	1.10	1.06	0.85
9	1.10	2.00	1.11	1.09	0.90
10	1.10	3.50	1.18	1.17	1.03
11	1.30	1.23	1.04	0.99	0.81
12	1.30	1.43	1.03	0.97	0.75
13	1.30	1.75	0.98	0.92	0.69
14	1.30	2.50	0.97	0.94	0.74
15	1.30	2.75	0.99	0.95	0.75
16	1.30	3.10	1.05	1.03	0.85
17	1.40	1.10	1.07	1.05	0.91
18	1.40	1.25	0.99	0.93	0.76
19	1.40	1.50	0.96	0.90	0.69
20	1.40	2.00	0.97	0.96	0.78
21	1.40	3.50	1.06	1.01	0.90
22	1.06	1.06	1.53	1.52	1.36
23	1.06	1.25	1.48	1.42	1.19
24	1.06	1.40	1.48	1.42	1.16
25	1.06	2.75	1.51	1.49	1.27
26	1.19	1.13	1.44	1.39	1.22
27	1.19	1.23	1.37	1.28	1.08
28	1.19	1.35	1.32	1.21	0.96
29	1.19	1.36	1.41	1.32	1.07
30	1.19	1.52	1.36	1.25	0.97
31	1.19	1.53	1.30	1.19	0.91
32	1.19	2.13	1.32	1.26	0.99
33	1.19	2.15	1.32	1.24	0.95
34	1.19	2.25	1.34	1.25	0.98
35	1.19	2.39	1.38	1.30	1.05
36	1.19	2.56	1.43	1.39	1.16
37	1.25	1.06	1.47	1.45	1.32
38	1.25	1.25	1.33	1.24	1.04
39	1.25	1.625	1.31	1.22	0.94
40	1.25	2.75	1.38	1.38	1.14

2.3. Space frames with mass discontinuity along their height

In this section, 18 steel space MRFs regular in plan view and with a non-uniform distribution of mass along the height are designed. These space frames constitute frame Group C. The mass discontinuity is located either at the bottom storey (Frame B) or at the middle storey (Frame M) or at the top storey (Frame T), as shown in Figure 3. The mass discontinuity is quantified by the mass ratio, m_r. The quantity m_r is defined as the ratio of the mass of the storey that sustains the large weight (critical storey) to the smaller mass of the masses of the adjacent storeys. This means that the critical storey of each frame carries higher gravity loads compared to the adjacent storeys and this has been considered in frames design. Based on the recommendation of ASCE 7-10 [32], a building structure is considered irregular in terms of vertical mass discontinuity, when the quantity m_r takes a value higher than 1.5. EC8 [3] does not provide any corresponding mr limit as a vertical irregularity criterion. In the examined space frames, m_r equals 2 and 3. The frames have 3, 6 and 9 storeys with 4 bays. An accidental eccentricity of 5% in directions x and y, separately, is taken into account in the design. Table 5 shows the final cross-sections of the 6-storeys and 9-storeys frames, while the three natural periods of these frames are provided in Table 6. Based on Table 6, it is observed that the period of frames increases when the mass discontinuity is located at the upper storeys. Cross-sections for the 3-storeys frames can be found in [22].

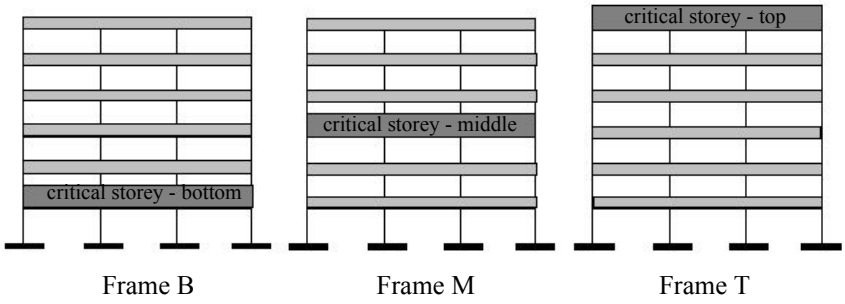

Figure 3. The location of mass discontinuity considered in this study

Table 5. Sections of the 6-storeys and 9-storeys space steel frames of Group C.

*Six storey space MRF							
	$m_r = 2$				$m_r = 3$		
	Frame B				Frame B		
Floor	IPE		SHS	Floor	IPE		SHS
	B_{xe}, B_{ye}	B_{xi}, B_{yi}	C_i, C_e		B_{xe}, B_{ye}	B_{xi}, B_{yi}	C_i, C_e
1	330	360	350x16	1	330	500	350x16
2	330	360	300x16	2	330	360	350x16
3	330	360	300x16	3	330	360	350x16
4	300	330	300x12	4	300	330	300x16
5	300	330	300x12	5	300	330	300x16
6	300	330	300x12	6	300	330	300x16
	Frame M				Frame M		
1	330	360	350x16	1	330	360	350x16
2	330	360	300x16	2	330	360	350x16
3	330	360	300x16	3	330	500	350x16
4	300	330	300x12	4	300	330	300x16
5	300	330	300x12	5	300	330	300x16
6	300	330	300x12	6	300	330	300x16
	Frame T				Frame T		
1	330	360	350x16	1	330	360	400x16
2	330	360	300x16	2	330	360	400x16
3	330	360	300x16	3	330	360	400x16
4	300	330	300x12	4	300	330	350x12
5	300	330	300x12	5	300	330	350x12
6	300	330	300x12	6	300	450	350x12

*$0.19 < \rho < 0.30$ and $4.26 < \alpha < 5.79$

*Nine storey space MRF							
	$m_r = 2$				$m_r = 3$		
	Frame B				Frame B		
Floor	IPE		SHS	Floor	IPE		SHS
	B_{xe}, B_{ye}	B_{xi}, B_{yi}	C_i, C_e		B_{xe}, B_{ye}	B_{xi}, B_{yi}	C_i, C_e
1	300	360	400x16	1	300	500	400x16
2	330	400	400x16	2	330	400	400x16
3	330	400	400x16	3	330	400	400x16
4	330	400	400x16	4	330	400	400x16
5	330	400	400x16	5	330	400	400x16
6	300	360	350x16	6	300	360	350x16
7	270	330	300x12	7	270	330	350x16
8	270	300	300x12	8	270	300	300x12
9	270	300	300x12	9	270	300	300x12
	Frame M				Frame M		
1	300	360	400x16	1	300	400	400x20
2	330	400	400x16	2	330	450	400x20
3	330	400	400x16	3	330	450	400x20
4	330	400	400x16	4	330	450	400x20
5	330	400	400x16	5	330	500	400x16
6	300	360	350x16	6	300	360	400x16
7	270	330	350x16	7	270	330	350x16
8	270	300	300x12	8	270	300	300x16
9	270	300	300x12	9	270	300	300x16

Frame T				Frame T			
1	300	360	400x16	1	330	400	400x20
2	330	400	400x16	2	360	450	400x20
3	330	400	400x16	3	360	450	400x20
4	330	400	400x16	4	360	450	400x20
5	330	400	400x16	5	330	400	400x16
6	300	360	350x16	6	330	360	400x16
7	270	330	350x16	7	300	330	350x16
8	270	330	300x12	8	300	330	300x16
9	270	330	300x12	9	300	450	300x16

*$0.15 < \rho < 0.27$ and $5.04 < \alpha < 6.28$

Table 6. Three first vibration periods of the 6-storeys and 9-storeys space steel frames of Group C.

Frames of Group C					
Frame case (See Figure 3)	Number of storeys	m_r	Period (sec) T_1	T_1	T_1
B	6	2	1.23	1.23	1.10
B	6	3	1.14	1.14	1.05
B	9	2	1.63	1.63	1.53
B	9	3	1.58	1.58	1.52
M	6	2	1.28	1.28	1.15
M	6	3	1.23	1.23	1.14
M	9	2	1.69	1.69	1.60
M	9	3	1.58	1.58	1.56
T	6	2	1.43	1.43	1.28
T	6	3	1.47	1.47	1.33
T	9	2	1.81	1.81	1.71
T	9	3	1.80	1.80	1.68

3. FRAME MODELING AND GROUND MOTIONS FOR INELASTIC ANALYSIS

3.1 Frame modelling

Nonlinear dynamic analyses were performed with the aid of Ruaumoko 3D software (Carr [33]) by taking into account the effect of large displacements. The frame modeling considers simple center-line representation for frame members with a rigid diaphragmatic action at every floor along the frame height. Rayleigh type damping corresponding to 3% of critical damping in the first and n^{th} mode (n is the number of the frame storeys), in conjunction with the tangent stiffness matrix was assumed. The abovementioned damping modeling assumptions are based on the recommendations of [33] to avoid potential unrealistic damping forces that result in underestimation of peak displacement demands and overestimation of peak strength demands. It is noted that for all models, the first and second periods were translational, while the third one was torsional. The use of the first and n^{th} mode in Rayleigh damping definition considers that the effective mass for the first n modes of vibration is at least 90% of the total mass of the structure.

Bilinear elastoplastic hinges were considered at beam and column ends with a strain hardening equal to 3% [33]. This modeling is considered adequate for time-history analysis under design level ground motions [3, 34]. Based on Skalomenos et al. [35], at high seismic intensities, the use of more refined models that capture stiffness and strength deterioration phenomena in beams, columns and panel zone connections is recommended in determining the ductility demands of plane composite frames and smaller behavior factors can be observed than those determined by simplified model assumptions [36]. The influence of the modelling sophistication to the frames under consideration is a subject of continuing study. The M-N interaction effect in three dimensions was taken into account. Considering plastic hinge formation in columns, the effect of the axial force on the plastic moment strength is taken into account through the interaction formulae [27]

$$\frac{N}{N_{pl,Rd}} + \frac{M_y}{M_{pl,y,Rd}} + \frac{M_z}{M_{pl,z,Rd}} = 1.0 \qquad (2)$$

where N, M_y and M_z are the axial force and the bending moments in the cross-section of the column, $N_{pl,Rd}$ is the axial plastic resistance, and $M_{pl,y,Rd}$ and $M_{pl,z,Rd}$ are the plastic moments of resistance. It should be noted that local buckling limits the ability of SHS to form stable plastic hinges and the behavior is highly dependent on the width-thickness (b/t) and the depth-thickness ratio (h/t). Based on the testing results of [37], SHS members subjected to bending due to cyclic loading start deteriorating behavior at 0.04 rad rotation level. This rotational

level is expected to occur at seismic levels beyond the design earthquake. A sufficient rotational capacity and strength of the columns may be achieved through connection detailing, e.g. by using stiffeners, which can lead to stable hysteretic behavior of the columns for the *IDR* values considered in this work, i.e. up to 4%.

3.2 Ground motions

The space steel frames were subjected to 42 pairs of far-fault seismic excitations [38], where a full list of all these ground motions with their characteristics can be found in [22]. Figure 4 depicts the elastic spectra of the ground motion components. The selection of ground motions was based on the comparison between the spectral ordinates of each ground motion against the spectral ordinates of the design basis earthquake at the fundamental period of each frame. In that way the scaling factor of each ground motion can be controlled in order not to take excessive values at higher performance levels. It should be noted that in the literature there are also different procedures for selecting and scaling acceleration histories such as the one described in FEMA P58 [39].

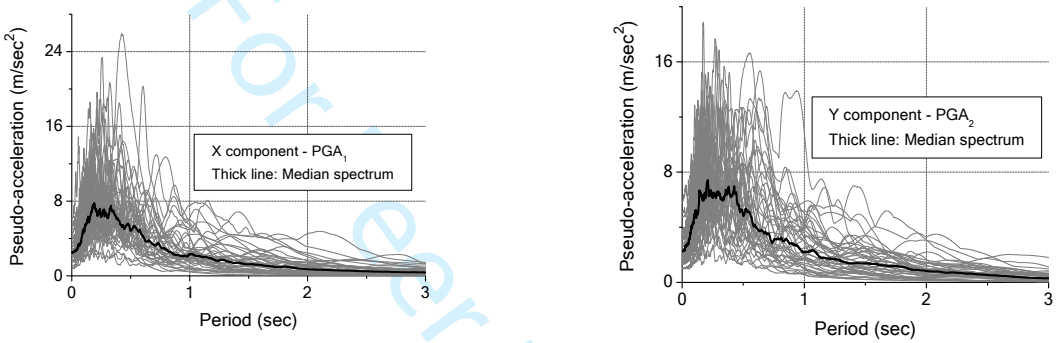

Figure 4. Response spectra for the x and y components of the ground motions.

3.3 Seismic response databank

The seismic response databank of the 88 space irregular MRFs was created by approximately 30000 dynamic nonlinear time histories in the framework of incremental dynamic analysis (IDA). Each IDA analysis subjects the structure to a single ground motion with repeatedly scaling its amplitude. The IDA curve that correlates the peak structural response quantity with the seismic intensity was made. The scaling factors (*SF*) of the ground motion that drives the structure to the four performance levels proposed by SEAOC [40] were identified and recorded for every structure and ground motion pair. Those four performance levels were: (a) formation of first plastic hinge in the frame; (b) peak value for the target interstory drift ratio along the frame height (IDR_{max}) equal to 1.8%; (c) IDR_{max} equal to 3.2 and (d) IDR_{max} equal to 4%. The two components of the 42 ground motions were alternated along the x and y axis of the buildings as those axes were defined in the schematic views of Section 2. The bisection method [21,22,24] was programmed in MATLAB [41] which operated the time history analyses and determined accurately the appropriate scale factor for each performance level (SF_{PL}).

Once the SF_{PL} was known, the response quantities of interest were obtained for each performance level. These were: (1) the roof displacement at the onset of first plastic hinge, $u_{r,y}$, (2) the peak roof displacement, $u_{r,max}$, (3) the IDR_{max}, (4) the maximum local rotational ductility of beams and columns, μ_θ, (5) the maximum roof displacement ductility, μ_r, (6) the behavior factor q, (7) irregularity metrics quantified through indices, e.g. Φ_s and Φ_b; and (8) the fundamental periods of vibration. The μ_θ is defined as $1+\theta_p/\theta_y$, where θ_y and θ_p are the yield chord rotation and the plastic rotation the member's ends, respectively. The μ_r is defined as $u_{r,max} / u_{r,y}$ for each performance level. The corresponding behavior factor q is calculated as the ratio of the SF_{PL} over the SF_y (scale factor that drives the structure to the first yielding) [35,39]. The proposed q factor, unlike the traditional constant q factor used in EC8 [3], is determined for each performance level and depends on the deformation demands in terms of *IDR* and μ_θ. It should be noted that peak floor acceleration (PFA) can be used as an additional performance metric for the non-structural elements, e.g. acceleration sensitive equipment. The inclusion of acceleration measures in HFD method can be considered as an important future development

4. TIME HISTORY ANALYSIS RESULTS

On the basis of the developments and assumptions presented in this work, the current section introduces the seismic behavior of the steel space irregular MRFs under consideration. A discussion on seismic responses for each type of structural irregularity is presented for representative frames. The results highlight the importance of considering the irregularity design parameters and are assessed accordingly to develop the proposed design method. A future goal is to further extend the current design method to other types of building structures with, e.g., strength and stiffness degradation, semi-rigid joints, I sections for columns, or combination of irregularities.

4.1. Space frames irregular in plan view

Figure 5 shows the normalized median of the *IDR* along the height of the 6 and 12 storey frames of Group A. Accordingly, Figure 6 shows the normalized median of the peak values of lateral storey displacements along the frame elevation. Results are shown only for the performance levels of IDR_{max}=1.8% and IDR_{max}=4.0%. For the performance levels at the first plastic hinge and IDR_{max}=3.2% one can look at [22]. It was found that the seismic response is similar along the x or y direction, and therefore, only the results of the x direction are presented. For comparison reasons, the responses of the corresponding regular-in-plan-view frames (with square plan view) are also plotted in these figures (labeled as Reg. Frame). It is noted that an accidental eccentricity of 5% was considered in the design of these regular-in-plan-view frames. An observation of Figures 5 and 6 and the remaining ones in [22], reveals that the response of the frames is similar with a dispersion that increases slightly with the number of storeys. In particular, the response of Frames type 1 – 5 is very similar with the response of the Reg. Frame, indicating that the plan irregularity considered in this study may not play an important role in the seismic response of the frames. However, the response of Frame 6 appears to be the one with the higher difference compared to the rest of frames and requires further investigation. In addition, it is observed from the *IDR* profiles that peak values in tall buildings are recorded in higher storeys. To make the *IDR* distribution more uniform along the frame elevation, a solution could be to increase the beam and/or the column dimensions at the upper floors. However, this may increase the weight of the building disproportionately. Finally, Figure 7 illustrates the normalized median inter-storey twist by the storey height at x and y direction of the 6 storey frames for the performance level with *IDR* = 4.0%. The torsional response is smaller in all Frames 1 – 6 of Figure 1a compared to the torsional response of the Regular Frame, as shown in Figure 7. This result can also demonstrate that the EC8 [3] slenderness λ criterion for regularity in plan is valid, considering that all the other regularity in plan criteria of clause 4.2.3.2 of EC8 [3] are met.

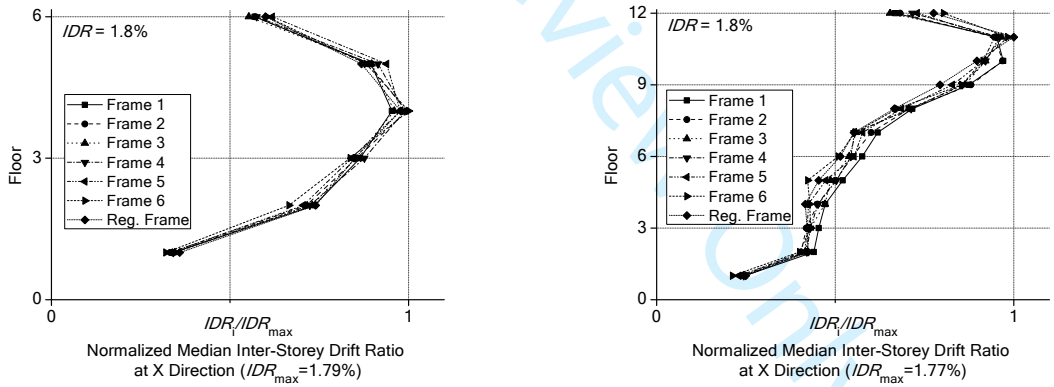

(a)

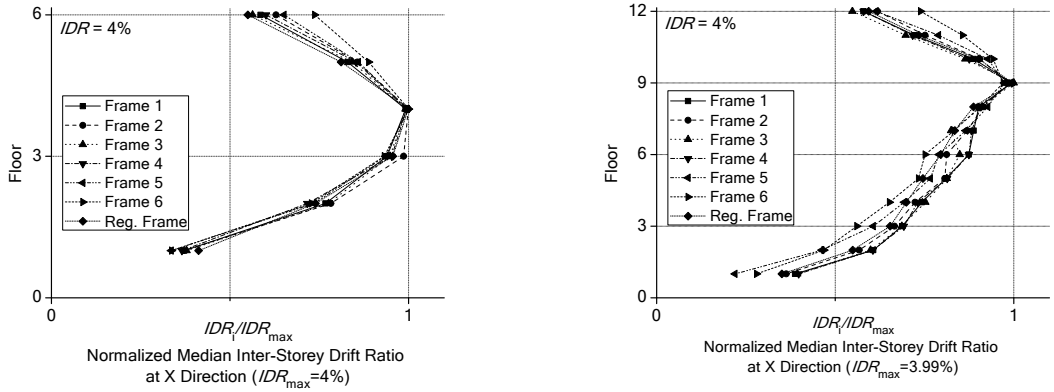

(b)

Figure 5. *IDR* profile of the 6 and 12 storey frames of Group A: (a) first plastic hinge; (b) *IDR* = 1.8%; (c) *IDR* = 3.2%; (d) *IDR* = 4%.

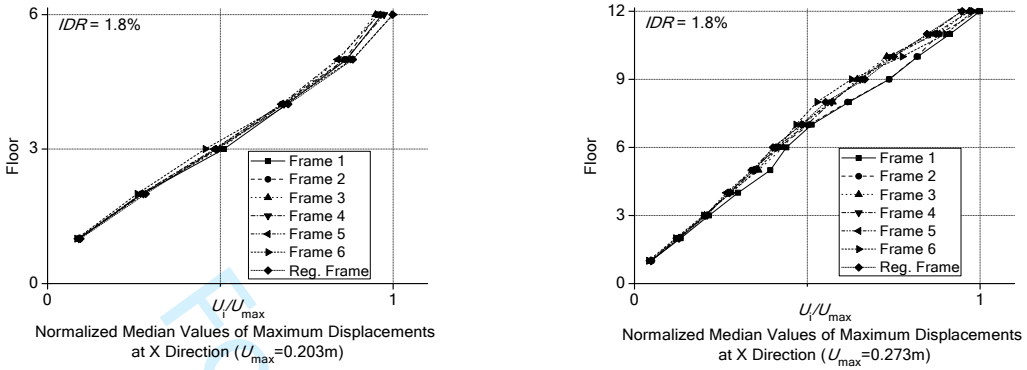

(a)

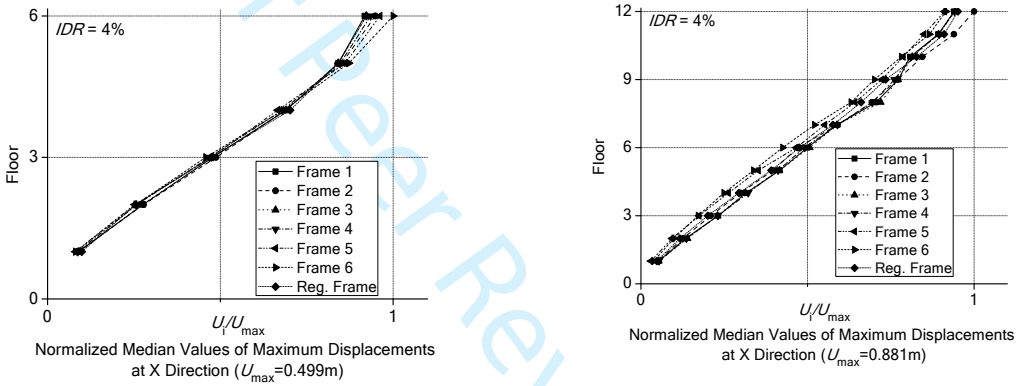

(b)

Figure 6. Floor displacements profile of the 6 and 12 storey frames of Group A: (a) *IDR* = 1.8%; and (b) *IDR* = 4%.

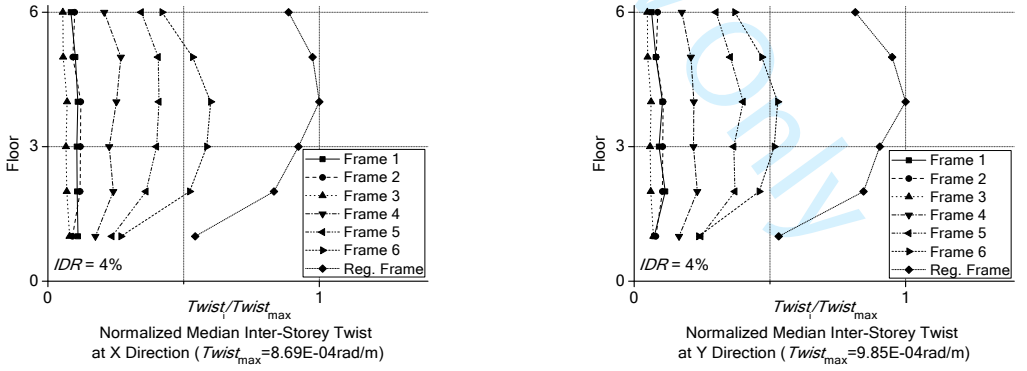

(a) (b)

Figure 7. Normalized median inter-storey twist of the 6-storey frames of Group A: *IDR* = 4.0% at: (a) x direction and (b) y direction.

5.2 Space frames with setbacks along the height

Figure 8 depicts with the same manner as Figures 5 and 6 the lateral storey displacements and *IDR* profiles of the Group B frames, for the first three performance levels. The 6-storey frames (See Figure 2, Frames 6 to 21) are shown in those figures. The figures illustrate the frame responses along the x direction. The displacement and *IDR* profiles were created by using the maximum values obtained from the frame nodes at the perimeter of

each storey. In Figure 8 the responses of Frame 10, 19 and 21 are highlighted with dark marked lines as more representative ones among the 16 six-storey frames, while the remaining frame responses are depicted by light gray lines. For comparison reasons, the responses of the corresponding regular frames (no setbacks and an accidental eccentricity of 5%) are also plotted in those figures (labeled as Reg. Frame).

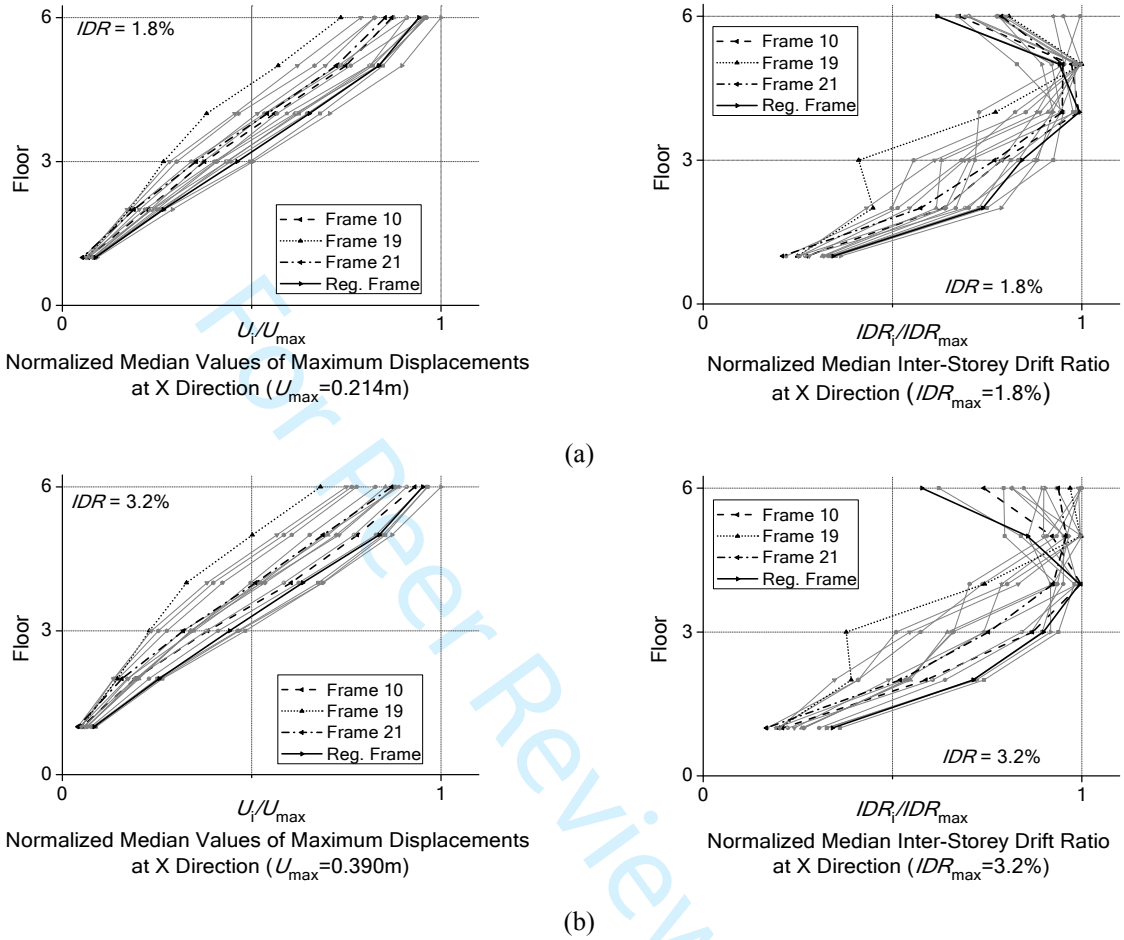

Figure 8. Peak floor displacements and *IDR* profiles of the 6-storey frames of Group B: (a) *IDR* = 1.8%; and (b) *IDR* = 3.2%.

Table 7. Frames exhibiting the minimum and maximum floor displacement along the x and y direction among all the frames of Group B (See Figure 2), including the corresponding regular frame.

3-storey				6-storey				9-storey			
x direction		y direction		x direction		y direction		x direction		y direction	
min	max	min	max	min	max	min	max	min	max	min	max
Frame 5	Regular Frame	Frame 5	Regular Frame	Frame 19	Frame 11	Frame 14	Frame 18	Frame 40	Regular Frame	Frame 39	Frame 26

The indices Φ_s and Φ_b considered here, appear to be adequate to quantify the influence of the setbacks on the dynamic behavior of frames. For all the performance levels, those frames with values of Φ_s and Φ_b close to unity exhibit larger floor displacements than those frames which form a "tower" along their height. This is also observed in Table 7, where the frames that exhibit the minimum and maximum displacement along the x and y direction among all the frames of Group B (including the corresponding regular frame) are summarized. It should be noted that the frame responses along the x direction show a larger dispersion compared with the ones along the y direction because of the flexibility of the "tower" along the x direction.

Figure 8 shows that *IDR* profiles among all the frames have the same shape for the low performance level. In high-damage performance levels, the shape of *IDR* profiles is becoming less uniform due to the inelastic deformations. The dispersion with respect to the amplitudes increases between the lower and higher floors. The

torsional behavior was also found to be larger in all frames of Group B compared to the torsional behavior of the Reg. Frame. Figure 9 illustrates the normalized median inter-storey twist by the storey height for the 6-storey and 9-storey frames associated with *IDR* = 3.2% along the x direction.

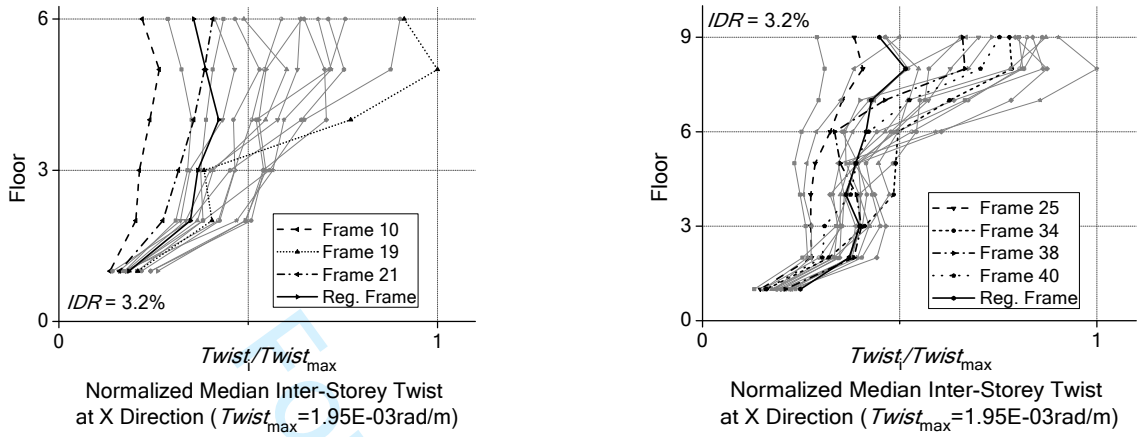

(a) (b)

Figure 9. (a) Normalized median inter-storey twist of the 6-storey; and (b) 9-storey frames of Group B associated with *IDR* = 3.2% along the x direction.

Frame structures with setbacks along their height are expected to exhibit a larger level of damage compared to the corresponding regular structures. To further justify this discussion on the frame considered, the inelastic behavior of the frames of Group B was evaluated for a common level of seismic intensity by conducting time-history nonlinear analyses with five pairs of semi-artificial accelerograms. The accelerograms were generated to be compatible to the elastic design spectrum of EC8 [3] (PGA = 0.36g and soil class B) in order to evaluate the response of the frames under a seismic intently beyond the design-based level. The two components of the artificial motions shown in Figure 10 were alternated in x and y direction, respectively. The analyses were performed for 10 of the 40 frames shown in Figure 2c (Frame 3, 4, 5, 10, 19, 21, 25, 34, 40) and their corresponding regular frames (labeled as R). Figure 11 shows bar charts of the results in terms of IDR_{max} and μ_θ for the 6-storeys and 9-storeys frames along the x and y direction.

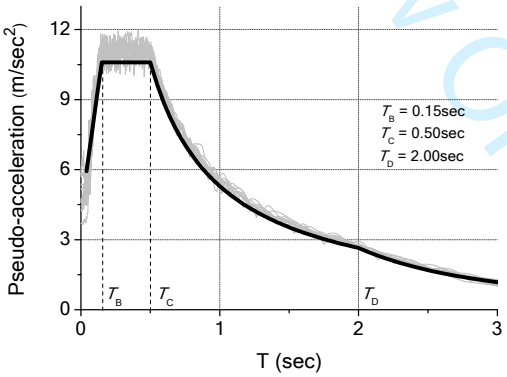

Figure 10. Response spectra of the semi-artificial ground motions.

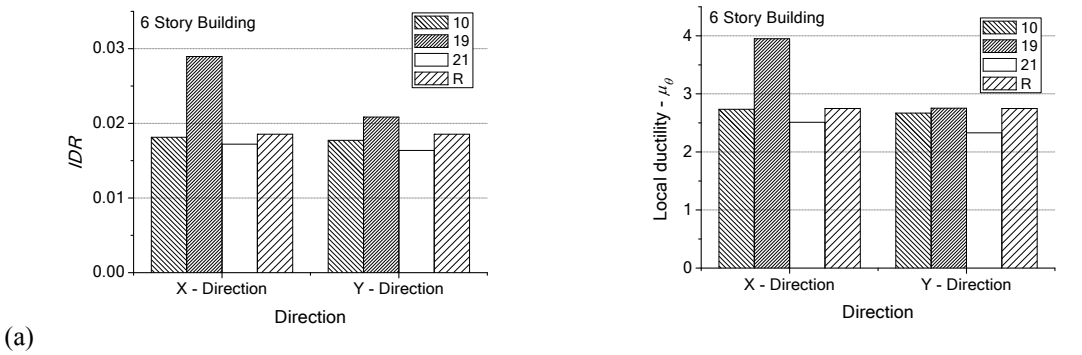

(a)

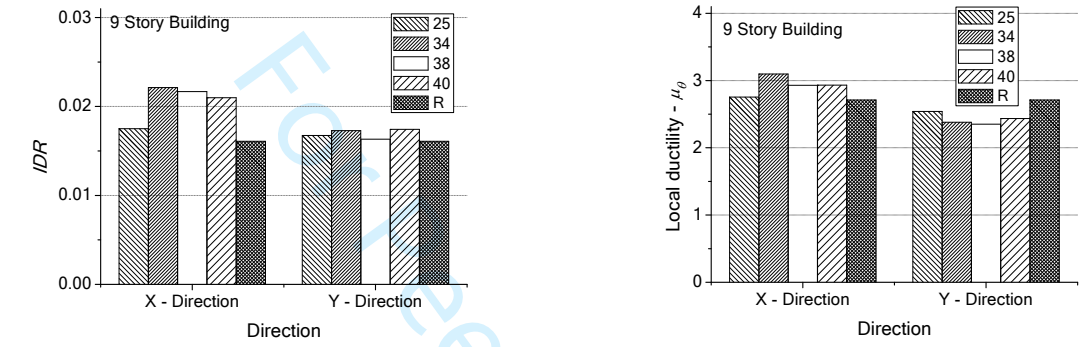

(b)

Figure 11. IDR_{max} and μ_θ along the x and y direction for the: (a) 6-storey [Frames 10, 19, 21]; and (c) 9-storey frames [Frames 25, 34, 38, 40] of Group B.

It is observed from Figure 11 that frames with setbacks experienced a larger damage along the x direction, while along the y direction regular frames often exhibited a larger level of damage than the irregular frames. In addition, regarding the x direction, increasing the height of the frames leads to an increase of drift and ductility demands for all irregular frames as compared with the regular ones.

5.3. Space frames with mass irregularity along their height

Figure 12 shows peak lateral storey displacements and *IDR* profiles in elevation of the 6-storey frames of Group C, for the two performance levels. The remaining performance levels can be found in [22]. For comparison reasons, the responses of the corresponding regular frames (no mass discontinuity and an accidental eccentricity of 5%) are also plotted in these figures (labeled as R). It is observed that the regular frames exhibited a larger displacement and *IDR* profile at the onset of the first plastic hinge compared with the irregular ones. Only the case of Frame T2 (mass discontinuity is at the top storey and mass ratio $m_r = 2.0$) provides with slightly higher values at the top storeys. The same trend with the results of the 6-storey frames is observed for the 3-storey and 9-storey frames.

The 6-storey and 9-storey frames behaved in a similar way at higher performance levels. In general, smaller displacements exhibited in frames with the mass discontinuity at the top storey (T) of the frame, followed by the frames with the mass discontinuity at the bottom storey (B) of the frame, and then by those with the mass discontinuity at the middle storey (M) of the frame. On the contrary, in case of 3-storey frames, the trend appears to be different. Frames with the mass discontinuity at the top storey (T) exhibited larger displacements.

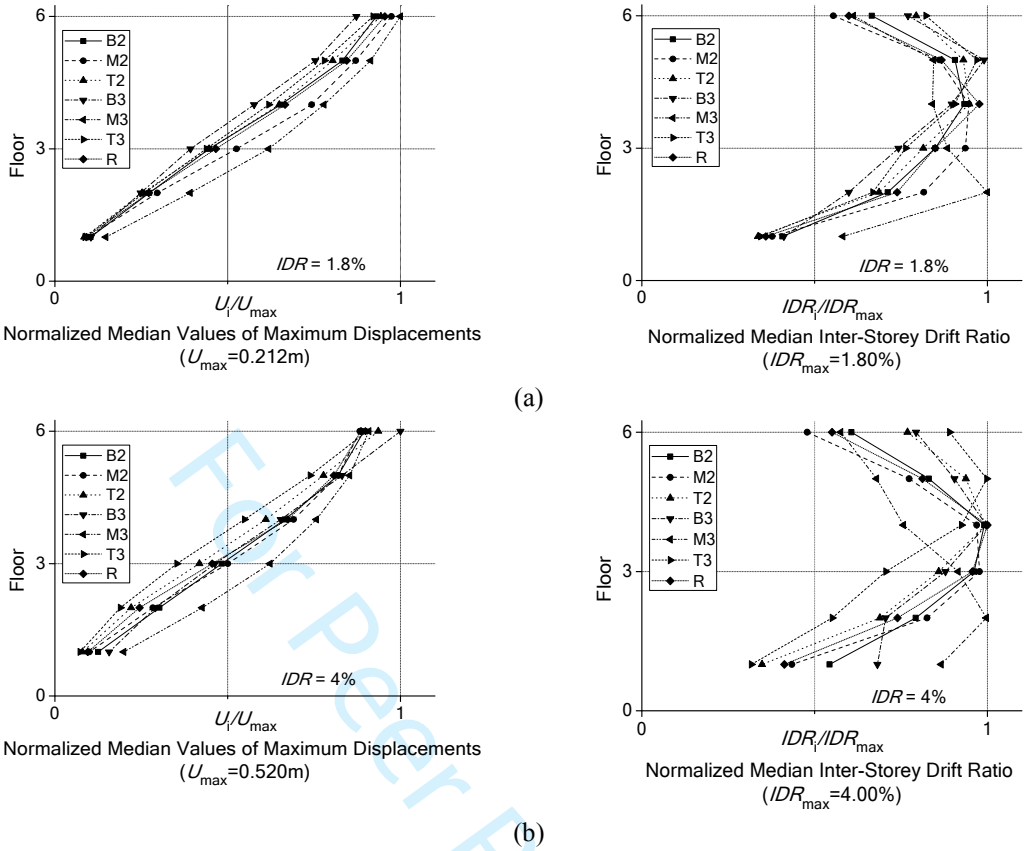

Figure 12. Peak floor displacements and *IDR* profiles of the 6-storey frames of Group C: (a) *IDR* = 1.8%; (b) *IDR* = 4.0%

5. HFD DESIGN METHOD

The HFD method [21-24] determines the roof displacement $u_{r,max(d)}$ at design as the minimum of the peak roof displacements $u_{r,max(IDR)}$ and $u_{r,max(\mu)}$ which correspond to non-structural and structural deformation respectively,

$$u_{r,max(d)} = \min\left(u_{r,max(IDR)},\ u_{r,max(\mu)}\right) \tag{3}$$

The roof ductility $\mu_{r,d}$ as the design quantity is then determined as

$$\mu_{r,d} = \frac{u_{r,max(d)}}{u_{r,y}} \tag{4}$$

The designer can obtain $u_{r,y}$ by conducting an elastic strength-based design (q=1) for frequent earthquake. The behavior factor q is given as a function of $\mu_{r,d}$.

In this section, empirical formulae for $u_{r,max(IDR)}$, $u_{r,max(\mu)}$ and q as functions of basic geometrical/dynamical characteristics of the frames are developed by a nonlinear regression analysis in MATLAB [41]. By analyzing the created response databank of frames with irregular plan view (Group A), $u_{r,max(IDR)}$ is expressed as

$$u_{r,max(IDR)} = b_1 \cdot H \cdot IDR^{b_2} \tag{5}$$

where *IDR* is the targeted interstory drift ration and *H* is the height of the frame (in m). The parameters b_1 and b_2 are provided in Table 8. By analyzing the response databank of frames with setbacks along the height (Group B), the ratio $\beta = u_{r,max(IDR)} / (H \cdot IDR)$ was found to be the most representative parameter to quantify the design demand. The ratio β is calculated by

$$\beta = 1 - b_1 \cdot (n_s - 1)^{b_2} \cdot \Phi_s^{b_3} \cdot \Phi_b^{b_4} \tag{6}$$

where constants b_1, b_2, b_3, and b_4 are given in Table 9 for motions along the x and y directions. Equation (6) is simple and satisfies the natural condition $\beta = 1$ for $n_s = 1$. By analyzing the response databank of frames with

mass discontinuities along the height (Group C), the $u_{r,max(IDR)}$ can be expressed as in Eq. (5). The parameters b_1 and b_2 are given in Table 10 with respect to the storeys number and the location of mass discontinuity (bottom, middle, or top).

With *IDR* to be known, the ratio $u_{r,max,app}/u_{r,max,exact}$ is taken for all irregular frames. The "appx" subscript stands for the word "approximate" and refers to the value obtained by the empirical Eqs (5) and (6), while the "exact" subscript refers to the seismic response databanks. The mean, median and standard deviation (Stdev) values are also provided. For the frames of Group A, Eq. (5) provides a mean value equal to 1.04, median value equal to 0.99 and dispersion value equal to 0.30 for the ratio $u_{r,max,app}/u_{r,max,exact}$. The same equation for the frames of Group C provides a mean value equal to 1.01, median value equal to 0.98 and dispersion value equal to 0.26 for the ratio $u_{r,max,app}/u_{r,max,exact}$. Similar results can be obtained from the use of Eq. (6) for the frames of Group B.

Table 8. Values of parameters b_1 and b_2 of Eq. (5) for steel space frames with irregular plan view

Number of storeys	$IDR_y - IDR_{1.8\%}$		$IDR_{1.8\%} - IDR_{3.2\%}$		$IDR > IDR_{3.2\%}$	
	b_1	b_2	b_1	b_2	b_1	b_2
3	0.84	1.01	1.03	1.06	0.99	1.05
6	0.37	0.88	0.93	1.11	1.51	1.25
9	0.29	0.88	2.07	1.37	2.38	1.41
12	0.28	0.91	1.46	1.32	5.58	1.71
15	0.22	0.89	5.04	1.67	6.88	1.76

Table 9. Values of parameters $b_1 - b_4$ of Eq. (6) for steel space frames with setbacks

Direction	b_1	b_2	b_3	b_4
x	0.18	0.36	0.85	0.24
y	0.18	0.36	0.17	0.10

Table 10. Values of parameters b_1 and b_2 of Eq. (5) for steel space frames with mass discontinuities

Number of storeys	Location of mass discontinuity	b_1	b_2
3	B	0.83	1.01
	M	0.83	1.01
	T	1.26	1.11
6	B	1.16	1.17
	M	0.72	1.03
	T	0.82	1.07
9	B	1.95	1.34
	M	1.47	1.24
	T	1.38	1.27

The $u_{r,max(\mu)}$ can be estimated from

$$u_{r,max(\mu)} = \mu_{r,\theta} \cdot u_{r,y} \tag{7}$$

where $\mu_{r,\theta}$ is the maximum ductility of the top storey with respect the μ_θ and can be calculated for the frames with irregular plan view (Group A) as

$$\begin{aligned} \mu_{r,\theta} &= 1 + 0.81 \cdot (\mu_\theta - 1) \qquad \text{for } \mu_\theta \le 4.68 \\ \mu_{r,\theta} &= 2.58 + 0.38 \cdot (\mu_\theta - 1) \qquad \text{for } \mu_\theta > 4.68 \end{aligned} \tag{8}$$

and for the frames with setbacks (Group B) and vertical mass discontinuities (Group C) as

$$\mu_{r,\theta} = 1 + b_1 \cdot (\mu_\theta - 1)^{b_2} \tag{9}$$

Table 11a and b provides the constants b_1 and b_2 respectively. Eq. (8) provides a mean value equal to 0.94, median value equal to 0.94 and dispersion value equal to 0.24 for the ratio $\mu_{r,\theta,app}/\mu_{r,\theta,exact}$. For the Group B frames, Eq. (9) provides a mean value equal to 1.02, median value equal to 0.97 and dispersion value equal to 0.28 for the ratio $\mu_{r,\theta,app}/\mu_{r,\theta,exact}$, while for the Group C frames and the same ratio, Eq. (9) provides a mean value equal to 1.04, median value equal to 1.02 and dispersion value equal to 0.24.

Table 11. Values of constants b_1 and b_2 of Eq. (9) for:

(a) Steel space frames with setbacks		
Direction	b_1	b_2
x and y	0.79	1.00
(b) Steel space frames with mass discontinuities		
Location of mass discontinuity	b_1	b_2
B	1.22	0.60
M	1.17	0.59
T	1.26	0.61

As it was mentioned in the Section 3.3, the behavior factor q was defined as $q = SF_{IDR} / SF_y$. Figure 13a illustrates schematically the relation of behavior factor q versus the targeted *IDR* for the 6-storey space frames of Group A, while Figure 13b plots the median values of all frames for each type of irregular plan-view introduced in Figure 1a. Number of storeys had no influence on q. The *q*-*IDR* relation did not significantly differ from the corresponding one for regular frames for the case studies examined in the present work. Moreover, the period of vibration and frequency of the ground motion was found to not have a significant effect on the *q*-*IDR* relation. A similar finding is also valid for the Groups B and C frames.

For the Group B frames there is an influence of the torsional response on the *q*-*IDR* relation as it is shown in Figure 14. Figures 14a and 14b show the *q*-*IDR* relation along the x and y direction, respectively, for some representative Group B fames and the corresponding regular frames. Figure 14 shows the median values for the four performance levels considered here. Having as reference the trend of the regular frame, a large dispersion of the *q*-*IDR* relation for the frames with setbacks is observed. Figure 15 illustrates the relation of behavior factor q with the *IDR* for mass ratio $m_r = 2$. Figure 15a shows the *q*-*IDR* relation of the 6-storey frames of Group C for the three cases of mass discontinuity considered against the corresponding regular frame, while Figure 15b the *q*-*IDR* relation of the 3-storey, 6-storey and 9-storey frames where the mass discontinuity is located at the middle storey (M) of the frames. The trend of the *q*-*IDR* relation was found to be similar for mass ratio $m_r = 3$. For frames with a mass discontinuity along their height, a larger behavior factor q than the corresponding one for regular frames can be used to satisfy the targeted *IDR*, as shown in Figure 15a. Accordingly, the q factor increases also with the number of storeys for a given level of performance, as shown in Figure 15b. Table 12 summarizes the median values of scale factors (SF) used in time-history analyses to drive the frames of Group C to reach the target performance level. Only results for the *IDR* = 1.8% and *IDR* = 4.0% performance levels are provided. Results for the remaining performance levels can be found in [22]. It is concluded that frames with a mass discontinuity along their height satisfy the various performance levels for a lower seismic intensity than the corresponding regular frames, since the SF is smaller for the former case study. It should be noted here that the design of the frames affects the analysis results and could lead into a different conclusion. More frame cases should be examined in the future with additional mass discontinuities to generalize the abovementioned findings.

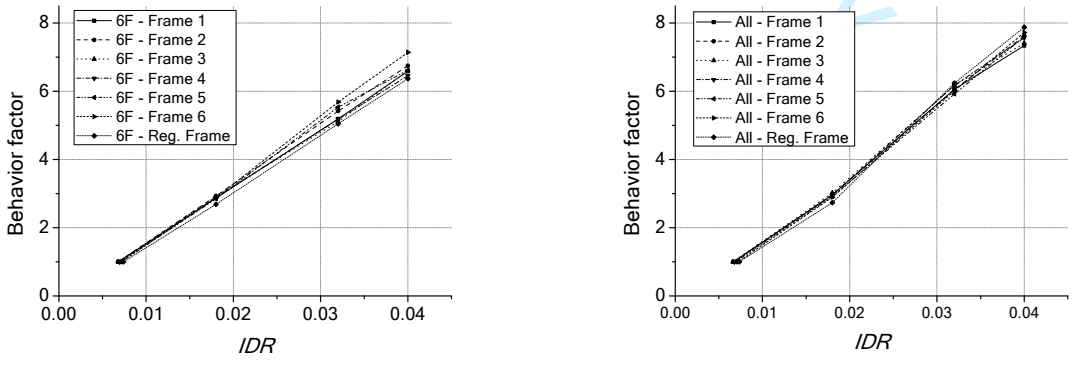

(a) (b)

Figure 13. Behavior factor q versus *IDR* for the frames of Group A: (a) 6-storey frames; and (b) all frames (median values)

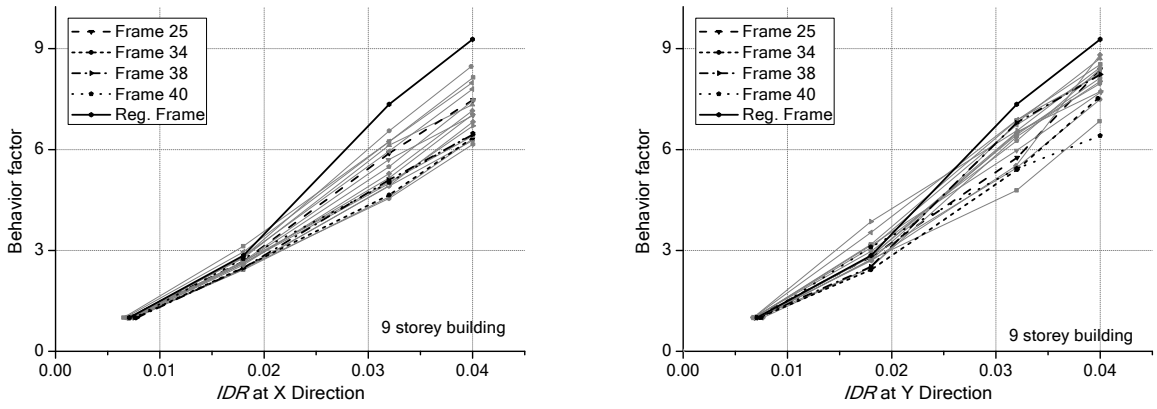

(a) (b)

Figure 14. Behavior factor q versus IDR for the 9-storey frames of Group B at: (a) along x direction; and (b) along y direction

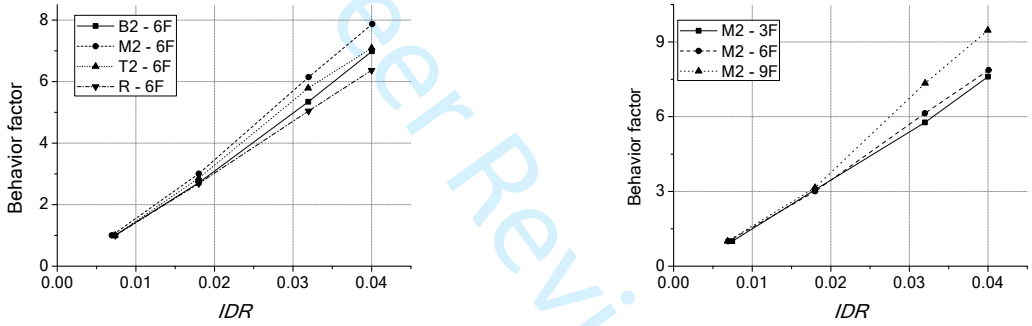

(a) (b)

Figure 15. Behavior factor q versus IDR for mass ratio $m_r = 2$: (a) 6-storey frames of Group C for the three cases of mass discontinuity considered against the corresponding regular frame; (b) 3-storey, 6-storey and 9-storey frames where the mass discontinuity is located at the middle storey (M) of the frames.

Table 12. Median values of scale factors (SF) that correspond to performance levels IDR = 1.8% and IDR = 4.0% for the Group C frames.

Performance level	Design case	Scale Factor (SF) 3 storey	6 storey	9 storey
	B2	1.74	1.97	1.85
	M2	2.02	2.02	2.19
	T2	1.97	2.04	2.10
IDR=1.8%	B3	1.91	1.91	1.70
	M3	2.03	2.27	1.87
	T3	2.14	2.04	1.70
	R	**1.76**	**1.87**	**2.00**
	B2	3.49	3.71	4.03
	M2	3.14	3.81	3.89
	T2	3.07	3.61	3.53
IDR=4%	B3	2.87	3.56	3.49
	M3	3.47	3.80	4.32
	T3	3.24	3.75	3.29
	R	**3.34**	**4.01**	**4.32**

Table 13. Values of parameters b_1 and b_2 for: Eqs (11) and (12).

(a) Steel space frames with setbacks – Eq. (11)			
Direction	b_1	b_2	b_3
x	1.39	1.05	-0.06
y	1.39	1.05	-0.34
(b) Steel space frames with mass discontinuities – Eq. (12)			
Location of mass discontinuity	b_1	b_2	
B	1.38	1.00	
M	1.50	1.00	
T	1.43	1.00	

The expression providing q was found to be of the form

$$q = 1 + 1.35 \cdot (\mu_r - 1) \quad \text{for the frames of Group A} \tag{10}$$

$$q = 1 + b_1 \cdot (\mu_r - 1)^{b_2} \cdot \Phi_s^{b_3} \quad \text{for the frames of Group B} \tag{11}$$

$$q = 1 + b_1 \cdot (\mu_r - 1)^{b_2} \quad \text{for the frames of Group C} \tag{12}$$

where the parameters b_1 and b_2 of Eqs (11) and (12) are obtained from Table 13 and μ_r is the $\mu_{r,d}$ of Eq. (4). Equations (10), (11) and (12) fulfill the condition q=1 for μ_r=1. These equations show that the equal-displacement rule of EC8 [3] overestimates the peak floor displacements.

The proposed equations can be applied to frames with stiffness parameter ρ and strength parameter α within their minimum and maximum values in Section 2. The created database can be further increased by considering buildings which will be designed using different values of behavior factor q. This will also contribute to the inclusion of the ρ and α parameters in the proposed equations and further development of the regression coefficients considered in this work. It should be also noticed that based on the analysis results no effect of the period of vibration and frequency content of the ground motion on the relationship between q and μ_r, $u_{r,max}$ and IDR_{max}, μ_r and μ_θ was identified and for this reason their effect has not been included in all proposed equations. In addition, the inclusion of peak floor acceleration as an additional performance metric of the HFD method can further control non-structural damage as well as residual drifts in the design equations and provide useful information for estimating potential losses and repair costs at different performance levels.

Figure 16 shows graphically Eqs (10) and (11) for the Group A and B frames together with the corresponding databank results and the equal displacement rule, while in Figure 18b the q-μ_r relation introduced in [11] for planar frames with setbacks is also plotted here for comparison reasons assuming Φ_s = 2. Accordingly, Figure 17 plots Eq. (12) for the Group C frames together with the corresponding databank results, the equal displacement rule and the relations introduced in [19] for planar frames with vertical mass discontinuities. Figures 16 and 17 show higher dispersion in the q value at higher roof ductility levels which can be related to the variability induced from each seismic record. The present results appear to be more accurate than those of EC8 [3], which overestimates ductility demands in all cases.

Furthermore, for a realistic range of q (less than 8), the comparison in Figures 16 and 17 of the proposed q-μ_r relations for space irregular frames to the corresponding relations for planar irregular frames, reveal a difference in their seismic response. For a targeted level of seismic performance, space frames require higher ductility demands and lower behavior factors than the corresponding planar ones. This finding is in accordance with the current design codes [3], where a proper reduction on the behavior factor is recommended for space irregular structures for which torsional response plays an important role. A larger lateral resistance seems to be required in order to control the seismic response of these type of structures.

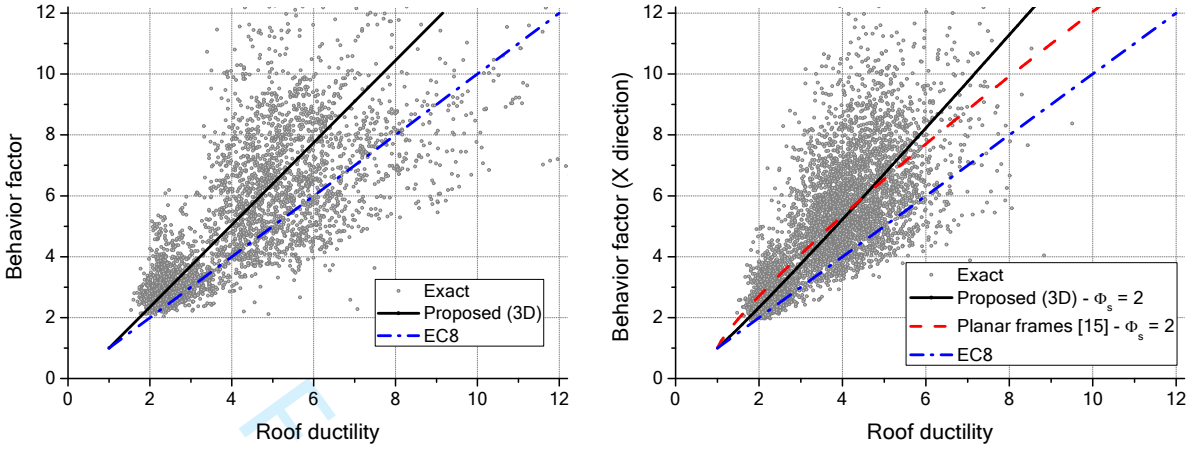

(a) (b)

Figure 16. Graphical depiction of the response databank results and approximation by the proposed relation for space MRFs. Comparison with the proposed in [11] relation for planar MRFs and the equal-displacement rule (EC8 [3]), for the case of frames with: (a) irregular plan view (Group A); (b) setbacks (Group B) with $\Phi_s = 2$.

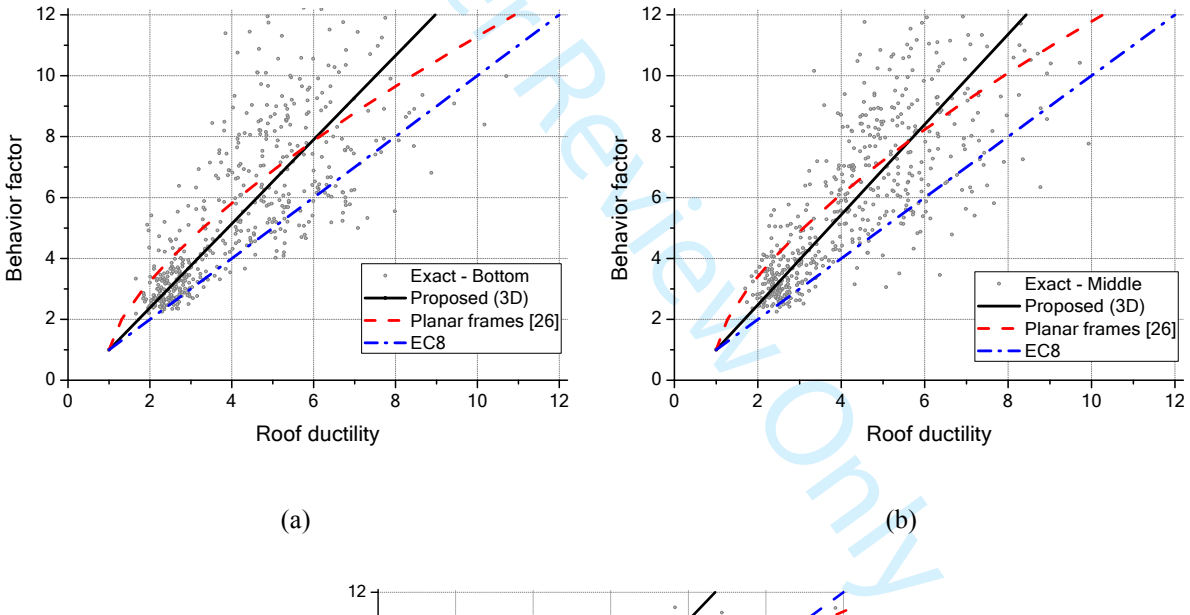

(a) (b)

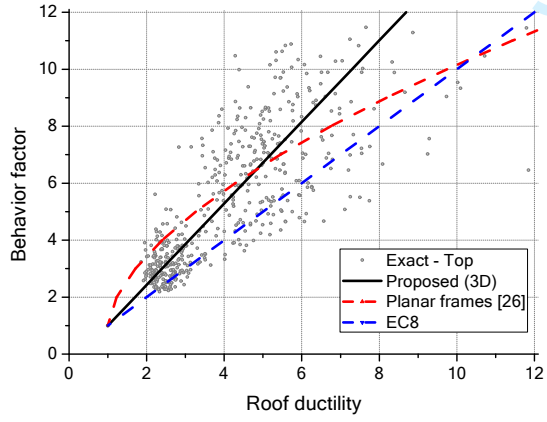

(c)

Figure 17. Graphical depiction of the response databank results and approximation by the proposed relation for space MRFs. Comparison with the proposed in [19] relation for planar MRFs and the equal-displacement rule (EC8 [3]) for the frames with vertical mass discontinuities (Group C) on: (a) bottom floor; (b) middle floor; and (c) top floor.

6. SEISMIC DESIGN EXAMPLES

This section utilizes the developed relationships within the framework of the HFD seismic design method [21-24] for designing the three space steel irregular frames shown in Figure 18. The frames were first designed according to EC8 [3] and EC3 [27] provisions assuming the same grade of steel and load combinations as those introduced in Section 2. All buildings have 3m storey height and 6m bay width in both directions (Figure 18). The performance levels for seismic design are: (a) IO (Immediate Occupancy) under the FOE (Frequently Occurring Earthquake), (b) LS (Life Safety) under the DBE (Design Basis Earthquake), (c) CP (Collapse Prevention) under the MCE (Maximum Considered Earthquake). Figure 19 shows the Type 1 (soil class B) elastic design spectra of EC8 [3] for the FOE, DBE and MCE levels. For the DBE level, the peak ground acceleration (PGA_{DBE}) was taken equal to 0.36g. The PGAs under the FOE and the MCE were taken equal to 0.25 x PGA_{DBE} and 1.5 x PGA_{DBE}, respectively. Based on ASCE 41-13 [42], the *IDR* and μ_θ should be lower than 0.7% and 1.0 under the FOE, lower than 2.5% and 9.0 under the DBE and lower than 5.0% and 11.0 under the MCE, respectively. Table 14 summarizes all the relevant information of the design.

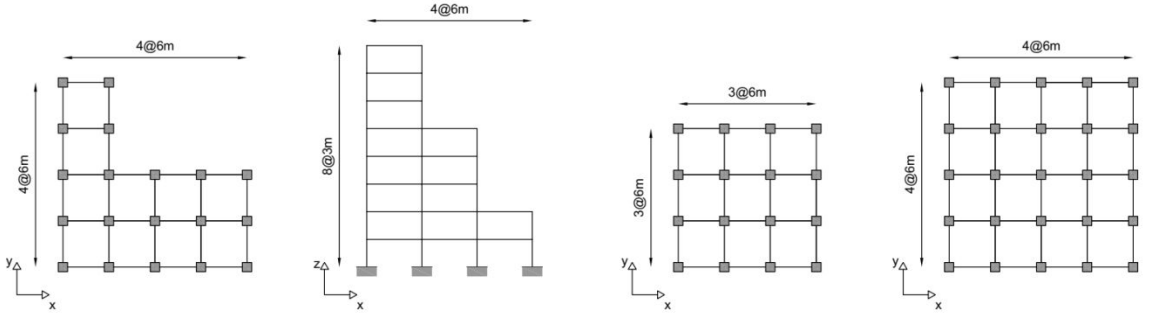

(a) (b) (c)

Figure 18. Building structures considered here for the design examples: (a) 6-storey space frame with L-shaped plan view; (b) 8-storey setback space frame; and (c) 9-story space frame with a vertical mass irregularity at 5th floor.

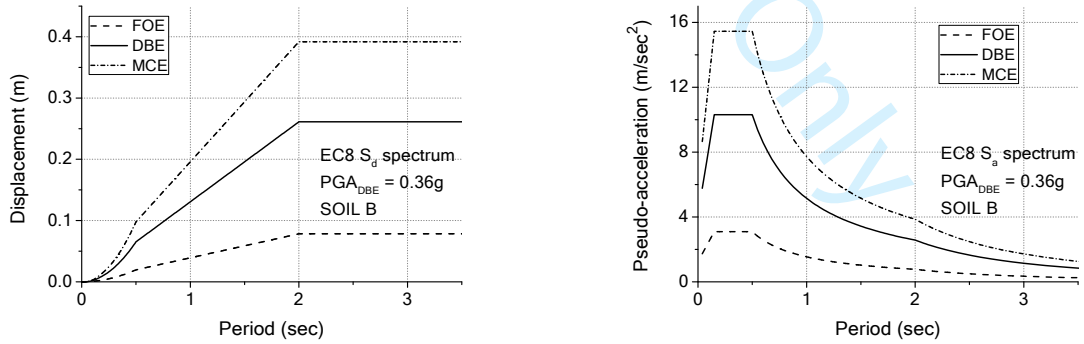

(a) (b)

Figure 19. Design spectra of EC8 [3] for soil class B and PGA_{DBE} = 0.36g: (a) displacement design spectra; (b) pseudo-acceleration design spectra.

Table 14. Types and steel grade for designed frames (3* means that the 5th floor has a mass three times larger the one of the adjacent floors)

Design Example	Storeys Number	Lateral-resistant system	PGA_{DBE}	Metrics of Irregularity			Grade of steel
				Φ_s	Φ_b	Mass	Beam - Column
1	6	MRF with L shaped plan	0.36g	-	-	-	S235 – S355

2	8	MRF Setback	0.36g	1.21	2.05	-	S235 – S355
3	9	MRF Mass Irregular	0.36g	-	-	3*	S235 – S355

6.1. Six storey space MRF with L shaped floor plan.

Figure 18a illustrates a six storey space MRF with L shaped floor plan. The story height is 3.0 m. Table 15 provides the sections under a first elastic design for the FOE and the natural periods. The fundamental period is translational and equal to 1.24 sec. Considering that the initial FOE design is to determine the yielding roof displacement, $u_{r,y}$ equals to 0.076 m and IDR_y = 0.58%. This value of *IDR* fulfils the limit states of IO performance level as defined in ASCE 41-13 [42]. The designed structure is further assessed for the LS and the CP performance levels. For estimating the frame response under the DBE, the behavior factor q in DBE level can be taken from PGA_{DBE}/PGA_{FOE} = 4.00. By using Eq. (10) and Eq. (4), $\mu_{r,d} = (4\text{-}1)/1.35+1 = 3.22$ and $u_{r,max} = 0.076\times3.22 = 0.245$ m, respectively. By employing Eq. (8) and Eq. (5), $\mu_\theta = (3.22\text{-}1)/0.81+1 = 3.74$ and $IDR_{max} = (0.245/(3\times6\times0.93))^{1/1.11} = 2.22\%$, respectively. For estimating the frame response under the MCE, the factor q in MCE level can be taken from $(PGA_{MCE}/PGA_{DBE})\times q_{DBE} = 6$. Accordingly, by using Eq. (10) and Eq. (4), $\mu_{r,d} = (6\text{-}1)/1.35+1 = 4.7$ and $u_{r,max} = 0.076\times4.7 = 0.357$ m, respectively. By employing Eq. (8) and Eq. (5), $\mu_\theta = (4.7\text{-}2.58)/0.38+1 = 6.58$ and $IDR_{max} = (0.357/(3\times6\times0.93))^{1/1.11} = 3.12\%$, respectively. In the view of the above results and considering the limit values of ASCE 41-13 [42], one can observe that the frame design which fulfils the IO performance level fulfils the LS and CP requirements as well.

A second design is made for the LS performance level. The target values of the IDR_{max} and μ_θ are equal to 2.5% and 9, respectively (ASCE 41-13 [42]). Eq. (5) estimates the target roof displacement $u_{r,max(IDR)}$ as $3\times6\times0.93\times0.025^{1.11} = 0.279$ m. Then, the target roof displacement ductility $\mu_{r,IDR}$ is estimated by employing Eq. (4) as 0.279/0.076 = 3.67. By using Eq. (8), the target local rotational ductility $\mu_{r,\theta}$ is calculated as $2.58+0.38\times(9\text{-}1) = 5.62$. The design roof ductility $\mu_{r,d}$ is determined by taking the minimum values of $\mu_{r,IDR}$ and $\mu_{r,\theta}$ and is equal to the min (3.67, 5.62) = 3.67. It is found that drift controls the LS performance level. For a SDOF system with the same period as the designed frame (T_1 = 1.24 sec), the peak displacement can be determined from the DBE displacement design spectrum shown in Figure 19a and is equal to 0.165 m. Then, this displacement is increased to account for the frame response. The calculations give $0.165\times1.4 = 0.231$ m, where the multiplier 1.4 is proposed by ASCE 41-13 [42] for six storey buildings. The estimated roof displacement appears to be smaller than the $u_{r,max(IDR)}$ = 0.279 m, and the target values of the IDR_{max} and μ_θ for DBE performance level require revision according to [25,27]. By revising the target displacement to 0.231 m, the target values of IDR_{max} and μ_θ for this design example should be around 2.11% and 3.52, respectively, based on the Eqs. (4), (5) and (8). Based on Eq. (10) and implementing the new values of IDR_{max} and μ_θ, the required behavior factor q is calculated equal to 3.75. The designer performs a response spectrum analysis using the DBE design spectrum (Figure 19b) reduced by the obtained q factor. The resulted cross-sections are the same as the ones determined in IO level (Table 15).

A third design is prepared for the CP performance level. The target values of the IDR_{max} and μ_θ are equal to 5% and 11, respectively (ASCE 41-13 [42]). Eq. (5) estimates $u_{r,max(IDR)} = 3\times6\times1.51\times0.025^{1.25} = 0.643$ m. Then, by using Eq. (4), $\mu_{r,IDR} = 0.643/0.076 = 8.46$. Based on Eq. (8), $\mu_{r,\theta} = 2.58+0.38\times(11\text{-}1) = 6.38$. Thus, the $\mu_{r,d}$ is equal to 6.38. It is found here that local ductility controls the CP performance level and $u_{r,max(d)} = u_{r,max(\mu)} = 6.38\times0.076 = 0.485$ m. Based on the MCE displacement design spectrum shown in Figure 19a and the assumption of the SDOF system introduced before, the maximum displacement is found to be $0.248\times1.4 = 0.347$ m. The estimated roof displacement appears to be smaller than the $u_{r,max(IDR)}$ = 0.485 m, and the target values of the IDR_{max} and μ_θ for the MCE performance level require revision. By revising the target displacement to 0.347 m, the target values of IDR_{max} and μ_θ for this design example should be around 3.04% and 6.24, respectively, based on the Eqs. (4), (5) and (8). The required behavior factor q = 5.82 based on Eq. (10). The designer performs a response spectrum analysis using the MCE design spectrum (Figure 19b) reduced by the obtained q factor. The resulted cross-sections are the same as the ones determined in IO level (Table 15). In the view of the above results, one can observe that IO performance level determines the frame dimensions in the current example.

The conventional FBD method [3, 27] using a behavior factor $q = 6.5 \times 0.8 = 5.2$ is also applied to design the current space irregular MRF. The obtained cross-section and first three natural periods are given in Table 15. It is observed that the LS performance level determines the frame dimension in the FBD (EC8 [3]). The frame behaves elastically under FOE and it is expected to experience $u_{r,y}$ = 0.073 m and IDR_{max} = 0.55%. Accordingly, under the DBE the $u_{r,max}$ can be computed as $0.073\times PGA_{DBE}/PGA_{FOE} = 0.292$ m and the IDR_{max} as $0.55\%\times PGA_{DBE}/PGA_{FOE} = 2.20\%$. Under the MCE the $u_{r,max}$ can be computed as $0.292\times PGA_{MCE}/PGA_{DBE} = 0.438$ m and the IDR_{max} as $2.20\%\times PGA_{MCE}/PGA_{DBE} = 3.30\%$.

6.2. *Eight storey setback steel space MRF*

Figure 18b illustrates a steel space MRF with setbacks consisting of eight storeys of height 3.0m each. According to Eq. (1), the values of the indexes Φ_s and Φ_b of the MRF are equal to 1.21 and 2.05, respectively. Eq. (6) determines a value equal to 0.49 for the parameter β. As was mentioned in Section 4.2, based on the analyses results of this work, in most cases the direction with setback determines the performance level and thus only the equations of that direction are considered in this example. Table 16 provides the sections under FOE and the natural periods. The fundamental period is translational. The $u_{r,y}$ equals 0.079 m, while IDR_y equals 0.58% satisfying the IO level [42]. The q factor of the frame in DBE is 4.00. By using Eq. (11) and Eq. (4), $\mu_{r,d} = ((4\text{-}1)/(1.39\times1.21^{-0.06}))^{1/1.05} + 1 = 3.10$ and $u_{r,max} = 3.10\times0.079 = 0.245$ m, respectively. By employing Eq. (9) and Eq. (6), $\mu_\theta = (3.10\text{-}1)/0.79+1 = 3.66$ and $IDR_{max} = u_{r,max} / (H\times\beta) = 2.07\%$, respectively. For estimating the frame response under the MCE, the q factor for the space MRF is 6. Accordingly, by using Eq. (11) and Eq. (4), $\mu_{r,d} = ((6\text{-}1)/(1.39\times1.21^{-0.06}))^{1/1.05} + 1 = 4.42$ and $u_{r,max} = 4.42\times0.079 = 0.350$ m, respectively. By employing Eq. (9) and Eq. (6), $\mu_\theta = (4.42\text{-}1)/0.79+1 = 5.33$ and $IDR_{max} = u_{r,max} / (H\times\beta) = 2.96\%$, respectively. Based on the limit values of ASCE 41-13 [42], designing the frame under IO, both the LS and CP performance levels are satisfied.

If the design starts from the LS performance level, the $u_{r,max(IDR)} = H\times\beta\times IDR_{max} = 0.294$ m and therefore, the $\mu_{r,IDR}$ is equal to 0.294/0.079 = 3.72. By using Eq. (9), the $\mu_{r,\theta} = 1+0.79\times(9\text{-}1) = 7.32$ and therefore, the $\mu_{r,d} = \min(3.72, 7.32) = 3.72$. It is found that drift controls the LS design. For a SDOF system with T = 1.47 sec, the maximum displacement is found 0.197×1.4 = 0.276 m under DBE (Figure 19a). The multiplier 1.4 is for eight storey buildings [42]. The displacement is smaller than the $u_{r,max(IDR)} = 0.294$ m and the revised values of IDR_{max} and μ_θ based on Eqs. (4) and (9) are 2.23% and 4.16, respectively. These values fulfil the limit states of ASCE 41-13 [42]. Based on Eq. (11) the required behavior factor q = 4.90. The resulted cross-sections are the same as the ones of IO level (Table 16).

If the design starts from the CP performance level, the $u_{r,max(IDR)} = H\times\beta\times IDR_{max} = 0.588$ m and therefore, the $\mu_{r,IDR}$ equals 0.588/0.079 = 7.44. By using Eq. (9), the $\mu_{r,\theta} = 1+0.79\times(11\text{-}1) = 8.90$ and thus $\mu_{r,d} = 7.44$. It is found that drift controls the CP design in current example as well. The maximum displacement expected under MCE would not be larger than 0.300×1.4 = 0.420 m (Figure 19a) which is smaller than the $u_{r,max(IDR)} = 0.588$ m. The revised values of IDR_{max} and μ_θ are 3.57% and 6.46, respectively. These values fulfil the limit states of ASCE 41-13 [42]. The use of $IDR_{max} = 3.57\%$ lead to similar structure with the IO level.

The FBD method [3, 27] is also applied here using factor q = 6.5 × 0.8 = 5.2. The LS performance level determines the frame dimension. The obtained cross-section and first three natural periods are given in Table 16. The frame behaves elastically under FOE and it is expected to experience $u_{r,y} = 0.079$ m and $IDR_{max} = 0.58\%$. Accordingly, under the DBE the $u_{r,max} = 0.316$ m and the $IDR_{max} = 2.32\%$. Under the MCE the $u_{r,max} = 0.474$ m and the $IDR_{max} = 3.48\%$.

6.3 *Nine storey steel space MRF with mass discontinuity along the height*

Figure 18c illustrate the floor plan of the nine storey steel space MRF with mass discontinuity along the height. The frame has an accidental eccentricity of 5% while the 5th floor has three times the mass of the adjacent floors. Table 17 provides the sections under FOE and the natural periods. The $u_{r,y} = 0.117$ m and $IDR_y = 0.62\%$ which fulfils the IO limit state values [42]. The q factor for DBE is 4.00. By using Eq. (12), $\mu_{r,d} = 1+(4.00\text{-}1)/1.48 = 3.03$, and Eq. (4), $u_{r,max} = 3.03\times0.117 = 0.354$ m. Eq. (9) determines $\mu_\theta = 1+((3.03\text{-}1)/1.17)^{1/0.59} = 3.54$ and Eq. (5) $IDR_{max} = (0.354/(1.47\times3\times9))^{1/1.24} = 2.22\%$. For estimating the frame response under the MCE, the q factor for the space MRF is 6. Accordingly, by using Eq. (12) and Eq. (4), $\mu_{r,d} = 1+(6\text{-}1)/1.48 = 4.38$ and $u_{r,max} = 4.38\times0.117 = 0.512$ m, respectively. By employing Eq. (9) and Eq. (5), $\mu_\theta = 1+((4.38\text{-}1)/1.17)^{1/0.59} = 7.03$ and $IDR_{max} = (0.512/(1.47\times3\times9))^{1/1.24} = 3.00\%$, respectively. Based on the limit values of ASCE 41-13 [42], designing the frame under IO, both the LS and CP performance levels are satisfied.

Under LS performance level design, Eq. (5) estimates $u_{r,max(IDR)}$ as $9\times3\times1.47\times0.025^{1.24} = 0.409$ and therefore, the $\mu_{r,IDR}$ is 0.409/0.117 = 3.50. By using Eq. (9), the $\mu_{r,\theta} = 1+1.17\times(9\text{-}1)^{0.59} = 4.99$ and thus $\mu_{r,d} = 3.50$. For a SDOF system with T = 1.95 sec, the maximum displacement is found to be 0.26×1.48 = 0.384 m under the DBE displacement design spectrum (Figure 19a). The multiplier 1.48 is for nine storey buildings [42]. The is smaller than 0.409 m and the revised values of the IDR_{max} and μ_θ are 2.24% and 4.10, respectively. These values satisfy the limit values of ASCE 41-13 [42]. Based on Eq. (12) the required behavior factor q = 4.38. The resulted cross-sections are the same as the ones of IO level (Table 17).

Under CP performance level design, $u_{r,max(IDR)} = 9\times3\times1.47\times0.05^{1.24} = 0.967$ m and therefore, $\mu_{r,IDR} = 0.967/0.117 = 8.26$. The $\mu_{r,\theta}$ is calculated as $1+1.17\times(11-1)^{0.59} = 5.55$ and thus $\mu_{r,d} = 5.55$. As a result, local ductility controls the CP design in the current example and placing the attention, the $u_{r,max(d)} = u_{r,max(\mu)} = 5.55\times0.117 = 0.65$ m. Under the MCE displacement design spectrum, the maximum roof displacement of the frame is expected to be $0.39\times1.48 = 0.577$ m (Figure 19a). The value is smaller than 0.65 m and revised values of IDR_{max} and μ_θ are 3.30% and 7.80, respectively. These values satisfy the limit value of ASCE 41-13 [42]. The use of IDR_{max} = 3.30% lead to similar structure with the IO level.

The FBD method [3,27] is also applied here using factor $q = 6.5 \times 0.8 = 5.2$. The LS performance level determines the frame dimension. The obtained cross-section and first three natural periods are given in Table 17. The frame behaves elastically under FOE and it is expected to experience $u_{r,y} = 0.087$ m and $IDR_{max} = 0.51\%$. Accordingly, under the DBE the $u_{r,max} = 0.348$ m and the $IDR_{max} = 2.04\%$. Under the MCE the $u_{r,max} = 0.522$ m and the $IDR_{max} = 3.06\%$.

Table 15. Columns and beams sections and first three natural periods of the 6-storey steel space MRF with irregular floor plan (L-shaped)

Design Example 1: 6-storey steel space MRF with L shaped floor plan						
Floor	Hybrid method			EC8 method		
	IPE		SHS	IPE		SHS
	B_{xe} - B_{ye}	B_{xi} - B_{yi}	C_i - C_e	B_{xe} - B_{ye}	B_{xi} - B_{yi}	C_i - C_e
1	330	450	340x20	400	450	350x16
2	330	500	340x20	400	500	350x16
3	330	450	320x20	400	500	350x16
4	300	400	320x20	360	450	300x16
5	300	360	300x20	330	360	300x16
6	300	360	300x20	330	360	300x16
	T_1=1.24sec - T_2=1.23sec - T_3=1.19sec			T_1=1.11sec - T_2=1.10sec - T_3=1.04sec		

Table 16. Columns and beams sections and first three natural periods of the 8-storey steel space MRF with setbacks

Design Example 2: Eight storey steel space MRF with setbacks						
Floor	Hybrid and EC8 method					
	IPE		SHS	IPE		SHS
	F_{xe}	F_{ye}	C_e	F_{xi}	F_{yi}	C_i
1	330	300	400x16	360	330	400x16
2	330	300	400x16	400	330	400x16
3	330	300	400x16	400	330	400x16
4	330	300	350x16	400	330	350x16
5	330	300	350x16	360	330	350x16
6	330	300	350x16	360	-	-
7	300	300	300x16	330	-	-
8	300	300	300x16	330	-	-
	T_1=1.47sec - T_2=1.37sec - T_3=1.13sec					

Table 17. Columns and beams sections and first three natural periods of the 9-storey steel space MRF with vertical mass discontinuities

Design Example 3: Nine storey steel space MRF with vertical mass discontinuity						
Floor	Hybrid method			EC8 method		
	IPE		SHS	IPE		SHS
	B_{xe} - B_{ye}	B_{xi} - B_{yi}	C_i - C_e	B_{xe} - B_{ye}	B_{xi} - B_{yi}	C_i - C_e
1	300	400	400x20	450	550	400x20
2	330	450	400x20	450	550	400x20
3	330	450	400x16	450	550	400x20
4	330	450	400x16	400	550	400x16
5	400	500	400x16	400	500	400x16
6	330	400	350x16	360	450	350x16
7	300	330	350x16	360	400	350x16

8	300	330	300x16	330	360	300x16
9	300	330	300x16	330	360	300x16
	T_1=1.95sec - T_2=1.95sec - T_3=1.91sec			T_1=1.56 sec - T_2=1.56 sec - T_3=1.49 sec		

6.4 Comparison and seismic assessment using semi-artificial accelerograms

The three design frames introduced in previous sections were subjected to the five pairs of semi-artificial accelerograms shown in Figure 10. The time history analysis results were then used to evaluate the frames performance as well as to both design methods.

The dynamic nonlinear analysis results are summarized in Table 18. Compared to the FBD method, one can observe that the hybrid design method provides a better control for the structural damage in terms of drift and ductility. This is because the hybrid design method utilizes a deformation and damage control q factor which can obtain several values based on the targeted performance level, while the FBD method employs a q factor that takes a general and constant value uncoupled from specific damage objectives. Moreover, IDR_{max} and $u_{r,max}$ obtained from the dynamic nonlinear analysis are constantly overestimated by FBD method, while those values are well predicted by the proposed method. However, a better prediction is observed for the six storey MRF by the hybrid method whereas an underestimation is observed for the nine storey MRF. Both design methods provided structures with similar weights. HFD and FBD designs of Example 1 have weight equal to 1211 kN and 1198 kN, respectively, while in Example 2 both methods determined a weight equal to 916. For the design Example 3, the hybrid design method provided a 15% lighter structure. The total weight of the steel (transformed in kN) was measured equal to 2536 kN. The FBD method provided a heavier structure with weight equal to 2946 kN. Table 19 provides the total mass of the structures and the performance level that controls the design in each case.

It should be noted that in all MRFs designed by the FBD, the interstorey drift sensitivity coefficient θ of EC8 [3] governs the design under the DBE thus determining a smaller actual behavior factor q than the one chosen initially. However, the initial choice of the q factor plays a direct role in the design solution by FBD and lighter solutions can very likely be adopted if a lower q factor was adopted instead. HFD appears to be more rational in estimating a behavior factor which satisfies both the targeted performance levels and drift requirements without implying later any indirect revision. As a result, a lighter structure is very likely to be adopted.

Table 18. Dynamic analyses results and comparison with both design methods for the 3 examples considered here

Six storey steel space MRF with L shaped floor plan - PGA_{DBE} = 0.36g												
Example 1	Hybrid method						Force based desing (EC8)					
	FOE		DBE		MCE		FOE		DBE		MCE	
	TH[a]	EST[a]	TH[a]	EST[a]	TH[a]	EST[a]	TH[a]	EST[b]	TH[a]	EST[b]	TH[a]	EST[b]
IDR (%)	0.58	0.58	2.06	2.22	2.78	3.12	0.55	0.55	1.75	2.20	2.40	3.30
$u_{r,max}$ (m)	0.078	0.076	0.245	0.245	0.346	0.357	0.074	0.073	0.225	0.292	0.332	0.438
μ_θ	1.00	1.00	3.17	3.74	4.22	6.58	1.00	1.00	2.93	-	4.80	-
Eight storey steel space MRF with setbacks - PGA_{DBE} = 0.36g												
Example 2	Hybrid method						Force based desing (EC8)					
	FOE		DBE		MCE		FOE		DBE		MCE	
	TH[a]	EST[a]	TH[a]	EST[a]	TH[a]	EST[a]	TH[a]	EST[b]	TH[a]	EST[b]	TH[a]	EST[b]
IDR (%)	0.60	0.58	2.01	2.07	3.02	2.96	0.60	0.58	2.01	2.32	3.02	3.48
$u_{r,max}$ (m)	0.086	0.079	0.278	0.246	0.418	0.350	0.086	0.079	0.278	0.316	0.418	0.474
μ_θ	1.00	1.00	3.08	3.66	4.39	5.33	1.00	1.00	3.08	-	4.39	-
Nine storey steel space MRF with vertical mass irregularity - PGA_{DBE} = 0.36g												
Example 3	Hybrid method						Force based desing (EC8)					
	FOE		DBE		MCE		FOE		DBE		MCE	
	TH[a]	EST[a]	TH[a]	EST[a]	TH[a]	EST[a]	TH[a]	EST[b]	TH[a]	EST[b]	TH[a]	EST[b]
IDR (%)	0.63	0.62	1.93	2.22	2.57	3.00	0.51	0.51	1.74	2.04	2.39	3.06
$u_{r,max}$ (m)	0.125	0.117	0.333	0.354	0.450	0.512	0.090	0.087	0.283	0.348	0.411	0.522
μ_θ	1.00	1.00	3.37	3.54	4.45	7.03	1.00	1.00	3.42	-	4.64	-

[a]TH: time history analysis; [a]EST: estimations of hybrid design method;
[b]EST (EC8): estimations using the equal displacement rule of EC8

Table 19. Mass and performance level (PL) that controls the design for the frames

Design Example	Hybrid method		Force based desing (EC8)	
	Mass (tons)	Control PL	Mass (tons)	Control PL
1	123.45	IO	122.12	LS
2	93.37	IO	93.37	LS
3	258.51	IO	300.31	LS

7. CONCLUSIONS

The main findings of the present study can be summarized as follows:

(1) Empirical expressions for a hybrid seismic design method (HFD) are developed for space steel moment resisting frames irregular in plan view and in elevation. Irregularity in elevation is either due to non-uniform distribution of mass or due to the presence of setbacks along the height of the frame. The proposed damage-control expressions apply to frames with low values of the mid-height stiffness parameter ρ and high values of the column-to-beam flexural strength parameter α.

(2) A torsional response component is observed in the irregular in-plan frames of this study. However, the level of this response is considerably smaller compared to the torsional response of the corresponding regular frames with 5% accidental eccentricity. This conclusion is limited to frames with the same bay widths and number of bays in both directions, similar to the frames of this work. The torsional response component of irregular setback frames can be more than two times the one of the corresponding regular frames with 5% accidental eccentricity.

(3) Buildings with setbacks only in one direction have different response and global ductility demands along the x and y in-plan direction. Thus, relationships between peak roof displacement – interstorey drift ratio (u_r - *IDR*) and behavior factor - maximum roof displacement ductility (q - μ_r) are different along the x and y direction. Based on the analyses results, in most cases, the setback direction determines the design controlling performance level.

(4) For a certain value of *IDR*, frames with mass discontinuity along their height have higher ductility demands compared to the corresponding regular frames. In addition, these frames satisfy the various performance levels for a lower seismic intensity than the corresponding regular frames.

(5) For a realistic range of q values (less than 8), the comparison of the proposed q-μ_r relationships versus the corresponding relationships proposed for planar irregular frames reveals a difference in the seismic response of space and planar irregular frames. For a targeted level of seismic performance, space frames require higher ductility demands and lower behavior factors than the corresponding planar ones. The above behavior seems to be related to the presence of the torsional response component in space irregular frames.

(6) Nonlinear time-history analyses revealed that HFD design method provides better estimations of critical response quantities, such as, the *IDR*, member ductility μ_θ, and roof displacement u_r under the three performance levels considered than the conventional FBD method.

(7) In the three design examples designed by the FBD method, the interstorey drift sensitivity coefficient θ of EC8 governs the design under the DBE level. As a result, a smaller behavior factor q than the one initially chosen is very likely to be determined by FBD. Following the HFD method, the immediate occupancy (IO) performance level controls the design in current examples without implying any indirect revision to the initial selection of q factor and a lighter structure could very likely be designed.

(8) In the three design examples, resulting total weights of the designed 6-storey irregular-in-plan-view and 8-storey with setbacks buildings by both design methods were found to be similar. In the design of the 9-storey building with vertical mass discontinuities the HFD method led to a 15% lighter structure.

REFERENCES

1. Zembaty Z, De Stefano M, editors. Seismic Behavior and Design of Irregular and Complex Civil Structures II. Switzerland: Springer; 2016
2. International Building Code, IBC. International code council, Inc. U.S.A.: ICC; 2012
3. Eurocode 8, EC8. Design of structures for earthquake resistance, Part 1: General rules, seismic actions and rules for buildings, European Standard EN 1998-1, Stage 51 Draft. European Committee for Standardization (CEN), Brussels; 2004

4. De Stefano M, Pintucchi B. A review of research on seismic behavior of irregular building structures since 2002. Bulletin of Earthquake Engineering 2008; 6: 285-308.
5. De la Llera JC, Chopra AK. Understanding the inelastic seismic behavior of asymmetric-plan buildings. Earthquake Engineering and Structural Dynamics 1995; 24: 549-572.
6. Dutta SC, Das PK. Inelastic seismic response of code-designed reinforced concrete asymmetric buildings with strength degradation. Engineering Structures 2002; 24: 1295-1314.
7. Anagnostopoulos SA, Kyrkos MT, Stathopoulos KG. Earthquake induced torsion in buildings: Critical review and state of the art. Earthquakes and Structures 2015; 8(2): 305-377.
8. Humar JL, Wright EW. Earthquake response of steel framed multistory buildings with setbacks. Earthquake Engineering and Structural Dynamics 1977; 5(1): 15-39.
9. Duan XN, Chandler AM. Seismic torsional response and design procedures for a class of setback frame buildings. Earthquake Engineering and Structural Dynamics 1995; 24: 761-777.
10. Chen C, Lam NTK, Mendis P. The Bifurcation Behavior of Vertically Irregular Buildings in Low Seismicity Regions. In WCEE: Proceedings of the 12th World Conference on Earthquake Engineering; 2000 Jan. 30 – Feb. 4; Auckland, New Zealand. Paper No. 1625.
11. Karavasilis TL, Bazeos, N, Beskos, DE. Seismic response of plane steel MRF with setbacks: estimation of inelastic deformation demands. Journal of Constructional Steel Research 2008; 64(6): 644-654.
12. Bosco M, Ghersi A, Marino E, Rossi PP. Effects of in elevation irregularity on the elastic seismic response of in-plan asymmetric buildings. In: Proceedings of the third European workshop on the seismic behavior of irregular and complex structures; 2002 Sept. 17-18; Florence, Italy. CD ROM.
13. Xilin Lu, Ningfen Su, Ying Zhou. Nonlinear time history analysis of a super-tall building with setbacks in elevation. The Structural Design of Tall and Special Buildings 2011; 22: 593-614.
14. Vasilopoulos AA, Bazeos N, Beskos DE. Seismic design of irregular space steel frames using advanced methods of analysis. Steel and Composite Structures 2008; 8: 53-83.
15. Valmundsson EV, Nau JM. Seismic response of building frames with vertical structural irregularities. Journal of Structural Engineering (ASCE) 1997; 123(1): 30-41.
16. Das S, Nau JM. Seismic design aspects of vertically irregular reinforced concrete building. Earthquake Spectra 2003; 19(3): 455-477.
17. Magliulo G, Ramasco R, Realfonzo R. Seismic behavior of irregular in elevation plane frames. In: Proceedings of the 12th European conference on earthquake engineering; 2002 Sept. 9-13; London, UK. Paper no. 219.
18. Tremblay R, Poncet L. Seismic performance of concentrically braced steel frames in multistory buildings with mass irregularity. Journal of Structural Engineering (ASCE) 2005; 131; 1363-1375.
19. Karavasilis TL, Bazeos N Beskos DE. Estimation of seismic inelastic deformation demands in plane steel MRF with vertical mass irregularities. Engineering Structures 2009; 30(11); 3265-3275.
20. Karavasilis TL, Bazeos N, Beskos DE. A hybrid force/displacement seismic design method for plane steel frames. In: Mazzolani FM, Wada A, editors. STESSA: Proceedings of the International Conference on the Behavior of Steel Structures in Seismic Area; 2006 August 14-17; Yokohama, Japan: Taylor & Fransis; 2006. p. 39-44.
21. Tzimas AS, Karavasilis TL, Bazeos N, Beskos DE. A hybrid force/displacement seismic design method for steel building frames. Engineering Structures 2013; 56: 1452-1463.
22. Tzimas AS. A New Hybrid Force/Displacement Method for Seismic Design of Space Steel Structures. Ph.D. Thesis, Department of Civil Engineering, University of Patras, Patras, Greece; 2013 (in Greek).
23. Tzimas AS, Karavasilis TL, Bazeos N, Beskos DE. Extension of the hybrid force/displacement (HFD) seismic design method to 3D steel moment-resisting frame buildings. Engineering Structures 2017; 147; 486–504.
24. Skalomenos KA, Hatzigeorgiou GD, Beskos DE. Application of the hybrid force/displacement (HFD) seismic design method to composite steel/concrete plane frames, Journal of Constructional Steel Research 2015; 115: 179-190.
25. Priestley MJN, Calvi GM, Kowalsky MJ. Direct Displacement-Based Design. Pavia, Italy: IUSS Press; 2007.
26. Bozorgnia Y, Bertero, VV. Earthquake Engineering: From Engineering Seismology to Performance-Based Engineering. CRC Press, Boca Raton, FL, USA; 2004.
27. Eurocode 3, EC3. Design of Steel Structures, Part 1. 1: General Rules for Buildings, European Prestandard ENV 1993-1-1. European Committee for Standardization (CEN), Brussels; 2005.
28. SAP2000. Static and Dynamic Finite Element Analysis of Structures. Computers and Structures inc., Berkeley, California; 2018.

29. Chopra AK (2007) Dynamics of structures. Pearson Prentice Hall, Berkeley
30. Macedo L, Silva A, Castro JM. A more rational selection of the behavior factor for seismic design according to Eurocode 8. Engineering Structures 2019; 188: 69-86.
31. Mazzolani FM, Piluso V. Theory and Design of Seismic Resistant Steel Frames. New York: FN & SPON an Imprint of Chapman & Hall, London; 1996
32. ASCE Standard ASCE/SEI 7-10. Minimum Design Loads for Buildings and Other Structures. American Society of Civil Engineers, Reston, Virginia, USA; 2010.
33. Carr AJ. Ruaumoko-3D - A Program for Inelastic Dynamic Analysis. Technical Report, Department of Civil Engineering, University of Canterbury, Christchurch, New Zealand; 2005.
34. Gupta A, Krawinkler H. Seismic Demands for Performance Evaluation of Steel Moment Resisting Frame Structures. Report No 132, John A Blume Earthquake Engineering Center, Department of Civil Engineering, Stanford University, Stanford, CA, USA; 1999.
35. Skalomenos KA, Hatzigeorgiou GD, Beskos DE. Modelling level selection for seismic analysis of concrete-filled steel tube/moment resisting frames by using fragility curves, Earthquake Engineering and Structural Dynamics 2015; 44(2): 199-220
36. Skalomenos KA, Hatzigeorgiou GD, Beskos DE. Seismic behavior of composite steel/concrete MRFs: deformation assessment and behavior factors, Bulletin of Earthquake Engineering 2015; 13(12): 3871-3896.
37. Fadden MF. Cyclic Bending Behavior of Hollow Structural Sections and their Application in Seismic Moment Frame Systems. Ph.D. Thesis, Department of Civil Engineering, University of Michigan, USA; 2013.
38. Pacific Earthquake Engineering Research Centre, PEER. Strong Ground Motion Database; 2009, http://peer.berkeley.edu/.
39. FEMA P58. Seismic performance assessment of buildings. ATC. Applied Technology Council: CA. USA; 2012.
40. Structural Engineers Association of California, SEAOC. Vision 2000 – A framework for performance based earthquake engineering. Sacramento, CA; 1995.
41. MATLAB. The language of technical computing. Natick MA: The Mathworks Inc; 2018.
42. ASCE Standard ASCE/SEI 41-13. Seismic Evaluation of Retrofit of Existing Buildings. American Society of Civil Engineers, Reston, Virginia, USA; 2014.